Nonaqueous organometallic electrochemistry : heterogeneous coupling of alkyl halides with reduced iron
by Jeffrey Louis Hall

A thesis submitted in partial fulfillment of the requirements for the degree of DOCTOR OF PHILOSOPHY in Chemistry
Montana State University

Abstract:
The electrochemical reduction of an N,N'-dimethylformamide, DMF, solution of iron (III) acetylacetonate, Fe(acac)3 , in the presence of 1-octyl bromide has been investigated. The strategy for the reaction is to selectively reduce the metal ion to a lower valent state without concomitant electrochemical reduction of the organic halide. The 1-octyl bromide was converted to octane, 1-octene, and hexadecane.

Electrolysis cells were operated with either a constant applied potential across two aluminum electrodes or with potentiostatic control of the working electrode potential. The latter cell required the generation of a stable reference electrode suitable for use in DMF. The cadmium amalgam reference electrode was such a reference.

The yields of hexadecane ranged from 0 to 33% for identically assembled two-electrode cells operating with a 1.5 volts applied across two aluminum electrodes. Potentiostatic control of the working electrode potential was hoped to decrease the wide range in yields of coupled product, however, this did not occur. Using an aluminum working electrode in identically assembled three-electrode electrolysis cells operating with the working electrode potential held at -0.9V vs Cd(Hg), the yields of hexadecane ranged from 35 to 59%.

The current-time behavior for the reduction of Fe(acac)3 in the presence of 1-octyl bromide using aluminum electrodes was recorded for both the two-electrode and three-electrode electrolysis cells. The current increased steadily with time for the two-electrode cell run at constant applied potential before falling to near zero levels. This is unusual for a simple reduction. The three-electrode cell held at a constant working electrode potential of -0.9V vs Cd(Hg) generated two current transients. The first current transient was generated as a result of iron plating onto the aluminum working electrode. The overpotential for reducing iron ions at an iron surface is less than the overpotential for the same reduction at aluminum, therefore the increase in current. The second current transient is assigned to the formation of an organoiron which is also electroactive.

The conversion of 1-octyl bromide to hexadecane, octane, and 1-octene is a one-electron heterogeneous reaction occurring at an iron-plated surface. The 1-octyl bromide is suggested to oxidatively add or dissociative!y adsorb onto the active iron surface. A one-electron transfer occurs expelling a bromide ion. This corresponds to the second current transient. Products are formed as a result of free radical reactions. The reaction is sensitive to the pretreatment of the aluminum electrodes, total cell current, and the nature of the plated iron surface. An epitaxial effect by the aluminum electrode is suggested to account for these observations.

42

NONAQUEOUS ORGANOMETALLIC ELECTROCHEMISTRY: HETEROGENEOUS COUPLING OF ALKYL HALIDES WITH REDUCED IRON

by

JEFFREY LOUIS HALL

A thesis submitted in partial fulfillment
of the requirements for the degree

of

DOCTOR OF PHILOSOPHY

in

Chemistry

Approved:

P. W. Jennings
Chairperson, Graduate Committee

E. W. Gnacker
Head, Major Department

Henry L Parsons
Graduate Dean

MONTANA STATE UNIVERSITY
Bozeman, Montana

April, 1977

to Karen and Sarah,

who made it all worthwhile

"Brevity, the soul of wit,

may become the very body of untruth."

A. Huxley

ACKNOWLEDGMENTS

My indebtedness to several individuals extends beyond a singular acknowledgment, but that is all that I can publicly offer while privately extending my friendship and respect. I hope that this humble offering is accepted.

George W. Keulks first introduced me to scientific research and heterogeneous catalysis. The offer he extended to me to work with him and his group was a turning point in my career. As a research director, instructor, and friend, he commands those faculties that make a great professional and provides a sound example to emulate. He has fired my zeal for heterogeneous catalysis.

Richard D. Geer has listened to my tales of electrochemistry and organometallic interactions, investing long and unrewarded hours of his own time. Without his timely contribution of a three-electrode potentiostat to this effort, the research might still be idling in the dark ages of the two-electrode constant applied potential cell. Bradford P. Mundy has sounded out my love for chemistry and kept the fires kindled through friendship and understanding. Arnold C. Craig developed a level of professionalism in me that can only come from a professional. I wish to thank Reed A. Howald for his stimulating tutorship in quantum mechanics and ligand field theory plus his willingness to instruct me in the ways of the dry fly. I wish to thank my

advisor, P. W. Jennings, for his support during this project. The graduate research assistantships he acquired for me during the course of this research effort helped accelerate the development of this project. To all of these individuals, thank you for increasing my understanding.

A thank you is also extended to two individuals who assisted with the analytical examination of the surface of the iron-plated aluminum working electrode. James Campbell obtained the X-ray fluorescent spectrum of the surface of the electrode while Phil McCandless obtained the scanning electron micrographs.

None of this would have been possible had I not had such proud, loving parents to be examples for me throughout my life. They have taught me to love and respect my Lord, my fellow man, and myself. I can never hope to repay them; all that I can do is give unto my family what they have given unto me.

TABLE OF CONTENTS

LIST OF TABLES

LIST OF FIGURES

ABSTRACT

The electrochemical reduction of an N,N'-dimethylformamide, DMF, solution of iron (III) acetylacetonate, $Fe(acac)_3$, in the presence of 1-octyl bromide has been investigated. The strategy for the reaction is to selectively reduce the metal ion to a lower valent state without concomitant electrochemical reduction of the organic halide. The 1-octyl bromide was converted to octane, 1-octene, and hexadecane.

Electrolysis cells were operated with either a constant applied potential across two aluminum electrodes or with potentiostatic control of the working electrode potential. The latter cell required the generation of a stable reference electrode suitable for use in DMF. The cadmium amalgam reference electrode was such a reference. The yields of hexadecane ranged from 0 to 33% for identically assembled two-electrode cells operating with a 1.5 volts applied across two aluminum electrodes. Potentiostatic control of the working electrode potential was hoped to decrease the wide range in yields of coupled product, however, this did not occur. Using an aluminum working electrode in identically assembled three-electrode electrolysis cells operating with the working electrode potential held at -0.9V vs Cd(Hg), the yields of hexadecane ranged from 35 to 59%.

The current-time behavior for the reduction of $Fe(acac)_3$ in the presence of 1-octyl bromide using aluminum electrodes was recorded for both the two-electrode and three-electrode electrolysis cells. The current increased steadily with time for the two-electrode cell run at constant applied potential before falling to near zero levels. This is unusual for a simple reduction. The three-electrode cell held at a constant working electrode potential of -0.9V vs Cd(Hg) generated two current transients. The first current transient was generated as a result of iron plating onto the aluminum working electrode. The overpotential for reducing iron ions at an iron surface is less than the overpotential for the same reduction at aluminum, therefore the increase in current. The second current transient is assigned to the formation of an organoiron which is also electroactive.

The conversion of 1-octyl bromide to hexadecane, octane, and 1-octene is a one-electron heterogeneous reaction occurring at an iron-plated surface. The 1-octyl bromide is suggested to oxidatively add or dissociatively adsorb onto the active iron surface. A one-electron transfer occurs expelling a bromide ion. This corresponds to the second current transient. Products are formed as a result of free radical reactions. The reaction is sensitive to the pretreatment of

the aluminum electrodes, total cell current, and the nature of the plated iron surface. An epitaxial effect by the aluminum electrode is suggested to account for these observations.

INTRODUCTION

Transition metals and main group metals have become common reagents in organic synthesis. Stoichiometric or catalytic quantities of the metal are used independently or in concert with other metals for both homogeneous and heterogeneous transformations of the organic substrates to products. Early attention was given to the main group metals but a growing body of literature has begun to explore the organo-coordination chemistry of the transition metals. The wealth of information that is now being accumulated on organotransition metal complexes is a consequence of the interesting chemistry of these metals due to the availability of the d-orbitals of the metal and the realization that organotransition metal complexes are not inherently thermally unstable. The carbon-metal σ-bond in these complexes is probably no weaker than bonds between carbon and other non-transition metal elements (1-4). The previously implied thermal instability simply reflects the plethora of decomposition pathways available for these organotransition metal complexes (2-6). The existence of these routes of decomposition is of eminent importance in the use of the organotransition metal complexes for organic synthesis. The following sections are offered to acquaint the reader with some general aspects of Group VIII transition metal chemistry, specific homogeneous organic chemistry of iron, and electrochemical processes of organic halides and organotransition metal complexes. These areas of the

literature have culminated in this examination of iron and alkyl halide reactions in an electrochemical cell.

General Group VIII Transition Metal Chemistry

The group VIII transition metals, of which iron is a member, participate in a wide variety of homogeneous reactions (7,8). Even a cursory examination of the group VIII transition metal chemistry requires several considerations to be put forth at the onset. First, the oxidation number of the central metal in the complex is defined as the charge left on the metal after all the ligands are removed in their closed-shell configuration (7,8). Thus, an alkyl radical is a one electron donor, but in computing the oxidation number of the metal, this group is considered a carbanion. A coordinated olefin is a two electron donor and, in computing the metal's oxidation number, it is removed as a two-electron ligand, therefore no change in the oxidation number of the metal occurs. Table I gives a brief classification of the number of electrons some commonly coordinated ligands donate to the metal. Second, the d-electron configuration about the central metal of the complex is assigned as a low-spin metal center with the d-orbitals split by the appropriate ligand field. The electrons fill the lowest energy d-orbitals with pairing, if necessary, before filling higher energy levels. Nonbonding and slightly π-bonding orbitals are filled before the antibonding orbitals. Finally, the 18-electron

Table I. Classification of Ligands on the Basis of Donated Electrons (8)

Number of Electrons Donated	Compound or Ligand
1	$R^{\bullet}$, aryl, $H^{\bullet}$, $X^{\bullet}$, $CN^{\bullet}$
2	CO, PL_3, ethylene, NH_3 L = aryl, alkyl, etc.
3	π-allyl$^{\bullet}$, NO (nitrosyl)
4	diene, triene, etc., but only two double bonds are coordinated
5	cyclopentadienyl
6	benzene, cycloheptatriene

rule, which is an empirical statement of the tendency of the transition metal center to acquire the next inert gas configuration, is usually obeyed by the group VIII metals although 16-electron square planar complexes for these metals are not unusual. Tolman (9) has noted a relationship between the 16- and 18-electron configuration about the central metal and the tendency for these complexes to participate in homogeneous catalytic cycles.

The normal range of the d^n electron configurations for the group VIII transition metals is from d^6 to d^{10} with a d^8 configuration being particularly widespread. Collman (8) has partitioned the even d^n configurations and coordination numbers of various possible complexes into saturated and unsaturated systems.

d^n	Saturated	Unsaturated
d^6	6 ligands	5 ligands
d^8	5 ligands	4 ligands
d^{10}	4 ligands	3 or 2 ligands

The utility of this classification lies in the experimental observation that coordinatively unsaturated systems are chemically active. Therefore, reasonable induction times are normally required to activate the saturated complexes (9).

Halpern (7) has further elaborated on this attempt of classification. He has examined the reactivity patterns of these transition

metals and compared the metal complexes to analogous intermediates in organic chemistry. Table II compares such a classification of the transition metals with organic intermediates. Appropriate examples are provided to accentuate the similarities.

The utility of this classification is best demonstrated with an example. The types of reactions associated with a particular electronic configuration and coordination geometry about the metal center can be related using the ligand field split d-orbitals of the preferred geometries of group VIII metals as shown in Figure 1. Consider the nature of the reaction in which an electron is added to an octahedral d^6 complex. The electron goes into an antibonding orbital of the octahedral complex. This is destabilizing. The detrimental effect can be relaxed if the system transforms into another geometry such as trigonal bipyramidal by loosing a coordinated ligand. This process, as pointed out by Halpern (7), is analogous to that which occurs when an electron is added to a saturated carbon compound:

$$\underset{\text{very stable}}{CH_3X} \overset{+e^-}{\rightleftharpoons} \underset{\text{unstable}}{[CH_3X]^-} \rightarrow \underset{\text{stable}}{CH_3\cdot} + X^- \qquad (1)$$

$$\underset{d^6}{Co(CN)_6^{3-}} \overset{+e^-}{\rightleftharpoons} \underset{d^7}{(Co(CN)_6^{4-}]} \rightarrow \underset{d^7}{Co(CN)_5^{3-}} + CN^- \qquad (2)$$

Extending this analogy to the systems in Table II while using the

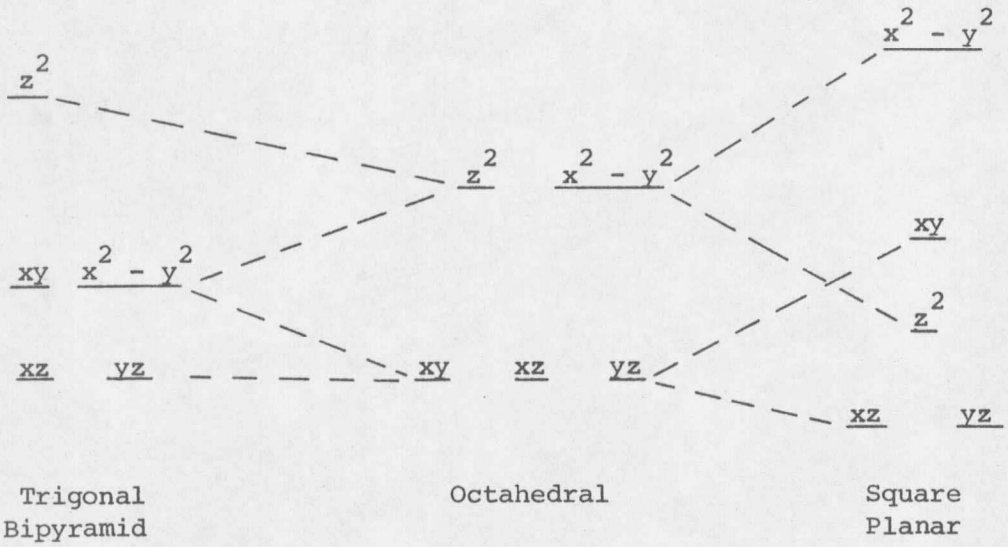

Figure 1. d-Energy Level Splitting for Preferred Geometries of Group VIII Transition Metals.

Table II. Comparison of Coordination Chemistry and Organic Chemistry Intermediates (7)

Species	Coordination Number	Nonbonding Electrons	Characteristic Reactions	Coordination Number	Nonbonding Electrons	Examples	Reactions
Saturated Molecule ($R_3C - X$)	4	0	Substitution	6	6	$RhCl_6^{3-}$	$RhCl_6^{3-} + H_2 \rightleftarrows RhCl_5H^{3-} + HCl$
Free radical ($R_3C^{\bullet}$)	3	1	Dimerization	5	7	$Co(CN)_5^{3-}$	$2Co(CN)_5^{3-} \rightleftarrows Co_2(CN)_{10}^{6-}$
			Abstraction				$Co(CH)_5^{3-} + CH_3I \rightarrow Co(CH)_5I^{3-} + CH_3^{\bullet}$
			Addition				$2Co(CH)_5^{3-} + HC{\equiv}CH \rightarrow (NC)_5CoCH{=}CHCo(CH)_5^{6-}$
Carbene $R_2C{:}$	2	2	Addition	4	8	$IrI(CO)(PPh_3)_2$	$IrI(CO)(PPh_3)_2 + C_2H_4 \rightleftarrows IrI(CO)(C_2H_4)(PPh_3)_2$
			Insertion				$IrI(CO)(PPh_3)_2 + H_2 \rightleftarrows IrH_2I(CO)(PPh_3)_2$
Carbonium ion (R_3C^+)	3	0	Addition of nucleophile	5	6	$Co(CN)_5^{2-}$	$Co(CN)_5^{2-} + I^- \rightleftarrows Co(CN)_5I^{3-}$
Carbanion ($R_3C{:}^-$)	3	2	Addition of electrophile	5	8	$Mn(CO)_5^{1-}$	$Mn(CO)_5^- + H^+ \rightleftarrows Mn(CO)_5H$

concepts of the unsaturated and saturated classification of Collman (8), the following generalized system of reactions can be developed:

d^6(5CN)*	$\xrightarrow{+L}$	d^6(6CN)	carbonium ion
d^7(5CN)	$\xrightarrow[+L]{-e^-}$	d^6(6CN)	free radical
d^8(4CN)	$\xrightarrow[+2L]{-2e^-}$	d^6(6CN)	carbene (oxidative-addition)
d^8(4CN)	$\xrightarrow{X}$	d^8(5CN)	carbene (X = CO or olefin)
d^8(5CN)	$\xrightarrow[+L]{-2e^-}$	d^6(6CN)	carbanion

*(coordination number)

In this scheme, L is any ligand and the number in parenthesis is the coordination number of the central metal. The importance of this type of classification is obvious; the reactivity patterns of the central metal depend on both its electronic configuration and the geometry, i.e., coordination number, of the complex. From such a classification, the oxidative-addition reaction which is widespread in the homogeneous reactions of the d^8 unsaturated square planar complexes of the group VIII transition metals arises from a concerted insertion of the d^8 complex into an X-Y bond. In so doing, the electron configuration and the coordination number about the metal center have changed by two. The existence of this reaction pathway is important in organotransition

metal chemistry in that it is often suggested to be a component of a homogeneous catalytic cycle. The propensity for undergoing the oxidative addition reaction increases upon descending a triad and passing from right to left (8). A word of caution should be injected at this juncture. The reaction scheme seems to suggest an inherent reactivity of saturated penta coordinated d^8 complexes. The trend for d^8 complexes to become coordinatively saturated (penta coordinated) increases on ascending the triad and going from right to left (8). Thus, the stability to CO dissociation for $M(CO)_5$ complexes is Fe > Ru > Os. Part of this stabilization is the availability of four π-backbonding orbitals in the trigonal bipyramid versus only three such orbitals in the square planar geometry (8,10).

The many pathways of decomposition that are available to the organotransition metal complexes have been reviewed elsewhere (5,6,11). Two decomposition pathways are of interest to this project. Reductive elimination reactions are essentially the reverse of oxidative addition reactions. The reaction involves a loss of two σ-bonded ligands together as a molecule. The coordination number and the oxidation state of the central metal decrease by two. β-hydride elimination occurs for alkyl transition metal complexes in which the alkyl group has hydrogens beta to the metal. This reaction requires a coordinately unsaturated site on the central metal. The beta hydrogen migrates to this site of coordinative unsaturation resulting in the formation

of an olefin-metal hydride complex. The olefin can then dissociate from the metal-hydride. The general sequence of events is depicted in the following equation:

$$M\text{-}CH_2CH_2R \rightleftharpoons \begin{matrix} H \\ | \\ M\text{-}\| \\ CHR \end{matrix}\!\!\begin{matrix} \\ \\ CH_2 \end{matrix} \rightleftharpoons H\text{-}M + H_2C{=}CHR$$

Iron Chemistry

The general chemistry of the group VIII transition metals is typified by the reactions of iron in various oxidation states. Five oxidation states are available to the iron and have been reported in the literature in various synthetic processes. These oxidation states are the -II which is not common but is found in the disodium tetracarbonyferrate salt, the zero, and the +I, +II, and +III states.

The disodium tetracarbonylferrate salt, $Na_2Fe(CO)_4$, has been suggested to be the transition metal analog of a Grignard reagent (12). The work of Collman et al. (13-15) has established the versatility of this reagent in synthetic organic chemistry. Two excellent reviews discuss the wide utility of this reagent from which Figure 2 has been abstracted (12,16). The reagent is useful in preparing aldehydes, unsymmetrical ketones, carboxylic acids, esters, and amides. The very high electron density on the iron (d^{10} configuration) makes the iron a particularly potent nucleophile (17). The reaction could proceed by either an S_N2 attack on the alkyl halide with inversion of

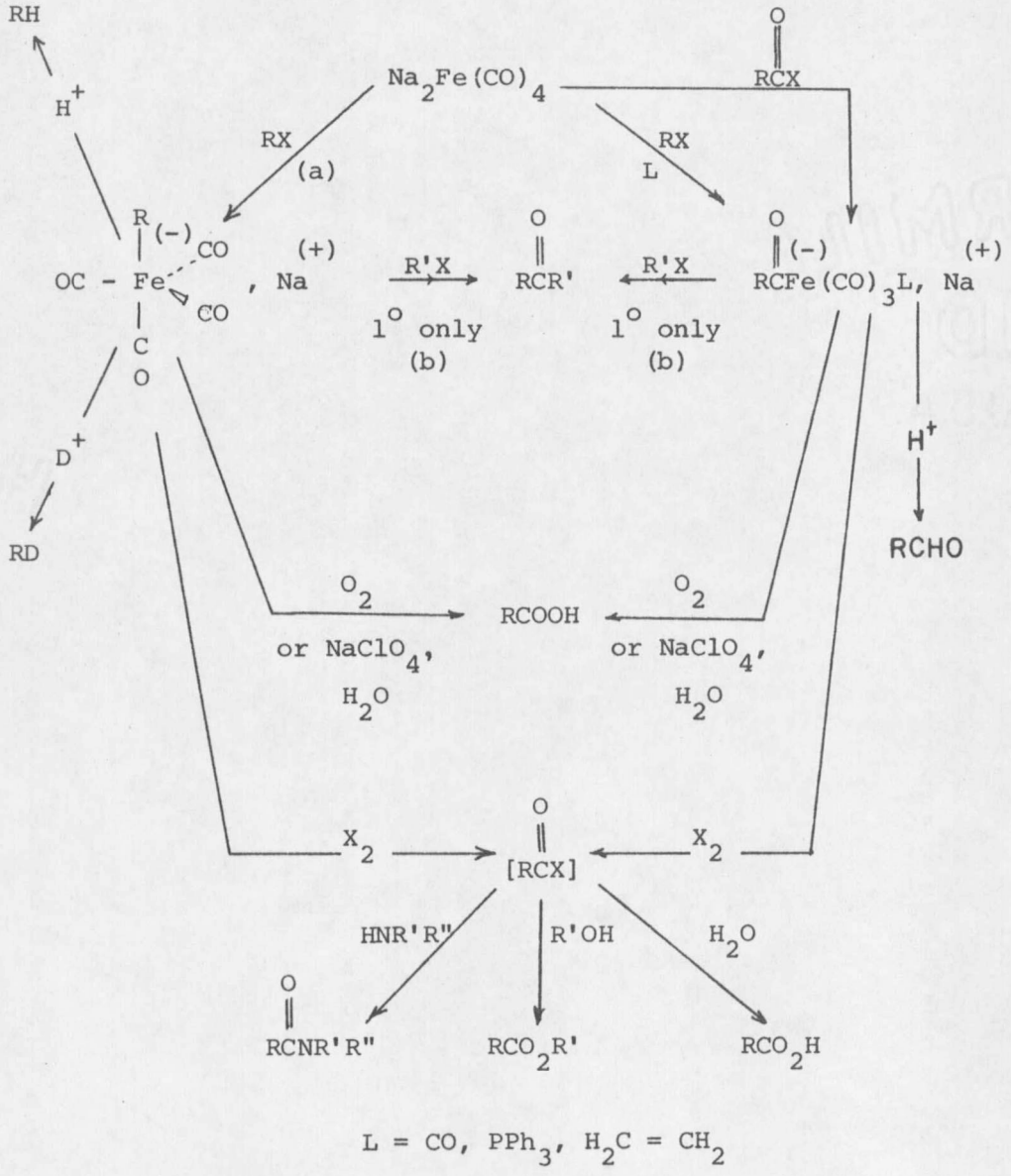

Figure 2. Organic Synthesis with $Na_2Fe(CO)_4$ (12,16,18).

configuration, or by oxidative addition to a d^{10} iron (-II)(13) defined to reflect the addition of a covalent molecule to the coordination sphere with reduction in the oxidation number of the metal (8). Both pathways would reduce the electron density about the iron center. Step (a) of the reaction sequence was observed to proceed with primary bromides, iodides, and tosylates as alkylating agents. The second alkylation, step (b), required more reactive reagents such as primary iodides or tosylates or benzylic halides. The overall order of reactivity for various reagents in the first step is ROTs $\sim$ RI > RBr > RCl and 1^{o} > 2^{o} > 3^{o}; in fact, the tertiary halide failed to react. This order of reactivity and the noted inversion about the carbon center was used to argue for a classical S_N2 alkylating step corresponding to the formation of the alkylated iron species. Subsequent formation of the acyl group proceeds with retention of configuration by migratory insertion of the carbonyl ligand into the alkyl metal bond (12).

The advantages which this complex has over the classical Grignard reaction are generally high yields of products, stereospecificity, and the toleration of several functional groups within the substrate such as -CHO, $-CO_2R$, -C≡N, and -Cl. There are some limitations to its usefulness. The high electron density on the iron makes it a particularly effective base in promoting elimination reactions. Allylic halides are also not usable because of their propensity to form π-complexes with the tricarbonyl iron. Like the Grignard reagents, the

iron complex must be used in excess to be effective in maximum conversion of organic substrate to product. Finally, the carbonyl insertion step is so facile in this complex that dialkylated iron species do not form which, on decomposition, could lead to coupled product without a carbonyl carbon inserted.

Iron zero, Fe(0), is a d^8 metal. Reactions of iron in atomic or aggregate form have been observed in homogeneous and heterogeneous systems respectively. Suspensions of iron powder in water have been noted to couple benzyl chloride (19) and α,α'-dichlorotoluene (20). Radicals are formed during this reaction. In the benzyl chloride case, these radicals were intercepted by anthracene which led to the generation of mixed organic products RR'. The proposed reaction for coupling was

$$PhCH_2Cl \overset{H_2O}{\underset{\Delta}{\rightleftharpoons}} PhCH_2^{(+)} + Cl^{(-)}$$

$$2PhCH_2^{(+)} + Fe^{\circ} \rightarrow 2PhCH_2^{\bullet} + Fe(II)$$

$$2PhCH_2^{\bullet} \rightarrow PhCH_2CH_2Ph$$

The oxidation state of iron changes to +II during the reaction which corresponds to a $d^8 \rightarrow d^6$ transition. Although the yields of bibenzyl were not reported, the formation of benzal chloride from

α,α'-dichlorotoluene was 9.6%. The coupling which does occur does not lead to a substantial generation of products.

The vapor phase reaction of iron atoms with organic substrates has also been examined. The method involves the vaporization of iron powder in a vacuum chamber and cocondensation of the gas-phase iron with organic substrate. The usual organic substrate was an unsaturated hydrocarbon. In one system, acetylene was observed to adsorb very rapidly onto the iron (21). Dienes were also found to form complexes with iron zero and, in the case of 1,3-cyclohexadiene, proceeded on to generate products (22): cyclohexene (33.4%), benzene (36.4%), and 1,4-cyclohexadiene (30.2%). This complex formation is reasonable. Olefins are particularly good coordinators to iron zero since π-backbonding through the olefin π^* orbital is a reasonable route in reducing the electron density about the iron zero.

Iron carbonyls are perhaps the best known iron (0) compounds. Several iron carbonyl complexes form: $Fe(CO)_5$, $Fe_2(CO)_9$, and $Fe_3(CO)_{12}$. The latter two represent cluster type compounds with bridging carbonyl ligands. The pentacoordinated iron (0) exists as a trigonal bipyramid and, as stated earlier, represents the most stable conformation of this d^8 metal complex. Any reaction that this species can undergo requires the initial removal of a CO ligand using either photochemical or thermal stimulation in order to obtain a coordinatively unsaturated 16-electron system (9). After such activation, the

tetracarbonyl iron (0) can react in one of two ways. The intermediate can coordinate an olefin which, like CO, is capable of π-backbonding. This type of substitution reaction would be classified a carbene-like reaction (7). Alternatively, the metal complex can undergo oxidative addition which is another carbene-like reaction in which the metal complex inserts into an activated C-X bond. Several examples of these reactions are presented.

Alper et al. (23) has reported that the iron pentacarbonyl complex will react with 1^{o}, 2^{o}, and 3^{o} aryl and alkyl α-haloketones in boiling 1,2-dimethoxyethane to give the coupled 1,4-diketone, reduced monoketone, and occasionally β-epoxyketones. They also noted that the iron pentacarbonyl will not react with the simple unactivated monohalides although the complex does react with activated geminal dihalides and vicinal dihalides. The reaction was not catalytic nor was it affected by free radical scavengers.

The reaction of a tetracarbonyl iron (0) complex with an olefin leads to the formation of cyclopentanones via a carbonyl insertion step. Weissberger et al. (24,25) photolyzed a sample of the pentacarbonyl iron (0) to generate the $Fe(CO)_4$ which subsequently coordinated an olefin. A reversible loss of another CO ligand from the monoolefin tetracarbonyl iron (0) complex allowed for further coordination of a second olefin. A five-membered metallocycle was formed from the coordinated olefins and metal center. A coordinated carbonyl group

inserts into one of the metal-carbon bonds thus forming a complex with a carbon-metal σ-bond and an acyl carbon-metal bond. Extrusion of the metal results in the formation of a cyclopentanone group linking the two olefins

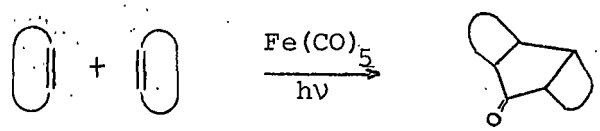

The formation of the products was stereospecific--exo-trans-exo was formed exclusively when substituted norbornene systems were used. This stereoselectivity has been suggested to be a consequence of the olefin π* acceptor orbital (26).

Mono coordinated olefins of the tetracarbonyl iron (0) complex can be treated with acid, HCl or HBr, to generate an iron (II)-alkyl intermediate. The intermediate then decomposes to alkane and an Fe(II) complex (27).

The ease of carbonyl insertion into a coordinated carbon-metal bond provides a route to possible ring expansion for appropriate systems. Weissberger (28) has observed the stereospecific expansion of pinene induced by iron pentacarbonyl to give the indicated products

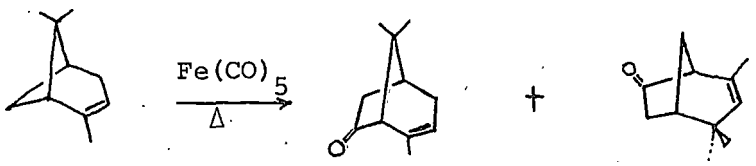

The reaction is felt to proceed via a σ-π-allyl metal complex and an acyl-π-allyl intermediate. Other ligands are capable of quenching the

reactive intermediate formed during the loss of a coordinated ligand. One such ligand is Ph_3P which is reported to be as effective in scavenging the iron (0) complex as is the olefin (29,30).

π-allyl metal derivatives of several metals have been recently reviewed (31). The π-allyl group is a three electron donor in π-complexes (8). It can coordinate with a metal as a σ-carbon species  or as an allyl group  . These possible bonding combinations are designated η^1- and η^3-allyl respectively. This allows for some very interesting chemistry. The reactive transition metal salts are coordinatively unsaturated. In the above case, it may be possible to use the η^3-allyl system to protect a site of unsaturation which is then exposed to an appropriate substrate during the transformation of the η^3-allyl group to an η^1-allyl system. Thus, depending upon the nature of the added ligand, the equilibrium between the σ-bonded and π-bonded allylic iron can shift. Cardaci et al. (32) observed that donor ligands caused the system to shift to σ-bonded carbon-metal bonds while acceptor ligands favored the π-allyl configuration.

The particular degree of complexation for polyolefins depends on the availability of good coordinating ligands which, as in the π-allyl case, can shift the nature of the bonding. A series of possible η^2-(monoolefin) to η^4-(diolefin)-1,4-diene complexes of iron (0) have been used to examine the consequences of the Woodward-Hoffman formalism as it applies to transition metal chemistry (33). Hughes et al.

(34) have demonstrated that the thermally disallowed 1,3-hydrogen suprafacial shifts which Mango postulates to occur in the presence of transition metals does not occur with the iron complex. They also observed direct metal insertion into a C-H bond and direct hydride transfer.

The above presentation has elaborated on systems of iron (0) in which a π acid has been coordinated to the zero valent iron. These π acids have been typed as such because of their ability to form π-back bonds. Can a stable σ-alkyl-iron zero compound form? A recent report has established the crystal and molecular structure of an iron zero-carbanionic salt (35). The salt, $[(\{C_6H_5\}_3P)_2N][Fe(CO)_4C_3H_7]$ contained a carbanionic propyl group attached to iron. This complex is very interesting in that the propyl group is formally a two electron donor without any ability to π-back bond. Since this complexing increases the electron density on the metal center, the existence of such a complex would not have been predicted on the basis of the pedestrian arguments posed here. The coordination about the anionic iron center was reported to be trigonal bipyramidal.

The cyclopentadienyl ligand stabilizes the low valent iron zero in the sodium salt, $Na[\eta^5\text{-}C_5H_5Fe(CO)_2]$. Again, the iron is the central metal of an anionic fragment. This complex is particularly suited to nucleophilic attack on the alkyl halides due to the electron density on the metal. Nucleophilic attack would generate a σ-bonded alkyl metal

derivative of iron (II). The attack by this nucleophilic complex is classified as a carbanion attack on an electropositive carbon (36).

$$Na[\eta^5\text{-}C_5H_5Fe(CO)_2] + RX \rightarrow \eta^5\text{-}C_5H_5FeR(CO)_2$$
$$d^8 \qquad \xrightarrow[+L]{-2e^-} \qquad d^6$$

This synthetic route has been used to prepare several σ-bonded alkyl-iron (II) complexes (37) including an optically pure chiral iron complex (38).

A very interesting reaction which is catalytic with respect to the reduced form of iron in the system is the Kharasch reaction (39,40) in which an organic Grignard reagent is mixed with a catalytic amount of ferric chloride in the presence of an organic halide.

$$RMgX + R'X \xrightarrow{FeCl_3} [RH, R(-H), R'H, R'(-H), RR, R'\text{-}R', RR']$$

The products of this reaction are monomeric alkanes and olefins (RH, R(-H), etc.) as well as coupled products (RR, etc.). The mechanism of this reaction has been extensively studied by Kochi et al. (41-46) and is suggested to be

$$RX + Fe \rightarrow R\bullet + FeX \qquad \text{(oxidation)}$$
$$R\bullet + Fe \rightarrow RFe \qquad \text{(oxidation)}$$
$$R'MgX + FeX \rightarrow R'Fe + MgX_2 \qquad \text{(metathesis)}$$
$$R'Fe, RFe \rightarrow \text{products} \qquad \text{(reduction)}$$

The reduced form of iron in this system has been shown to be the d^7 iron (I) species generated by a metathesis reaction between the Grignard reagent and the iron (III or II) of the added salt (44). The reduction of the iron involves an alkyl iron (III) species which proceeds through several steps before forming iron (I). An example of this reduction is given for an ethyl Grignard and $FeCl_3$.

$$Fe(III)Cl_3 + CH_3CH_2MgBr \rightarrow CH_3CH_3Fe(III)Cl_2 + MgClBr$$

$$CH_3CH_2Fe(III)Cl_2 \rightarrow \begin{matrix} CH_2 & H \\ \| & | \\ CH_2 & \end{matrix}\!\!-\!\!Fe(III)Cl_2 \rightarrow \begin{matrix} CH_2 \\ \| \\ CH_2 \end{matrix} + Fe(III)HCl_2$$

$$CH_3CH_2Fe(III)Cl_2 + Fe(III)HCl_2 \rightarrow CH_3CH_3 + 2Fe(II)Cl_2$$

$$Fe(II)Cl_2 + CH_3CH_2MgBr \xrightarrow{O} Fe(I), \text{ etc.}$$

The absence of butane in the reduction of the iron (III) eliminates any free radical component since six times more butane than ethane should have formed (44). The iron complex Kochi used in this analysis to generate the iron (I) center was iron (III) acetylacetonate, $Fe(acac)_3$.

The coupling reaction which leads to the dimeric product is sensitive to the number of available beta hydrogens on the organic substrate. As noted above, the reduction of iron (III) ion by the Grignard reagent proceeds in several steps, one of which includes

β-hydride migration. The availability of beta hydrogen on the organic halide substrate would also provide a low energy path of decomposition for the organoiron complexes formed from this material thus reducing or eliminating any coupling reaction. As an example, ethyl bromide, ethyl Grignard, and ferric chloride produced a 1:1 ratio of alkane to alkene with less than 0.1% n-butane (42). When t-butyl bromide was used in place of ethyl bromide, iso-butane and iso-butene were formed with ethane and ethylene. No products from the t-butyl bromide were obtained when styrene was present indicating a free radical component of the overall mechanism.

The generation of alkane and alkene was felt not to occur by a free radical reaction involving the homolysis of an iron-alkyl bond since no coupled product was obtained. Either a two step hydride migration or a direct hydride migration via a bimolecular reaction of two alkyl-metal complexes was suggested to generate alkane and alkene.

$$\text{2-step} \quad RCH_2CH_2M \overset{\rightarrow}{\leftarrow} RCH{=}CH_2 + HM$$

$$HM + RCH_2CH_2M \rightarrow RCH_2CH_3 + 2M$$

$$\text{direct} \quad 2RCH_2CH_2M \rightarrow RCH{=}CH_2 + RCH_2CH_3 + 2M$$

Coupling was suggested to proceed via a bimolecular reaction of two alkyl-metal complexes. Substrates without beta hydrogens coupled readily because the facile β-hydride migration decomposition

route was blocked. Added Ph_3P also increased the yield of coupled product for those systems without beta hydrogen (41).

The mechanism of the Kharasch reaction can be compared with recent work reported on gas phase ion-molecule reactions between iron (I) and CD_3CH_2I (47). Iron was observed to insert into the carbon-halogen bond forming an alkyl metal halide moeity. Furthermore, the β-hydride shift was explicitly observed to occur (47) thus supporting the existence of this step in the Karasch reaction. Although this work was performed in the gas phase and the Kharasch reaction is run in a solvent (THF), there does appear to be a conflict between the carbene-like insertion (oxidative-addition) in the gas phase versus the free radical reaction between alkyl halide and iron (I) in the solvent. The gas phase work with methyl iodide gave nearly a 50/50 mixture of organic free radicals and iodine atoms. d_5-Ethyl iodide, on the other hand, generated only 14% ethyl radicals and 86% deuterium iodide leaving a stable coordinated olefin-iron complex. Thus, the gas phase reaction suggests that radical formation is not particularly facile compared to oxidative-addition/β-hydride migration bringing into question the initial step of the Kharasch reaction, free radical generation.

Reactivity patterns of the Grignard reagent have established the pattern Et > n-Pr > i-Pr > neopentyl > CH_3 > ϕCH_2 > C_6H_5. Similarly,

the reactivities of the alkyl bromides have demonstrated the following order of decreasing reactivity: t-Bu > i-Pr > n-Pr (43).

Vinyl bromides were also observed to be reactive in the Kharasch reaction (42,45,46). This coupling reaction was observed to be stero-selective for products were cis or trans depending on the conformation of the vinyl moiety. The reaction is thought to proceed via coordination of the olefinic double bond to iron (I) with subsequent activation of the coordinated complex to halogen abstraction.

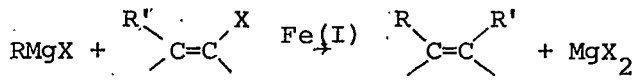

The stereospecificity of the reaction is suggested to reflect a concerted process in which a reduced iron species, Fe(I), is again the active agent.

$$Fe(I) + R'Br \rightleftarrows Fe(R'Br)$$

$$Fe(R'Br) + RMgX \rightarrow RR' + MgXBr + Fe(I)$$

This mechanism differs from the alkyl halide case in that no homolysis of the alkyl halide bond occurs. The mechanism is consistent with the coordinating abilities of the olefin. The coordination of the olefin allows for sterochemical specificity if the metathesis reaction between the Grignard and the olefin-iron complex results in the coordination of the Grignard's alkyl moeity on the iron center.

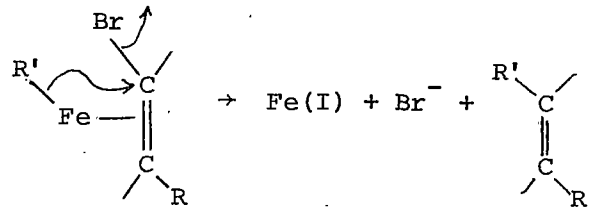

Recently Smith and Kochi (46) have suggested that the process involves oxidative addition of the vinyl bromide to the reduced iron with retention of configuration. They postulated the catalytic cycle

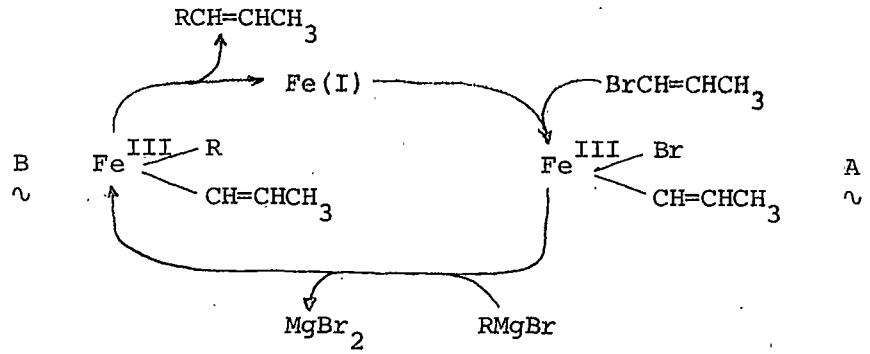

The catalytic effects of small amounts of iron (III), $\sim 10^{-5}$, in the Kharasch reaction has been observed for nearly sixteen years. It is interesting to read reports of peculiar effects that different sources of magnesium have on typical Grignard reactions (48,49). Examination of the magnesium from different sources found that the concentration of various transition metals varied with the source of magnesium. In particular, the effect of traces of iron impurities was monitored in the range of 4 to 40,000 ppm (48). Iron increased the yield of coupled product.

Iron (II) is a d^6 metal ion forming either octahedrally coordinated or tetrahedrally coordinated solution complexes depending on the particular ligand attached to the metal center. Iron (II)-alkyl metal complexes can be formed from the iron (0) anionic complex $Na[\eta^5\text{-}C_5H_5Fe(CO)_2]$ and alkyl halides generating the complex $\eta^5\text{-}C_5H_5Fe(CO)_2R$ which is thermally stable and insensitive to air oxidation in the solid state. Solutions of these complexes are air sensitive but, at room temperature, the complex is not labile. Whitesides et al. (50) have observed that the formation of the iron (II) complex proceeds with greater than 95% inversion of configuration at the carbon in the organic moeity. Generally, the reaction of low valent transition metals with alkyl halides can proceed with different stereochemical consequences depending on the method of reaction. If the metal acts as a nucleophile and displaces X^- from the organic substrate, the reaction is S_N2-like and proceeds with inversion of configuration (43). On the other hand, oxidative addition, particularly of d^8 complexes, proceeds with retention of configuration (43). Finally, ligand transfer of X^- to the metal reductant proceeds with racemization (43). The observation of 95% inversion substantiates the claim that the reaction is S_N2-like with the nucleophile being the iron (0) complex which has high electron density about the metal center. When the alkyl group is PhCHDCHD subsequent cleavage of the

alkyl-iron bond using Br_2, I_2, and $HgCl_2$ proceeds with retention of configuration of the alkyl ligand (51,52). If the alkyl group is $(CH_3)_3C$-, treatment of the complex with $HgCl_2$ cleaves the carbon-iron bond with retention of configuration (53,54) but Br_2 causes inversion at the carbon center (54).

Other reaction pathways are thermally accessible for this complex with R being the n-butyl moiety. Studies in hot solvent and in melts (55) have demonstrated that the thermal decomposition proceeds via β-hydride migration as demonstrated in Figure 3. Isolated products include the olefin and the metal hydride complex which was so stable, that it remained unreactive, therefore no saturated alkane was produced. Excess Ph_3P inhibited the formation of olefin by forcing the initial equilibrium to the left, therefore no sites of coordinative unsaturation were available for β-hydride migration. Recently, Norton (56) has suggested that hydride bridges between two metal centers are important in the elimination of alkane from a hydride and alkyl metal complexes. This suggestion appears to be in conflict with the noted generation of greater than 90% olefin from this iron (II) complex which generates both olefin and hydride. Since the olefin formation requires the generation of a coordinatively unsaturated site on the metal center, the availability of this vacant site for hydride bridging seems a reasonable pathway to initialize alkane production.

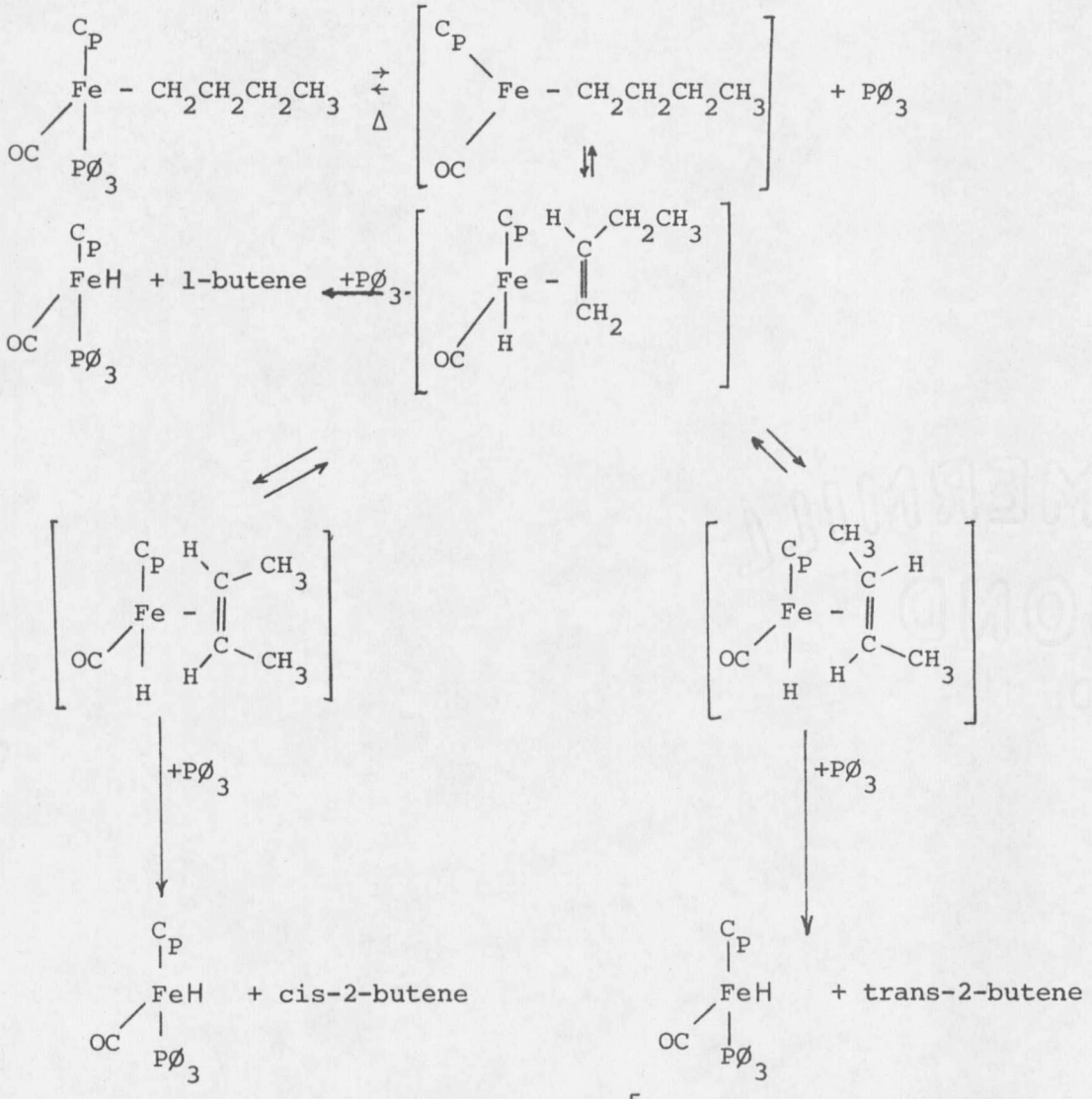

$PØ_3$: triphenyl phosphine; C_P: η^5-cyclopentadienyl

Figure 3. Thermal Decomposition Route for η^5-$C_5H_5Fe(CO)(PØ_3)(n\text{-}Bu)$ (55).

The work done on this bridging hypothesis involves osmium (II) which is also a d^6 metal in the same triad as iron.

Alkyl-iron (II) complexes have also been reported which are free of both the carbonyl and cyclopentadienyl ligands. Yamamoto et al. (57,58) have isolated diethylbis(dipyridyl)iron complexes from a catalyst system containing iron (III) acetylacetonate, diethyl aluminum monoethoxide, and dipyridyl. Iron (0), (II), and (III) complexes of the dipyridyl ligand were prepared by thermal degradation of the diethyl complex. The reaction scheme is given in Figure 4. Thermalosis is seen not to lead to any coupled product. Coupling can be initiated, but it is not the preferred route of decomposition. This diethyl complex was found to be an active catalyst in butadiene cyclodimerization. For this complex to function in such a process, the mechanism must involve the generation of a coordinatively unsaturated complex in order to allow for olefin coordination (58).

Iron (II) is also a good radical trap. The reaction of iron (II) with free radicals has demonstrated its versatility as a trap and a one-electron reductant (59-62). Functioning as a free radical trap, the iron (II) was observed to give coupled products from methyl free radicals via the proposed scheme (59):

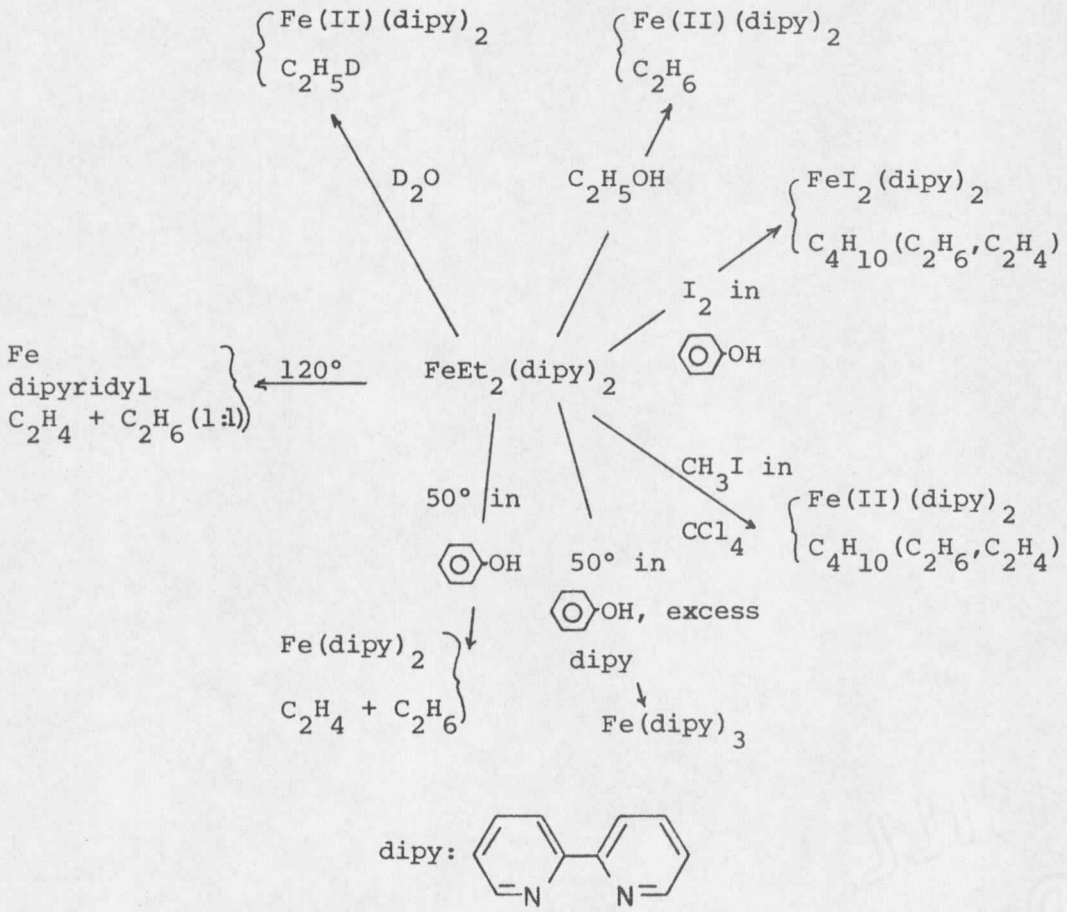

Figure 4. Reactions of $FeEt_2(dipy)_2$ (57,58).

$$R\cdot + M^{2+} \rightleftarrows (R\cdot M)^{2+}$$

$$R\cdot + (R\cdot M)^{2+} \rightarrow RR + M^{2+}$$

$$2(R\cdot M)^{2+} \rightarrow RR + 2M^{2+}$$

This reaction was particularly facile with Ni(II).

Iron (III) is the final oxidation state of iron that will be discussed. Iron (III) is a d^5 ion. The iron ion can effectively perform the functions of a free radical trap through its relative ease of reduction to iron (II). In particular, ferric chloride is a very effective trap for alkyl radicals, the product of the reaction being an alkyl chloride and ferrous chloride (63,64). The reaction is felt to proceed via a bridging chloride, i.e., an outer sphere reduction.

$$R\cdot + Fe(III)Cl_3 \rightarrow [R\cdots Cl\cdots Fe(III)Cl_2] \rightarrow RCl + Fe(II)Cl_2$$

The effect of free iron (III), that is without coordinated chloride, is to oxidize the free radical to the corresponding cation which proceeds to form products (65). The iron (III) ion is effective as a free radical trap, but of little utility in forming alkyl metal complexes, probably because of the low stability of an iron (IV) ion.

This discourse on iron organometallic chemistry suggests that the formation of the lower valent states of iron can lead to particularly effective reagents in organic synthesis. The oxidation states of iron (0) and iron (I) are noted to be more reactive than the

oxidation states (II) and (III) as demonstrated by both the iron carbonyl chemistry and the Kharasch reaction. The formation of these lower valent states has usually been accomplished with chemical reducing agents which have fixed but wide varying reduction potentials. This method of reduction generally limits the synthetic method in that the organic substrate is susceptible to reduction of unprotected functional groups. Secondly, the chemical reducing agent is usually required in excess concentrations to insure that all the iron remains reduced in which case a catalytic cycle is available. Alternatively, the iron is prereduced to a low oxidation state such as the iron in the disodium tetracarbonylferrate reagent. The reduced iron is susceptible to oxidation and therefore requires special handling. Another method of reduction uses an electrochemical cell to effect the reduction of an air stable iron salt in the presence of an organic substrate. The initial investigation into the utility of this method was done by Pillsbury (66). The method was successful. Electrochemical cells have also been used to form d^8 organometallic complexes from the d^6 organometallic parent (67). The synthesis outlined by Pillsbury is different in that the reduction, organometallic formation, and product generation are preformed in one cell without prior preparations.

Reduction of Organic Halides

The electrochemical reactivity of organic compounds has been thoroughly reviewed by Fry (68), Mann and Barnes (69), Baizier (70), and Rifi (71). The reaction of particular concern for this dissertation is the reductive cleavage of organic halides. The classical work of von Stackelberg and Stracke (72) established an electrochemical reactivity pattern for the organic halides that has recently been modified by Fry (68).

1. The ease of reduction of organic halides follows the order

$$\text{allylic} \simeq \text{benzylic} > \text{saturated} \simeq \text{aryl} > \text{vinylic}$$

Thus, allyl bromide has an $E_{1/2} = -1.29V(SCE)$, ethyl bromide has an $E_{1/2} = -2.09V(SCE)$, n-butyl bromide has an $E_{1/2} = -2.27V(SCE)$, and vinyl bromide has an $E_{1/2} = -2.47V(SCE)$. All of these reductions occurred in 75% dioxane-water solvent with tetraethylammonium bromide as the supporting electrolyte. SCE refers to the saturated calomel electrode used as a reference electrode.

2. The double bond in unsaturated halides is not electrochemically reducible.

3. The ease of reduction of a particular organic halide is a function of the attached halogen. The ease of reduction decreases (requires increasing cathodic potential) in the order

$$I > Br > Cl > F$$

In fact, except for unusual cases, the alkyl chlorides are not electrochemically reducible.

4. Geminal and vicinal polyhalides are easier to reduce than simple halides. This trend is adequately demonstrated in the following two series given in the order of decreasing ease of reduction:

$$CCl_4 > CHCl_3 > CH_2Cl_2 > CH_3Cl$$

$$BrCH_2CH_2Br > CH_3CHBr_2 > CH_3CH_2Br$$

5. An increase in chain length of the aliphatic group attached to a carbon atom reduces the ease of reduction:

methyl bromide > n-butyl bromide > n-octyl bromide

The nature of this effect has been attributed to adsorption phenomena.

6. In general, the half wave potentials for the reduction of organic halides are pH independent indicating that proton transfer to form the saturated system cannot occur either before or in the transition state of the reaction.

von Strackelberg and Stracke (72), on the basis of the above evidence, proposed the following mechanism for organic halide reduction:

$$RX + e^- \rightarrow R\cdot + X^-$$

$$R\cdot + e^- \rightarrow R^-$$

$$R^- + H^+ \rightarrow RH$$

Two other mechanisms have been suggested by Elving (73) one involving an S_N2 type reaction the other an S_N1 reaction:

S_N2 $\quad RCH_2X + 2e^- \rightarrow RCH_2^- + X^-$

or

$RCH_2X + 1e^- \rightarrow [RCH_2X]^{\bullet -}$

$[RCH_2X]^{\bullet -} \rightarrow RCH_2^{\bullet} + X^-$

$RCH_2^{\bullet} + 1e^- \rightarrow RCH_2^-$

S_N1 $\quad RCH_2X \rightarrow RCH_2^+ + X^-$

$RCH_2^+ + 2e^- \rightarrow RCH_2^-$

The latter mechanism was felt feasible by considering the effects of the intense electrical field within the electrical double layer. Petrovich and Baizer (74) have shown that the ease of reduction of alkyl halide followed the order of Br << OTs $\lesssim$ Cl. This order is inconsistent with an S_N1 displacement mechanism. Annino et al. (75) and Webb et al. (76) examined the reduction of optically active cyclopropyl halides and found partial retention of configuration. Again, the evidence was used to discount the S_N1 mechanism.

Lambert (77,78) and Marple (79) have been strong proponents of the S_N2 mechanism. They have demonstrated qualitative correlations between S_N2 reactivity and half-wave potentials. In this stead, the

cathode acts as an extremely large nucleophile. Ulery (80) indicated that two possible routes exist for this type of attack:

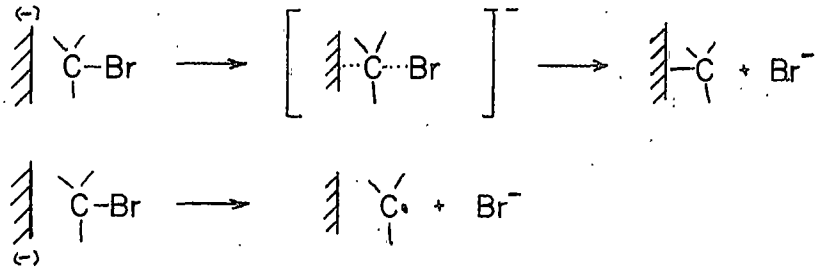

Sease (81) demonstrated that for bridge-head bromides, the S_N2 mechanism is not possible since backside attack is impossible. Noting that halogens can specifically adsorb on the surface of mercury, Sease considered the halogen functioning as a bridging group between the electrode surface and the alkyl group. In this configuration, an electron flows through the bromine atom from the cathode to the carbon. Lambert (82) argues against this mechanism and suggests that the orientation of the carbon-bromide dipole dictates that bromide cannot align itself with the cathode in this manner. He proposes either a perpendicular adsorption relative to the carbon-bromide bond axis or a possible S_N1 effect.

The intermediacy of the anion radical, $[R\text{-}X]^{\bullet-}$, has been contested by Fry (68). The $[R\text{-}X]^{\bullet-}$ may be a transition state but not a true intermediate. Studies of the reduction of alkyl halides by solvated electrons do involve intermediates with the structure $[RX]^{\bullet-}$. This argues against their formation in an electrochemical

cell since the rates of reduction by hydrated electrons are unrelated to carbon-halogen bond strength while the electrochemical reductions do demonstrate such a relationship.

The first step of the reduction in the classical mechanism is felt to be rate limiting. Thus, the second electron transfer is very rapid and, if the first step of the reduction of the original halide occurs at potentials more cathodic than the reduction of the alkyl radical thus formed, a net two electron transfer occurs. The evidence for the intermediacy of free radicals comes from two sources. First, Hoffman et al. (83) observed two polarographic waves of one electron each for the reduction of t-butyl iodide. Using t-butyl bromide, only one two electron polarographic wave was obtained. The second source is indirect evidence such as the formation of organometallics (84) at mercury (85,86), at lead (87,88), and at tin (89). The formation of coupled products is suggested to be indicative of free radical reactions although an S_N2 reaction of an electrochemically generated carbanion on alkyl halide starting material can not be exclusively ruled out. Brown (85) argues that dimers are formed from the organomercury products which form from a free radical attack on mercury. Fleischmann et al. (89) rule out the carbanion attack on RX as being responsible for coupled product on the basis that if such an attack occurs for one reaction, it should occur for all alkyl halides. This latter argument can be attacked by noting that the reduction of alkyl

halide is potential dependent (90), see Table III. The products generated are related to the working electrode potential therefore such a naive statement ignores the complexity of the problem.

Evidence for carbanions comes from coulometric work, trapping by CO_2 to form carboxylic acids (68), or by isolation of the Hofmann elimination products (76) when the solvent is aprotic.

$$R^- + CH_3CH_2\overset{(+)}{N}Et_3 \rightarrow RH + CH_2{=}CH_2 + 2Et_3N$$

Organometallic Electrochemistry

The synthesis of organometallic compounds has already been suggested to provide evidence of free radical formation during the reduction of organic halides (84-89). Settineri and McKeever (91) and Lehmkuhl (90,92) have reviewed the area of synthetic organometallic electrochemistry and the subsequent electrochemical degradation of the organometallic has been reviewed by Dessey (93).

The electrochemical formation of organometallics can proceed via one of three routes (90,92).

1. The reduction of organic compounds to form organic radicals which subsequently attack the cathode metal to form the organometallic (sacrificial cathode).

2. Metallic compounds can be reduced to a lower valence state of the metal. As noted in the introduction, this state is often not

Table III. Cathode Potential versus Product Distribution (90)

C Potential V vs Ag/AgCL	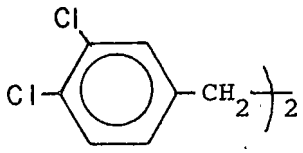 %	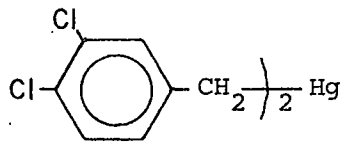 %
-0.94	2.1	39.0
-1.05	25.0	26.6
-1.30	21.0	4.6

stable per se but may be stabilized by suitable organic complexing agents.

3. Anodic oxidation of organometallics containing carbanions to generate free radicals which can then attack the anode material to form new organometallics.

The reductive routes of organometallic synthesis are particularly germain to this problem. The proposed scheme to account for the organometallic products formed at a sacrificial cathode is (86,87)

$$\begin{array}{l} \qquad\qquad\qquad\qquad\qquad\qquad\quad RM \\ \qquad\qquad\qquad\qquad\qquad\qquad\quad \uparrow M_{cathode} \\ RX + 1e^- \rightarrow R^{\bullet}_{ads} + X^- \xrightarrow{1e^-} R^- \xrightarrow{H^+} RH \end{array}$$

The formation of the organometallic is a function of the cathode potential as noted in Table III. The major tools used to identify reduction pathways for organic halides has been polarography with a dropping mercury electrode and controlled potential electrolysis using a mercury cathode or some other sacrificial electrode. Brown (85) claims that simple dimers are seldom formed as the major product of halide reduction and, when they are reported, they have been formed from organomercury products during the analysis after the reduction. This view is particularly harsh, but does suggest that "free" radicals are adsorbed radicals and the lifetime of a carbanion

is too short even in aprotic solvents to engage in nucleophilic attack on the starting material.

The formation of organometallic compounds by reducing the metal in the presence of an organic substrate has led to the preparation of several organometallic complexes. Usually the organic ligand is a complexing agent with multiple π-bonds which are effective in stabilizing low valent metals. Several examples follow.

$$Fe(acac)_3 \xrightarrow[\text{stainless steel cathode}]{\text{reduction } CO,\ 86^\circ} Fe(CO)_5 \quad 65\% \qquad (94)$$

$$Ni(acac)_2 \xrightarrow{\text{Al-anode, THF}} \frac{1}{n}[Ni(C_8H_8)]_n + \frac{2}{3}Al(acac)_3 \qquad (90)$$

$$Ni(acac)_2 \xrightarrow[Ph_3P]{\text{Al-anode, THF}} Ni(PPh_3)_4 + \frac{2}{3}Al(acac)_3 \qquad (90)$$

$$Co(acac)_2 \xrightarrow[\text{2) butadiene}]{\text{1) +2e, Al anode, THF}} CH_2{=}CHCH(CH_3){-}CH{=}CH{-}CH{=}CH_2 +$$

$$CH_2{=}CH{-}CH{=}CH{-}CH_2{-}CH_2{-}CH{=}CH_2 \qquad (90)$$

The latter example represents a reaction that has led to the dimerization of butadiene via a reduced form of cobalt and assumed organocobalt intermediate.

The formation of organometallics is important in systems where they are assumed to be generating product. Dessy's work on the electrochemical degradation of the organometallics is shown in Figure 5 (90,93). Lehnkuhl (90) has given examples of these routes and the reader is referred to his article.

Electrochemical Cells

The methodologies for examining an electrochemical reaction have been discussed by Headridge (95), Sawyer and Roberts (96), Cauguis (97), Meites (98), and Fry (68). Fundamental electrochemical concepts are thoroughly developed by Bockris and Reddy (99) and the reader is referred to this text for detailed study.

Of the available electrochemical techniques used to examine an electrochemical system, the least articulate is macroscopic synthesis. The transition from microelectrochemistry to macroelectrolysis cells is not necessarily smooth for it involves increasing the concentration of the electrophore 100 to 10,000 times that used in a polarographic technique (100). The practical problems of electrolysis on large samples have been reviewed (101).

Three types of electrolysis cells are available for large scale electrolysis. Two of these cells are two-electrode assemblies which operate at either constant current or constant applied potential. The third cell is referred to as a three-electrode cell. Its operation

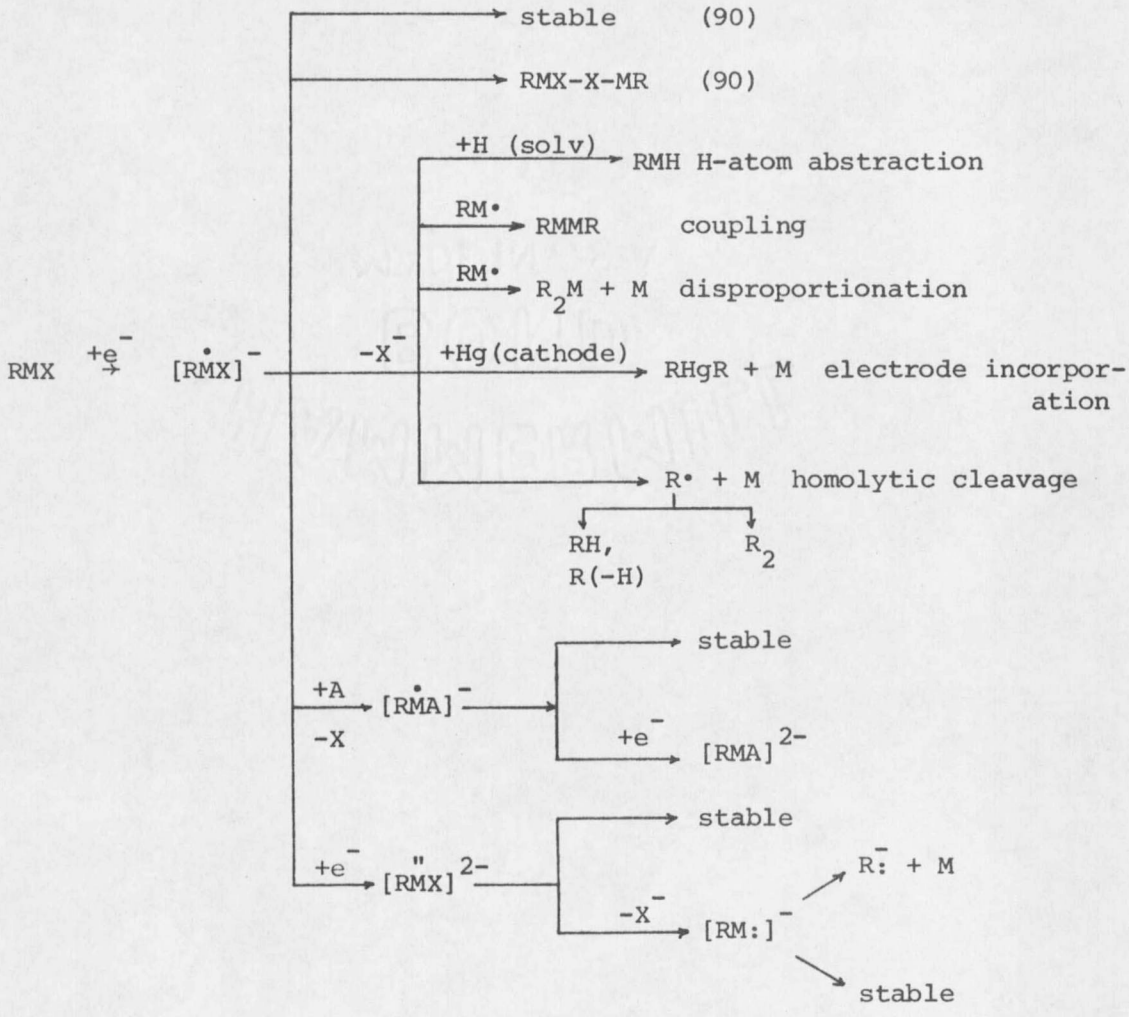

Figure 5. Electrochemical Degradation of Organotransition Metals (90,93).

involves the control of the working electrode potential (102). All three cell types have been used in this work and a more thorough presentation will be given in the discussion.

Statement of the Problem

Two advantages which an electrode has over a chemical reducing agent are (1) control of the reduction potential of the electrode which then introduces energy selectively into a system and hence varies the number of electrons transferred, and (2) the electrode often simply adds or removes an electron from the electrophore without entering into bonding as is often the case with chemical reagents (103). An electrochemical cell will be used to examine the plausibility of generating low valent metal ions or atoms in the presence of an organic halide. The organic halide can subsequently react with the low valent metal according to the homogeneous processes outlined in the introduction. The strategy is to selectively reduce the metal ion without concommitant electrochemical reduction of the organic halide thus the inorganic ion functions as a homogeneous mediator in the overall conversion of organic halide to products (104).

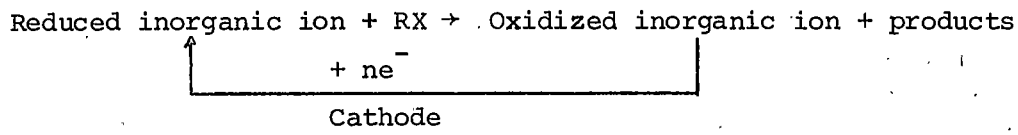

DISCUSSION

Two-Electrode Systems

The reaction we are attempting to effect is the conversion of alkyl halides to coupled dimer, R_2, and disproportionated products, RH and R(-H) where RH represents an alkane and R(-H) the olefin. This transformation is known to occur

$$RX \xrightarrow{[M]} [R_2, RH, R(-H)]$$

in several organic reactions using reduced forms of the metal such as the classical Wurtz reaction and the Kharasch reaction.

Our initial investigations into this transformation used a two-electrode cell run under constant current or constant applied potential (66,105). Table IV indicates that coupled products were formed during the reaction. The cell used in this phase of the examination is shown in Figure 6. The operation of the two electrode cells under constant current and constant applied potential will be considered.

Two solution electrophores are available for reduction in the electrolysis cell, the metal ion and the organic substrate. Each electrophore has its own reduction potential corresponding to $E^{M}_{1/2}$ and $E^{RX}_{1/2}$ where M and RX represent the metal ion and the organic halide, respectively. Figure 7 shows a possible polarographic trace for two solution electrophores. A judicious selection of metal ion and organic halide will generate a cell in which the metal is reduced before the organic

Table IV. Coupling of Organic Halides (105)

Substrate	Metal Acetylacetonate	Electrode (Cathode/Anode)	Stabilizing Ligand	Product	% Yield
1-Bromobutane	Fe	Ni/Ni	Ph_3P	Octane	28
2-Bromobutane	Fe	Ni/Ni	Ph_3P	3,4-Dimethyl hexane	20
2-Bromo-2-methyl-butane	Fe	Ni/Ni	Ph_3P	No coupling	
1-Octylbromide	Fe	Al/Al	Ph_3P	Hexadecane	32
				Octane	11
				1-Octene	3
1-Octyl bromide	Fe	Al/Al	—	Hexadecane	30
				Octane	49
				1-Octene	18
Benzyl chloride	Ni	Cu/Ni	Ph_3P	Bibenzyl	87
Benzyl bromide	Ni	Cu/Ni	Ph_3P	Bibenzyl	85
Phenyl bromide	Ni	Cu/Ni	Ph_3P	Biphenyl	65

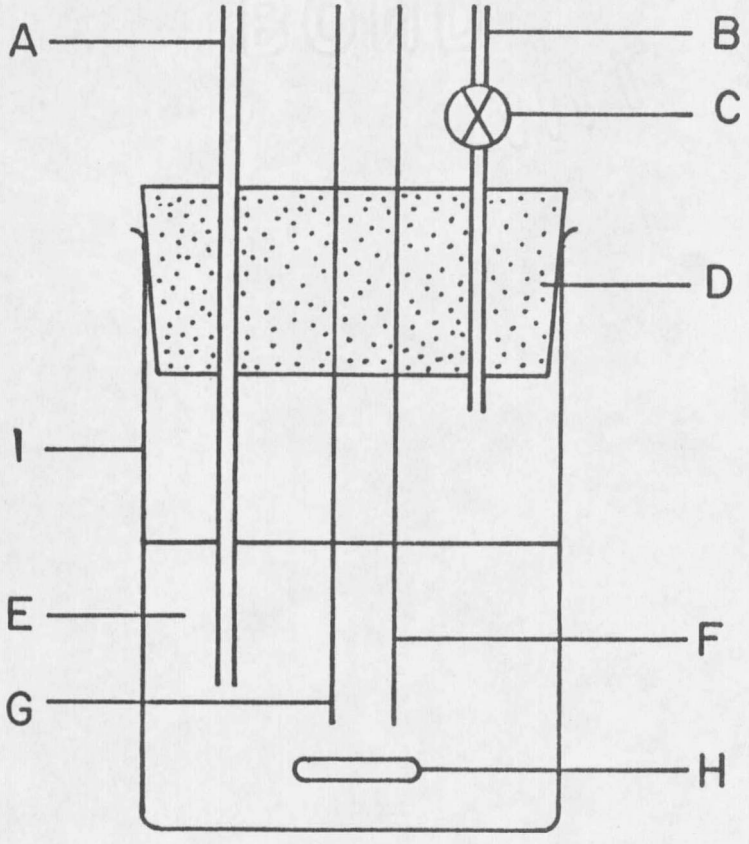

Figure 6. Two-electrode Electrolysis Cell: (A) nitrogen inlet for purging the solution and maintaining a positive pressure; (B) gas outlet which is open during purging and closed during electrolysis; (C) stopcock for closing gas outlet; (D) rubber stopper; (E) electrolysis solution; (F) cathode; (G) anode; (H) magnetic stirring bar; (I) 100-ml Berzelius beaker.

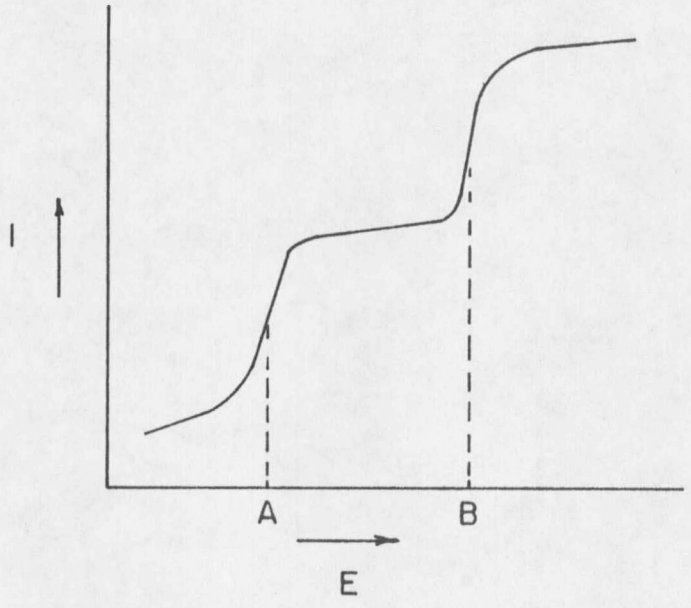

Figure 7. Polarogram for Two Electrophores. I is current, E is potential of dme versus suitable reference, A is $E_{1/2}$ of metal ion, B is $E_{1/2}$ of alkyl halide.

substrate, $E^{M}_{1/2} > E^{RX}_{1/2}$. Although the polarographic cell operates with solution concentrations of 10^{-4} M, the macroscopic cell using concentrations of 1.0 to 0.1 M is expected to behave similarly, that is $E^{M}_{1/2} > E^{RX}_{1/2}$. Figure 8 presents an I-E curve for such a macroscopic system containing two reducible electrophores (101). When the cathode potential is less than E_A no current will flow through the cell since no electron transfer reactions occur across the electrode-solution interface. When the potential of the cathode reaches E_A, current begins to flow. As the potential of the cathode is adjusted from E_A to E_B, the current increases with the changing potential much like that observed in a polarographic cell. The current in this region is potential dependent. Between potentials E_B and E_C, the current is independent of the cathode potential and the electrode is said to be polarized. All of the molecules or ions of the electrophore that arrive at the electrode and can undergo this reduction are reduced as soon as they reach the electrode. The current associated with this plateau is the limiting current, i_d. Continued cathodic shifts past E_C result in the reduction of the second electrophore.

Constant current electrolysis is also demonstrated in Figure 8. If a current is selected such that the control current, i_o, is less than the limiting current, i^{I}_{d}, for the first reduction, the electrophore corresponding to the first curve--in this example the metal ion --is reduced. This is the idealized system envisioned to be occurring

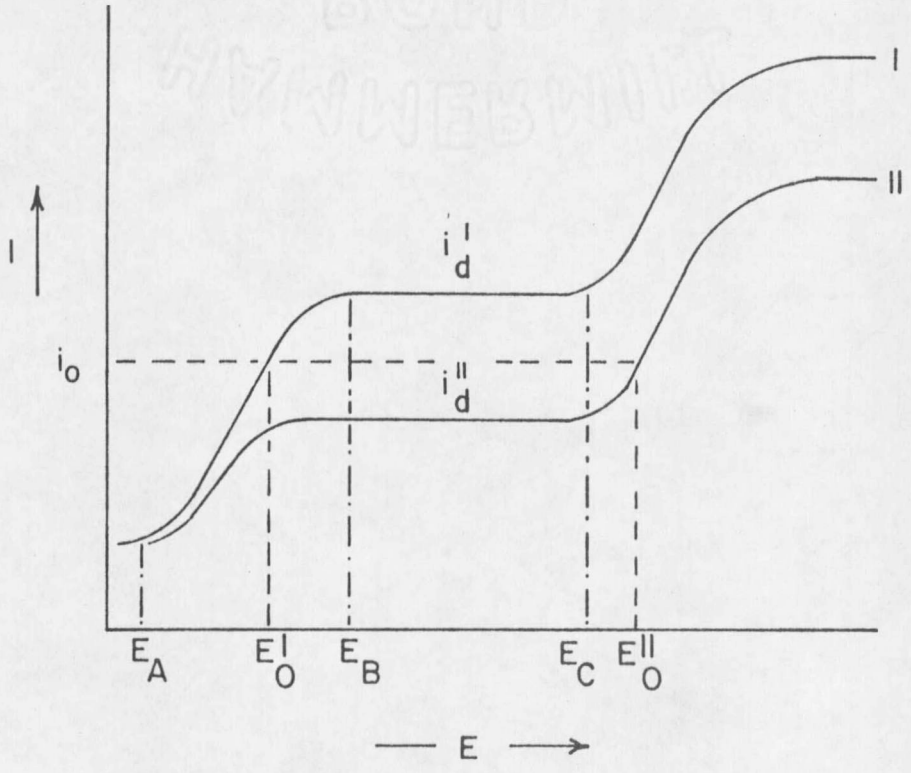

Figure 8. Macroscopic Cell with Two Solution Electrophores (101).

within the electrolysis cell. The cathode potential for this current level is E_o^I. As the electrolysis continues, the concentration of the metal ion decreases resulting in a decrease in magnitude of the limiting current for the metal ion, i_d^{II}. However, i_d^{II} is less than the preselected current, i_o, therefore the cathodic potential must shift to E_o^{II} in order to compensate for the current difference between i_d^{II} and i_o. This shift in the cathodic potential with the concommitant increase in the current in order to maintain the current level, i_o, means that another solution electrophore is being reduced. In the system under investigation, this reflects the direct reduction of the organic substrate. The strategy of selective reduction of the metal ion is forfeited.

Figure 8 depicts an ideal system in which the cathode potential E_C, is being followed. Without a reference electrode in the system, the cathodic potential is not known. The potential that is observed to change in a two electrode cell is the applied potential. This change in the applied potential is not necessarily a simple function of the current as indicated for the cathodic process in Figure 8. The applied potential is a function of several components given by the equation (106)

$$E_{APP} = E_C - E_A - iR - E_{overpotential}$$

where E_{APP} is the applied potential, E_C is the cathode potential, E_A the anode potential, iR the potential drop due to the resistance of the

solution to current passage, and $E_{overpotential}$ is the voltage in excess of the theoretical value for the cell calculated from the Nernst equation that is required to get the electrolytic reaction to occur at an appreciable rate. Both the overpotential and the solution resistance can change during the electrolysis, the changes not being fundamentally related to the cathodic potential or the overall current. For instance, the conductivity of the solution might increase if the anode reaction is a discharge (oxidation) of a metal. This could cause the applied potential to be reduced in a constant current cell since the resistance of the solution is reduced. Likewise, the overpotential may be less as the surface of the cathode undergoes modification such as occurs in plating a solution ion onto an inert electrode. This would result in a decrease in the applied potential even though the current is held constant.

The problems of the two-electrode cell run at constant current are not completely removed when the system is operated using two electrodes at constant applied potential. V. T. Brice initiated the study using constant applied potential (105). Under this method of operation, the potential applied across the two electrodes is held at some constant value. The current-time behavior for this type of cell using an aqueous solution and the simple reduction

$$Ox + ne^- \rightarrow Red$$

is shown in Figure 9. The current for such a simple reduction is expected to decay in an exponential manner. This current decay is described by a logrithmic function in terms of current or concentration of the electrophore (68).

$$\log i_t = -\beta t + \log i_{lim}$$

or

$$\log C^{*,t} = -\beta t + \log C^*$$

where i_t is the current at time t and i_{lim} is the limiting current for the initial concentration of the electrophore, C*. The bulk solution concentration at time t is given by $C^{*,t}$. Beta is referred to as the electrochemical rate constant. Beta is a function of several parameters

$$\beta = \frac{0.43\ DA}{V\delta}$$

where D is the diffusion constant for the electrophore, A is the surface area of the electrode, V is the volume of the electrolysis solution, and δ is the Nernst diffusion layer thickness. Controlling the magnitude of these terms can generate a faster electrolysis. Figure 9 shows two curves for the same concentration of an electrophore in two different cells. Curve A represents a cell of high β and consequently short electrolysis times. Curve B represents a curve of much smaller

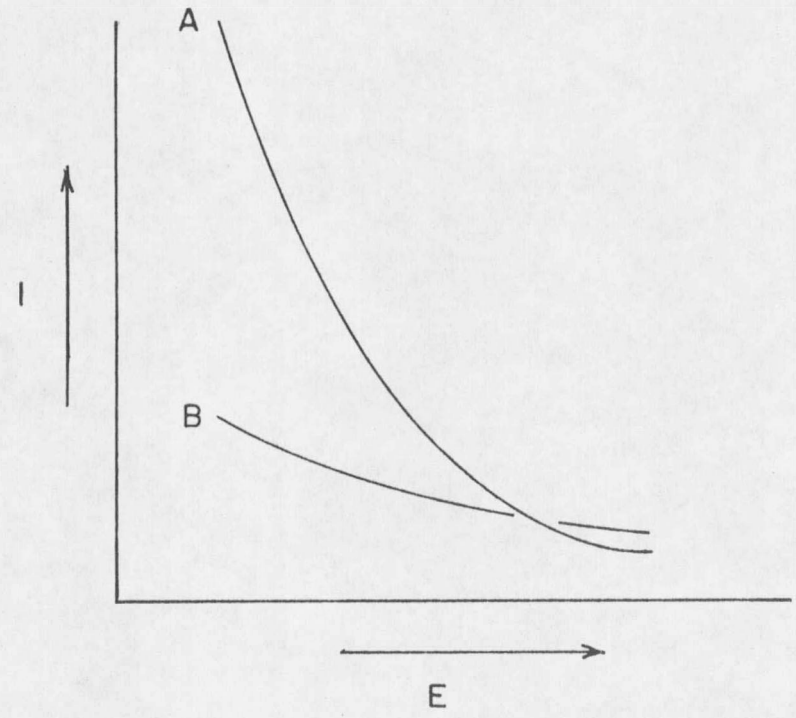

Figure 9. Current-Time Curves for Two Systems with Different Electrochemical Rate Constants (68).

β and hence longer electrolysis times. The general characteristics for both curves is a smooth decay of the current with time.

For the ideal case in a constant applied potential electrolysis cell, the current falls smoothly with time. Such ideality is not always available. Recall that the total applied potential of the electrolysis cell not only includes the potential difference of the cathode and the anode, but also the internal resistance and overpotential of the cell. The internal resistance of an aqueous solution with a high concentration of a base electrolyte is normally not very large. Thus $E_{cathode} - E_{anode}$, the thermodynamic cell potential, is not very different from $E_{Applied}$ if the overpotential for the particular reaction is small. However, for nonaqueous solutions, the high internal resistance of the solvent influences the magnitude of the applied potential. Hence the thermodynamic potential and the applied potential are not so readily related. Should the internal resistance change during the electrolysis, E_{anode} and $E_{cathode}$ must also change in order to maintain a constant applied potential. If the nature of the cathode changes during reduction as it can if plating occurs, the overpotential of the new surface may be less than the overpotential of the original surface. If the cathodic potential for this new surface does not change, that is the applied constant potential holds this new surface at the same potential as the old surface, the permissible current density at the new surface can vary widely (107) or an entirely new

electrolysis reaction can occur. This effect of the electrode material on the overpotential for hydrogen gas evolution is demonstrated in Table V. As the exchange current density decreases, a greater applied potential is required to reduce the proton to H_2 at an appreciable rate.

Table V. Approximate Exchange Current Densities for the Hydrogen Reaction on Metals at 25°C (108)

Metal	Exchange Current Density (A/cm^2)	Metal	Exchange Current Density (A/cm^2)
Pb,Hg	10^{-13}	Fe,Au,Mo	10^{-6}
Zn	10^{-11}	W,Co,Ta	10^{-5}
Sn,Al,Be	10^{-10}	Pb,Rh	10^{-4}
Ni,Ag,Cu,Cd	10^{-7}	Pt	10^{-2}

The two-electrode cell run under constant applied potential does provide some information concerning the reaction being investigated. The system used as a probe into the nature of the electrochemical reaction incorporated iron (III) acetylacetonate, $Fe(acac)_3$, as the inorganic transition metal salt and 1-octyl bromide as the organic substrate. The results in Table IV indicated that the organic products for this reaction were hexadecane, (R_2), n-octane (RH), and 1-octene, [R(-H)]. Triphenylphosphine, Ph_3P, was used in the cell for two purposes. Kochi (41) noted a greater amount of dimerization occurs for those favorable systems in the Kharasch reaction when Ph_3P

was present than when it was absent. Secondly, the weak π-back bonding ability of the Ph_3P can help stabilize and solubilize the reduced forms of the iron by removing some of the electron density from the reduced iron.

Table VI presents additional results obtained with this two-electrode cell for the reduction of $Fe(acac)_3$ in the presence of 1-octyl bromide. Several points should be noted. First, the yields of hexadecane, octane, and 1-octene are based on the amount of unrecovered starting material. The per cent reaction represents how much of the starting material was consumed. Summing the yields of recovered products demonstrates that not all of the unrecovered material is accounted for. Secondly, the suggested general reaction does appear to occur with 1-octyl bromide generating dimer, alkane, and olefin. Finally, the reactions listed in Table VI were prepared so that all the systems were identical. However, the yields of products are rather widespread. In one instance, no products were obtained yet in another identical reaction as much as 33% coupling occurred. Obviously, the reproducibility of the system is questionable.

Current-time traces for three representative experiments obtained from the two-electrode constant applied potential cell are given in Figure 10. Although these cells are assembled so that the solution concentrations are duplicated, the current-time behavior suggests that the reactions occurring in the solutions are not identical. The

Table VI. Product Yields for the Two-Electrode Constant Applied Potential Electrolysis Cell with Octyl Bromide and $Fe(acac)_3$ using Aluminum Electrodes.

Reaction No.	NI025	NI085	NI114	NI118	NI127
% $C_{16}H_{34}$	0	27.6	20.7	23.9	25.4
% C_8H_{18}	0	} 9.6	17.2	10.1	7.7
% C_8H_{16}	0		6.2	4.1	4.3
% Reaction	None	100%	100%	100%	100%
I_{max} (mA)	15	42	42	37	22
Δt (hours)	76½	92½	88½	91	114

Reaction No.	NI147	NI170	NI190	NI193	NII033
% $C_{16}H_{34}$	32.4	31.9	33.8	2.5	9.5
% C_8H_{18}	11.1	28.5	30.8	12.0	6.3
% C_8H_{16}	3.2	7.0	9.1	1.9	2.6
% Reaction	72.3	59.9	64.5	34.2	64.2
I_{max} (mA)	37	32	36	16	36
Δt (hours)	65	73	73	124	119½

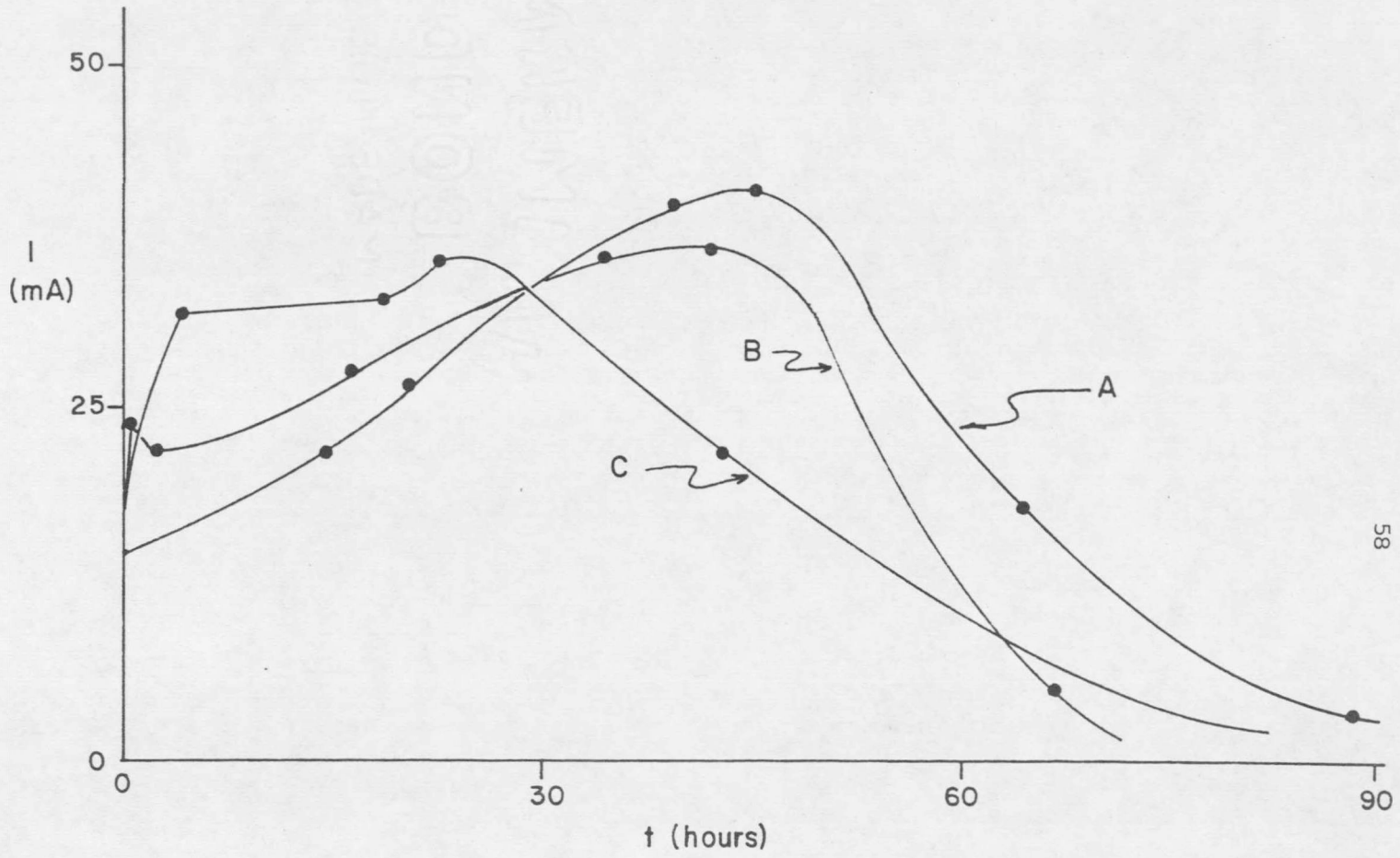

Figure 10. Current-Time Behavior for Three Representative Two-Electrode Constant E_{APP} Electrolysis Cells with Aluminum Electrodes. (A) Reaction NI114; (B) Reaction NI118; (C) Reaction NII033. E_{APP} = 1.5V for each reaction.

current-time behavior is not typical. The rise in current is unexpected for a simple reduction of a metal ion electrophore in an constant applied potential electrolysis cell.

Several possible systems could account for this current-time behavior. Two trivial situations are associated with the method of electrolysis. The aluminum electrode is covered with an oxide layer before immersion into the electrolysis cell. This is an insulating layer which may be removed during the electrolysis. Alternatively, the aluminum electrodes are rendered passive when placed into the electrolysis cell. Such passivation of the aluminum is known to occur with amines (109). Activation of the electrode is demonstrated by a current rise. The increase in current during the initial electrolysis could also indicate a change in either the internal resistance of the solvent or a change in the reaction overpotential or both. The anticipated change would be a reduction in the resistance and/or overpotential so that the potential drop between the cathode and the anode increases. This is analogous to making the cathode potential more negative (cathodic). Such a drift in the cathode potential could increase the current in two ways. First, if the initial cathode potential is near the foot of the reduction wave corresponding to point E_A in Figure 8, the negative drift in the cathode potential would cause the current to increase. Alternatively, this potential drift is sufficiently cathodic to initiate the reduction of a second solution

electrophore. Finally, if iron is plating onto the aluminum electrode and the overpotential for reducing iron ions at an iron surface is lower than the overpotential for reducing iron ions at an aluminum electrode, the current would again increase. Alternatively, the direct electrochemical reduction of the 1-octyl bromide may proceed at this newly plated iron surface although it would not have occurred at the aluminum electrode. This latter situation conflicts with the reaction strategy. As noted in the introduction, such direct reductions of the organic halides are not known to lead to coupled products, therefore this latter situation is not expected to be occurring in the reactions of Table VI.

A reference electrode was used to monitor the cathode potential in the two-electrode constant applied potential electrolysis cell. Figure 11 shows that the cathode potential does shift during the electrolysis.

Ideally, the increase in current may be indicative of a chemical reaction occurring after the initial electron transfer step. The original view postulated by Pillsbury (66) with some slight modifications associated with this research is contained in Figure 12. This postulated reaction scheme generates a reducible form of iron, $Fe^{II}X_2L_{n-2}$ during the cycle going from reduced to oxidized iron which is mediated by the 1-octyl bromide. The original iron salt, $Fe(acac)_3$, has a bidentate ligand attached to the metal center. Iron (III) may be easily

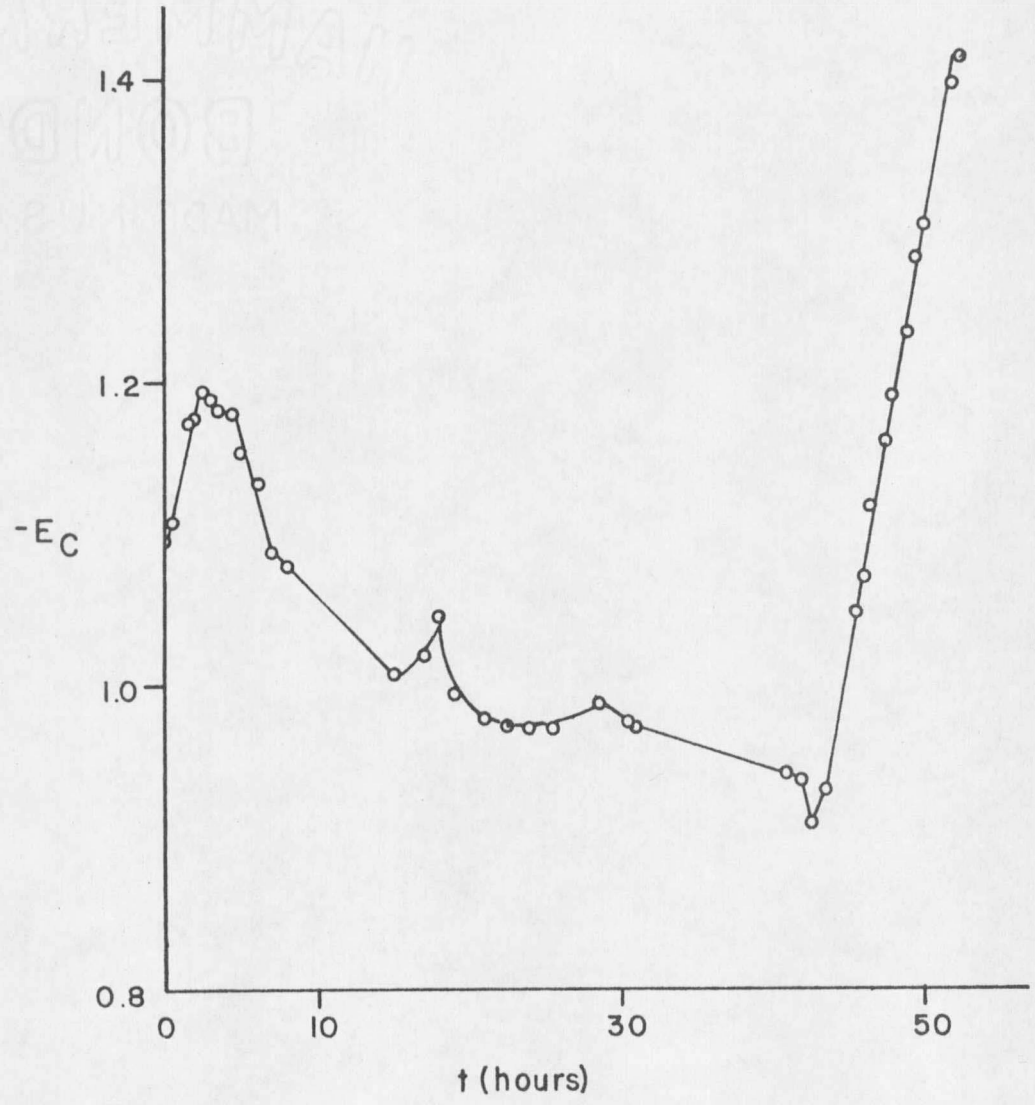

Figure 11. Cathode Potential versus Time for a Two-Electrode Constant E_{APP} Electrolysis. Potential Monitored with Cd(Hg) Reference. E_{APP} = 1.5V.

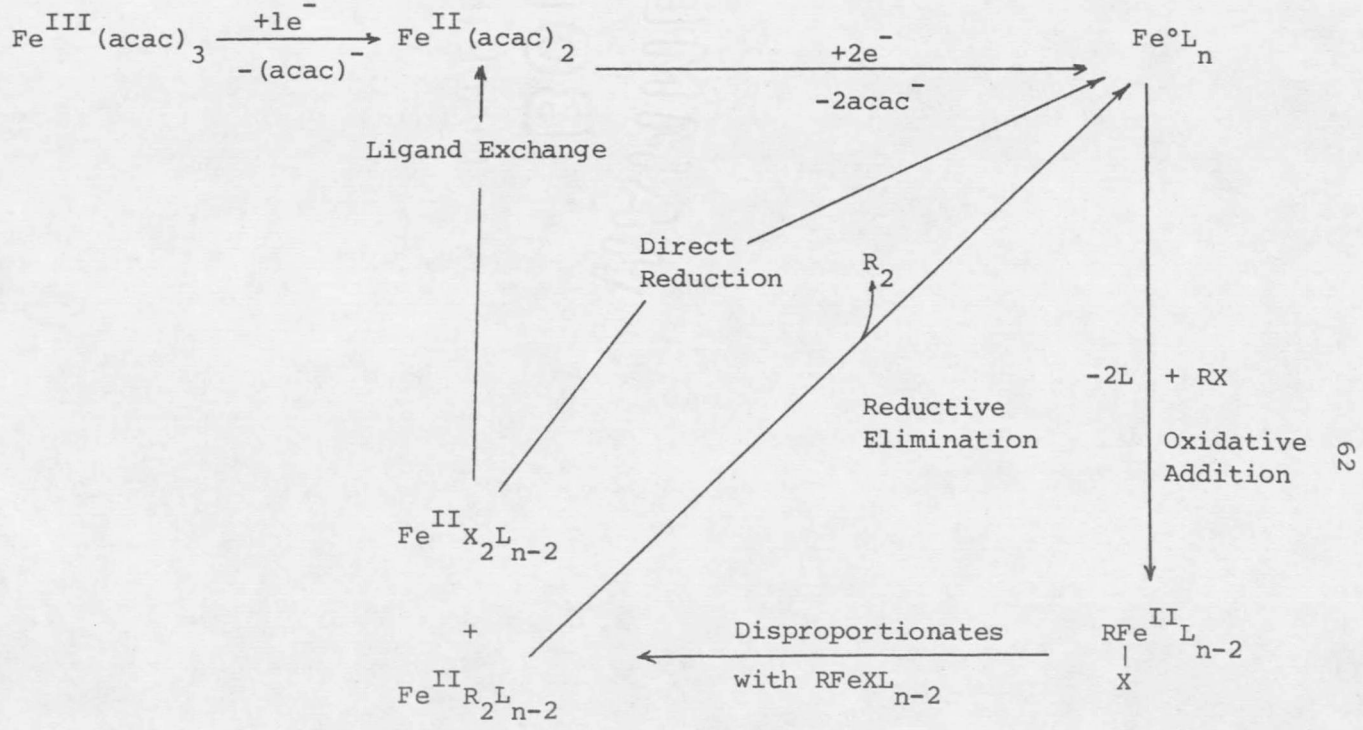

L = solvent or Ph_3P; n = 4 or 6

Figure 12. Idealized Cyclic Reaction with Iron Mediator and Alkyl Halide.

reduced to $Fe(acac)_2$, but the subsequent reduction of iron (II) to iron (0) may occur at more negative potentials for the bidentate ligand, $acac^{1-}$, than for the monodentate ligand, Br^-, i.e., $E^{FeBr_2}_{1/2} > E^{Fe(acac)_2}_{1/2}$. During the chemical transformation mediated by 1-octyl bromide, a new electrophore, $Fe^{II}X_2L_{n-2}$, is generated which may subsequently be reduced; the current would increase as this new electrophore is formed. The complete sequence of events can be summarized as an initial electron transfer followed by a chemical reaction which generates a new reducible electrophore that is subsequently electrochemically reduced. This process is typed an ECE mechanism

Oxidized (1)	$\overset{+ne^-}{\rightarrow}$	Reduced (1)	E
Reduced (1) + X	$\rightarrow$	Oxidized (2)	C
Oxidized (2)	$\overset{+me^-}{\rightarrow}$	Reduced (2)	E

If the electrophore generated in the chemical step is the same as in the original solution, Oxidized (2) $\equiv$ Oxidized (1), then the processes is termed electrocatalytic. Such a system occurs in the napthyl radical anion reduction of an alkyl chloride that is itself electrochemically inactive (68). Such a catalytic

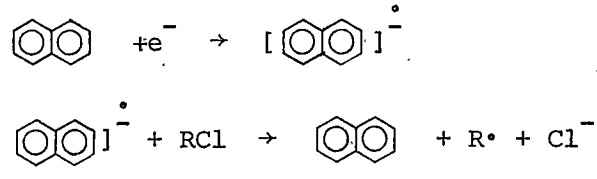

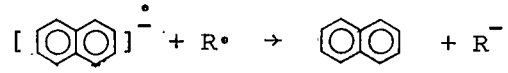

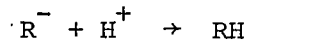

cycle fits the framework of the proposed reaction.

The two-electrode constant applied potential electrolysis cell cannot distinguish between the possible systems suggested above because the potential of the cathode drifts in the solution. Such drifting may subvert the reaction strategy of selective cyclic reduction proposed in Figure 12. The reaction is indicated to be promising since coupled products were formed. This represents an improvement over the Karasch reaction which also used reduced iron. In this reaction, the generation of coupled products would not occur if the organic substrate had beta-hydrogens available.

Three-Electrode Electrolysis

The problems associated with the two-electrode cell can be dealt with using another cell design. Specifically, a three-electrode cell is designed to eliminate the effects of the iR drop between the anode and the cathode. Depending on the nature of the investigated electrochemical reaction (oxidation or reduction), the appropriate electrode is termed the working electrode and the other electrode is the counter electrode. For all of the work dealt with in this thesis, the working electrode is the cathode. The potential of the working electrode is

maintained constant via the incorporation of a third electrode, the reference electrode. A simplified diagram follows.

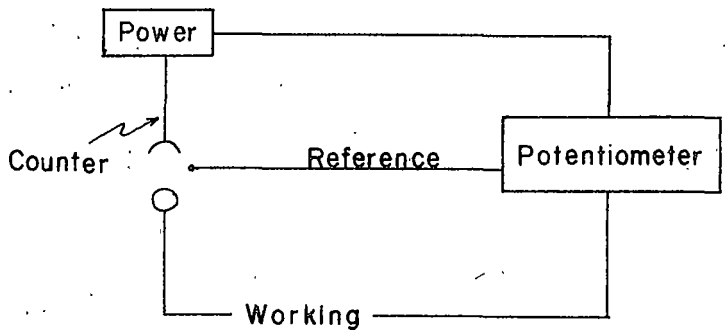

Several authoritative texts describe the assembly and operation of the potentiostat (68,95,96,98,102). Only a few highlights of its operation are included here. The three-electrode cell is designed to vary the applied potential while controlling the working electrode potential. The latter is accomplished by comparing the potential drop between the working and the reference electrode to some preselected value stored in the potentiometer. When this comparison is valued rather than null, appropriate signals are sent to the power pak to either increase or decrease the applied potential. The critical component of this system is the reference electrode. The reference electrode is the point of zero potential on which the potential of the working electrode is based. If the potential of the reference electrode varies, the system analyzes this change as a drift in the working

electrode potential. The net effect is no better than the problem faced with a two-electrode cell. The potential drop between the working and the reference electrode is known, but the potential of the working electrode with respect to the solution is unknown.

The reference electrode has specific design requirements. The electrode must be completely insensitive to changes in the solution composition during the electrolysis. It must have stable junction potentials between the reference cell and the electrolysis solution. The potential of the internal half-cell must be invariant with time, stable to small passages of current, and reversible. The internal half-cell must be reproducibly prepared. The whole system should be easy to assemble. Since passage of current involves the transport of matter to the electrode and chemical transformations at the electrode/solution interface, the ideal behavior of a reference electrode can only be approached. Critical surveys of the literature dealing with reference electrodes have been prepared by several groups (69,96,110-113). These sources should be consulted for further detail.

Reference electrodes for nonaqueous solutions are not readily available. This paucity of equipment reflects the severe restrictions placed on the reference electrode. Much work has been performed using the common saturated calomel electrode (SCE) for nonaqueous electrochemistry. Generally, this reference electrode is isolated in a reference compartment that is physically separated from the nonaqueous

solvent. The reference compartment makes electrical contact with the cell via an appropriate salt bridge made of agar or methyl cellulose saturated with a base electrolyte. The whole assembly looks like a capital H, hence the name H-cell for this configuration. The ends of the salt bridge are usually sealed with fine or medium porosity glass frits. For a standard stirred mercury pool electrolysis cell, this arrangement has resulted in a nonuniform potential over the surface of the electrode, the closest portion of the working electrode to the reference electrode corresponding to the preselected potential that is monitored by the reference electrode (101). This H-cell configuration has been elegantly redesigned to eliminate some of these difficulties (98).

The entire concept of a bridge can be attacked on fundamental grounds. Each junction of the bridge introduces large and unknown junction potentials as it makes contact with an aqueous solution on one side of the bridge and a nonaqueous solution on the other side (111). Furthermore, there is no way at present to relate thermodynamic potentials in different solvents to the same aqueous reference electrode (96) albeit extrathermodynamic methods have been used (96,114). The continued use of such bridges is simply a matter of convenience.

An attempt to prepare appropriate salt bridges for the aqueous SCE in a standard H-cell electrolysis vessel failed. An agar bridge (70% DMF, 30% H_2O) mixture containing either tetraethylammoumium

bromide, TEAB, or tetraethylammonium perchlorate, TEAP, was used to separate the two halves of the cell. This bridge was initially assembled to separate the two electrolysis compartments for a two-electrode electrolysis reaction. These reactions generally proceeded for 60 to 90 hours during which time the agar plug was noted to deteriorate, a visual indication of changing junction potentials. Therefore, this bridge was considered inappropriate for isolating the SCE reference electrode.

Another reported salt bridge that was suggested to be of measurable improvement over the agar plug used methyl cellulose as the gelling agent (115). This plug was assembled similarly to that of the agar plug, but it too decomposed while standing in N,N'-dimethylformamide, DMF, for 70 hours. This apparent dissolution of the bridging material suggests, of course, changing and erratic junction potentials, intolerable in any controlled potential electrolysis.

Attempts were made to isolate the SCE in a DMF solution of TEAP. This solution would be separated from the primary electrolysis cell with a DMF/TEAP bridge--a solution bridge rather than a solid bridge. The quaternary ammonium perchlorate salt was used instead of the bromide because the perchlorate salt is more soluble in DMF than is the bromide salt. The design was not satisfactory. The yellow iron acetylacetonate was observed to migrate rapidly through the liquid salt bridge. The aqueous solution leaking from the SCE could be

diffusing as rapidly through the bridge into the electrolysis cell thus contaminating the nonaqueous solvent. Secondly, the SCE had a fiber junction to establish electrical contact between the internal aqueous solution of the reference electrode and the external nonaqueous solution. This junction is for electrical contact and, operating under conditions of continuous impeded flow, allows the internal filling solution to slowly pass across the fiber into the monitored solution. A constant leakage is necessary to establish stable junction potentials between the reference solution of the reference electrode and the monitored solution. Since potassium chloride, KCl, and water leak across the fiber junction of an SCE, these components would be expected to be discharged into the DMF. Unfortunately, the TEAP in the DMF solution allowed potassium perchlorate to form at the junction. This potassium salt is insoluble and clogs the junction. Since a constant and substantial flow rate is probably the most critical factor for obtaining reproducible junction potentials (96), this precipitate changes the junction and increases the resistance of the fiber making the reference electrode unsatisfactory.

A final attempt to make use of the SCE involved changing the aqueous internal filling solution to a tetraethylammonium chloride saturated DMF solution. Sodium chloride, the salt of first choice for the intended filling solution, was not appreciably soluble in the DMF, therefore the use of the quaternary ammonium chloride salt. Just prior

to filling the reference electrode with the DMF solution, a report was read that mercurous chloride, Hg_2Cl_2, disproportionates in DMF (113). This mercury salt establishes part of the internal half cell reaction. The SCE was abandoned.

Another commonly used reference electrode system in DMF is the silver/silver ion electrode, Ag/Ag^+, either as an electrode of the first kind in which the silver metal is in equilibrium with its own ion (116), Ag^+, or as an electrode of the second kind in which the silver metal is in equilibrium with a sparingly soluble silver salt like silver chloride (117), AgCl. The latter reference electrode requires an internal filling solution which maintains a high, constant concentration of chloride, Cl^-. Unfortunately, Cl^- complexes with AgCl in most organic solvents to form the readily soluble $(AgCl_2)^{1-}$ complex (96) which makes this reference suspect since this new component may establish [1] a new half-cell reaction occurring at some different potential and [2] changes the activity of the silver ion thus affecting the Nernst equation. Although the Ag/Ag^+ electrode of the first kind continues to be used, it has been demonstrated to be unstable in DMF as the reduction of Ag^+ to silver metal is noted to occur (69,113).

Glassy carbon has been used as a cathode for reductions in aqueous solutions (118). During the examination, the authors noted there were no drifts in the potential of the glassy carbon indicating

the electrode was capable of carrying current with minimal electrical disruption of the solid. The possibility of using this electrode as a reference was experimentally evaluated. Potential drifts in the polarographic half wave potential of a 10^{-3} M Ni(II) aqueous solution fortified with 1.0 M KCl were monitored. The initial drift was anodic during the first 24 hours. Another more dilute solution was prepared, 10^{-4} M in Ni(II), while maintaining the same base electrolyte (KCl) concentration. In this instance the half-wave potential drifted cathodically. Table VII reports the results.

Table VII. Glassy Carbon Reference, $E_{1/2}$ of Ni(II) in 1.0 M KCl

Concentration	10^{-3} M	10^{-4} M	10^{-4} M
Initial $E_{1/2}$	-1.118V	-0.959	-0.954
Final $E_{1/2}$	-0.966V	-0.991	-1.014
Time (hours)	24	72	48

Although the flow of current does not appear to affect the characteristics of the glassy carbon when it functions as a cathode, its performance as a reference electrode was considered marginal. The problem may reflect the difficulty in establishing an equilibrium junction potential across the surface of the glassy carbon and the solution. The glassy carbon reference electrode does not flow, therefore the junction is influenced by changes in the solution. Particularly during

large scale electrolysis of a concentrated solution, the characteristics of the solution are drastically changing, placing the equilibrium junction in jeopardy. A flowing reference electrode is more appropriate.

Two reference electrodes for use in DMF have been suggested, the sodium amalgam, Na(Hg), and the cadmium amalgam, Cd(Hg) (113,119). The sodium amalgam is susceptible to air oxidation thus requiring special handling. This problem restricts its utility. The cadmium amalgam is particularly attractive for, unlike the Na(Hg), this amalgam is not sensitive to air oxidation. Secondly, unlike the Na(Hg), traces of water are not detrimental but actually assist in reducing the overpotential for a given current compared to a completely anhydrous assembly (113).

The Cd(Hg) reference electrode was first prepared by Marple (120) and then later improved upon by Manning and Purdy (121). The cadmium amalgam was prepared by heating stock cadmium with triply distilled mercury, cooling to room temperature, and finally adding sufficient mercury to form a slurry (120). Manning and Purdy (121) improved the amalgam by adding sodium chloride, NaCl, and anhydrous cadmium chloride, $CdCl_2$, to this slurry. The modification of the amalgam provided intimate contact between a constant activity of Cl^-, of Cd(II), and the amalgam. This assisted in stabilizing the internal half-cell. Secondly, this preparation of the slurry assists in eliminating

problems of mercury coalescence which forms a pool in the bottom of the reference assembly. This pool of mercury essentially stops the flow of internal filling solution into the electrolysis cell and hence changes the junction potential. The internal filling solution is a saturated $CdCl_2$ and NaCl solution of DMF. The reference is reported to have been stable for over a 6-month period. This stability was evaluated by monitoring the reduction of vanadium in vanadyl sulfate using a polarographic cell (121,122).

$$E_{1/2} = -1.31V \pm 0.014V$$

Furthermore, the reported potential of the cadmium amalgam versus the SCE was (121)

$$E_{Cd(Hg)}\ V \text{ vs SCE: } -0.7340 \pm 0.0007$$

The stability of the Cd(Hg) has been examined by others (117, 123). The junction potential for the $CdCl_2$/Cd(Hg) half-cell is very small because of the limited formation of complex ions such as $CdCl_3^{1-}$ and $CdCl^{1+}$ making the $CdCl_2$ stable to polarization. For molarities of $CdCl_2$ greater than 0.06 M, the potential of the amalgam is unchanged. These data as well as that of Manning and Purdy (121,122) suggest that this reference electrode is particularly advantageous for use in DMF.

Our initial efforts to prepare the amalgam failed. The literature preparation, albeit non-reproducible in this laboratory, is also unsafe since mercury must be heated to generate the amalgam. The probable cause for our unsuccessful attempts may be associated with oxide formation on the cadmium metal that could insultate it to dissolution into the hot mercury. After many attempts this method of preparation was abandoned.

The cathodic reduction of Cd(II) from an aqueous solution of cadmium sulfate at a mercury cup cathode produced a crystalline amalgam (124). Although the ratio of mercury to cadmium was not determined, solid cadmium amalgams at room temperature range from 15% to 55% cadmium in mercury (125) and are reported to be crystalline (126). The noted decrease in overpotential when hydrated cadmium chloride is used, added an additional perturbation to Manning and Purdy's modification. Finally, the reference electrode assembly was modified to eliminate the porous Vycor plug (thirsty glass) of the original electrode. The plug was replaced by a cracked glass junction. Results in Table VIII compare the original literature preparation and the electrolysis preparation.

The generation of a stable reference electrode completed the electrode assembly of the three-electrode cell. A potentiostat was required to drive the system. A modified Heathkit power pak failed to give satisfactory control. The response time of the power pak was

Table VIII. Comparison of Reference Electrodes[a] (124)

Reference Electrode	$E_{1/2}$ for vanadium
1. Dissolved Cd(Hg) with porous Vycor junction (121,122)	-1.31 ± 0.014V
2. Electrolyzed Cd(Hg) with porous Vycor junction	-1.32 ± 0.016V[b] (6)
3. Electrolyzed Cd(Hg) with cracked glass junction	-1.30 ± 0.019V[c] (6)
4. Same as 3 above after 4 months of continual use	-1.31 ± 0.006V[d] (3)

(a) Parenthetical values after the half-wave potentials are the number of polarographic scans used to calculate the average $E_{1/2}$ and standard deviation for that wave.

(b) 0.0343 g $VOSO_4 \cdot x H_2O$ in 100.0 ml of 0.1002 M DMF solution of TEAP.

(c) 0.0526 g $VOSO_4 \cdot x H_2O$ in 100.0 ml of 0.1003 M DMF solution of TEAP.

(d) 0.0409 g $VOSO_4 \cdot x H_2O$ in 100.0 ml of 0.0974 M DMF solution of TEAP.

slower than the response time of the operational amplifier control loop used to maintain a constant working electrode potential. This resulted in oscillating behavior. Secondly, the potentiostat was not capable of passing through zero potential. Without this capability, current versus working electrode potential curves for the macroscopic cells could not be generated. A solid-state in-house manufactured poteniostat, designed and built by Dr. R. Geer, Montana State University, has been used for the majority of the three-electrode work. The system is stable and can scan potentials from the anodic side of zero through zero to cathodic potentials. An added feature built into the system is overriding current control diagrammatically shown in Figure 13. The working electrode potential is maintained at the preselected potential until some limiting current level, i_ℓ, is attained. The system then goes into current limiting control with the working electrode remaining constant or changing to anodic values of the preselected potential. When the current falls below this limiting value, i_ℓ, the system again shifts to constant working electrode control. The important point here is that although the working electrode's potential may drift, it never becomes more cathodic but rather drifts anodically. One final note. Although the effect of the internal resistance of the solvent between the counter electrode and the working electrode has been eliminated, a small but finite uncompensated iR drops still persists between the working electrode and the reference electrode (127). Although this iR

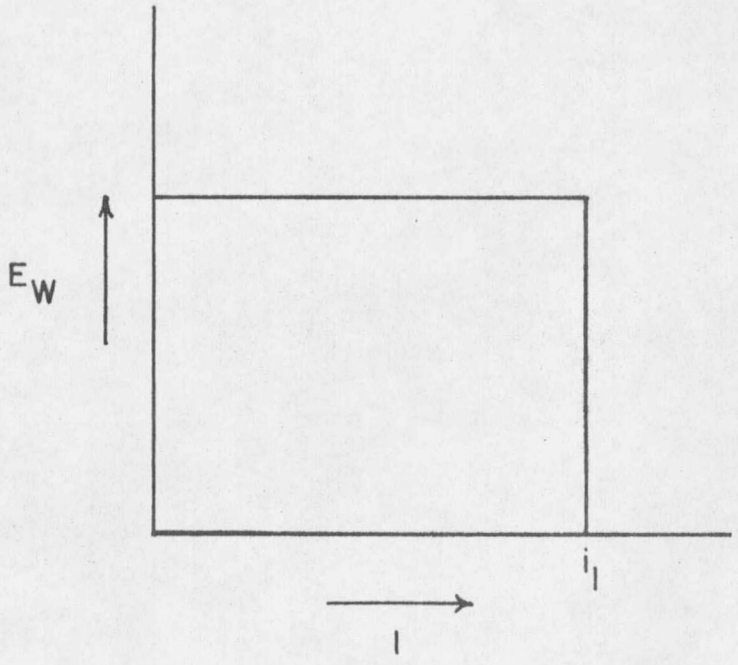

Figure 13. Idealized Working Electrode Potential versus Total Cell Current for Solid State Potentiostat with Current Limiting Override.

drop is not eliminated, its effect can be maintained constant if the geometrical arrangement of the working electrode and the reference electrode is maintained constant.

Potentiometry

Both iron (III) acetylacetonate and 1-octyl bromide solutions in DMF were examined in a polarographic cell using a dropping mercury electrode, DME, in order to establish the integrity of the selective reduction concept. Table IX lists the results of this analysis. Within repetitive runs the reproducibility is superb. However, repeating the polarographic scan at other times appeared to indicate the potential was drifting, i.e., the reference was unstable. This was later ascribed to the ±300V power supply in the Heathkit EUW-19B operational amplifier system. Any excessive voltage drift in this power supply results in a drifting initial potential (128). This instability of the power source and hence the unreliability of the initial potential is reflected in the apparant changes of the reduction potentials. This table clearly demonstrates the integrity of the reduction, i.e., the metal can be reduced independently of the organic substrate in a polarographic cell using a dropping mercury electrode as the working electrode, a platinum counter electrode, and a Cd(Hg) reference electrode.

Table IX. Half-wave Potentials for $Fe(acac)_3$ and $n\text{-}C_8H_{17}Br$.

Substrate (Concn, M)	Base Electrolyte (Concn, M)	$E_{1/2}$ V(vs Cd(Hg))[a]
$Fe(acac)_3$ (10^{-3} M)	TEAP (0.1 M)	+0.086 ± 0.003 (7)
$Fe(acac)_3$ (10^{-3} M)	TEAP (0.1 M)	+0.132 ± 0.009 (6)
$Fe(acac)_3$ (10^{-3} M)	TEAB (0.1 M)	+0.185 ± 0.000 (6)
$Fe(acac)_3$ (10^{-3} M)	TEAB (0.1 M)	+0.192 ± 0.012 (4)
$1\text{-}C_8H_{17}Br$ (3.6×10^{-3} M)	TEAP (0.1 M)	-1.409 ± 0.026 (6)[b]
		-1.588 ± 0.021 (6)

(a) Numbers in parenthesis after the half wave potentials are the number of polarographic scans used to calculate the average $E_{1/2}$ and standard deviation for that wave

(b) Potentials at the foot of a polarographic wave with a large maxima

The overpotential for hydrogen evolution has been noted to vary with different electrodes. This is common for most electrochemical reactions. The polarographic work assures adequate separation of reduction potentials if a stirred mercury pool was used, but the data becomes less convincing if a different cathode material is substituted. Secondly, the polarographic examination uses concentrations of the order of 10^{-3} M for the electrophore while the intended electrolysis cell operates with about 0.2 M $Fe(acac)_3$. This scale up for a mercury pool would cause the $E^1_{1/2}$ at the mercury pool to shift cathodically (100) as described by the equation

$$(E^1_{1/2})_{Hg\ pool} = E^0_{1/2} + \frac{RT}{\alpha nF} \ln \frac{k_e \delta}{D}$$

where α is the transfer coefficient, δ the Nernst diffusion layer thickness, and $E^0_{1/2}$ is the standard potential at which the heterogeneous rate constant k_e for the irreversible wave is defined. Since both k_e and δ are small, their product is smaller than the diffusion coefficient D and the stirred pool half wave is more cathodic. This simple relationship fails when the electrode material is switched since the heterogeneous rate constant changes. The three-electrode system requires that current-working electrode potential curves be generated to again insure the separability of the reductions.

The components of the three-electrode electrolysis cell were again examined using two aluminum electrodes and the cadmium amalgam

reference electrode. Figure 14 shows the reduction of $Fe(acac)_3$ and 1-octyl bromide at an aluminum working electrode. The breaking potential, defined as the potential where the observed current abruptly leaves the base line, is well separated for the two components. The reduction of 1-octyl bromide is seen to begin at -1.8V which is near the solvent limit. This observation establishes that the two-electrode cells run at constant applied potentials of 1.5V or less were not in danger of directly reducing the 1-octyl bromide at the aluminum cathode since the Heathkit power pack cannot pass through zero volts. If the iR drop of the solution were zero volts, the most cathodic the system could drift is -1.5V. The anode would be at zero volts and the cathode at -1.5V.

Current-Time Behavior

A current-time trace for a typical 3-electrode electrolysis cell is shown in Figure 15. An aluminum working electrode with an aluminum counter electrode was used to generate this current-time plot. This current-time behavior is unique and indicates a level of complexity not appreciated from the current-time behavior of the 2-electrode constant applied potential configuration. In the 3-electrode cell, the potential of the working electrode is fixed so that this intriguing plot is not, on first considerations, associated with a drifting working electrode potential. This was a suggested source for the current time

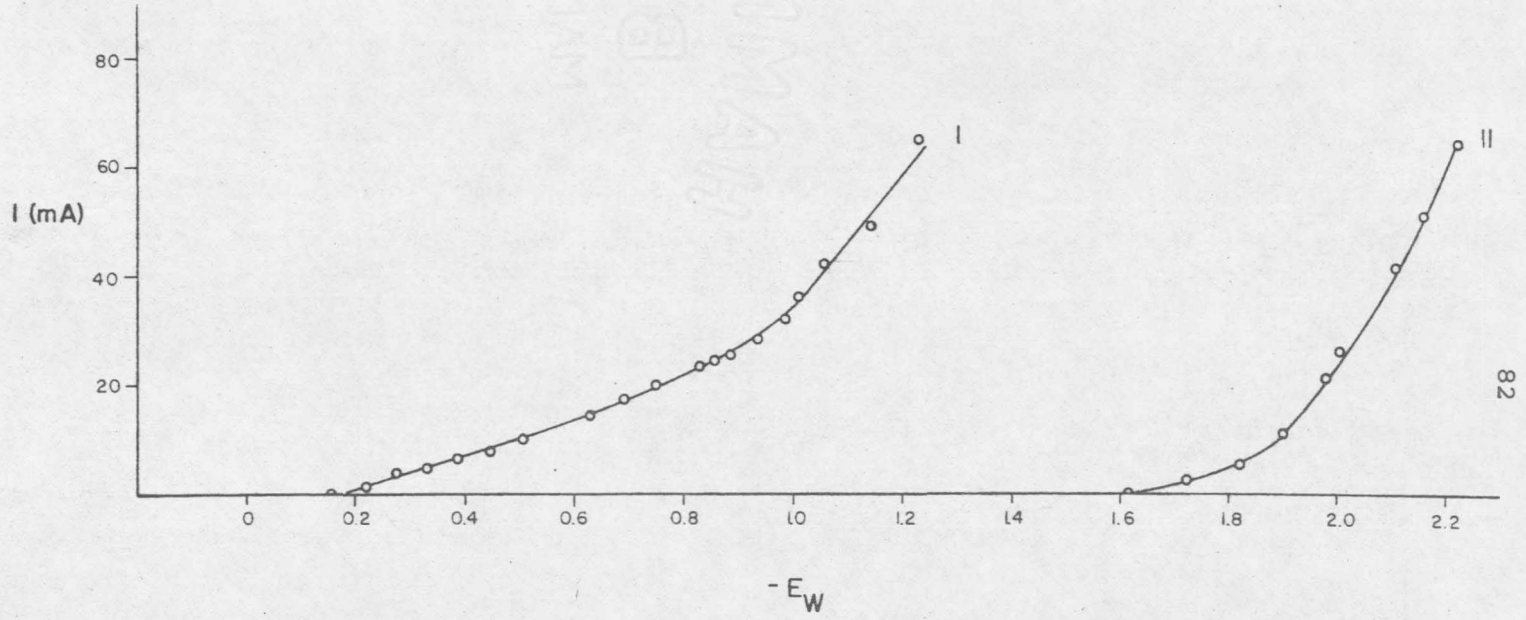

Figure 14. Cell Current versus Working Electrode Potential Curves for (I) 0.2M $Fe(acac)_3$ and (II) 0.8M 1-$C_8H_{17}Br$ at an Aluminum Working Electrode.

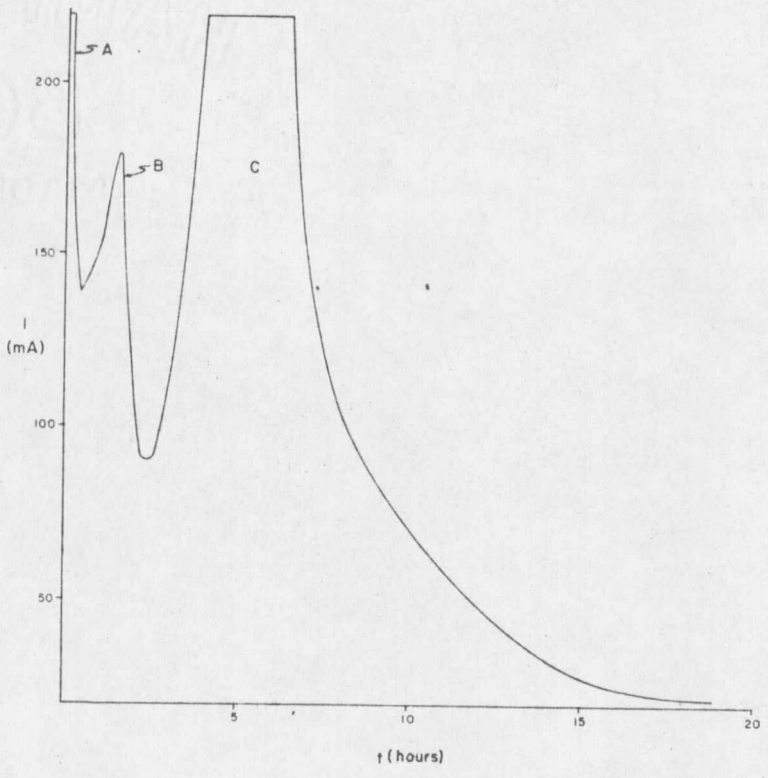

Figure 15. Cell Current versus Time Behavior for a Three-Electrode Cell with $Fe(acac)_3$, $1\text{-}C_8H_{17}Br$, Aluminum Electrodes, and E_{ref} = -0.90V vs Cd(Hg).

seen with the two-electrode cell run at constant applied potential which had been documented by monitoring the cathode potential with a reference electrode, Figure 11. Secondly, the current behavior is not associated with an activational process since such a system should begin with the current at some low level and then increase the current as the activational process proceeds. The above trace shows an initially high current falling with time, Curve A. The decrease in current represented by curve A is the expected behavior for a simple reduction step. The current transients corresponding to curves B and C are unexpected.

Buchta and Evans (129) observed an increase in the electrolysis current during the electrochemical reduction of 1,3-diphenyl-1,3-propanedione in DMSO. They attributed the rise in current to an electrocatalytic process. Similar electrocatalysis was observed in the electrochemical reduction of 1-phenyl-1-hexyne (130). Again, the current transient was attributed to the generation of a more easily reducible material. Thus, curves B and C may represent two possible electrocatalytic steps or possible ECE-type mechanisms.

Further investigations into the nature of this unique current-time behavior have shown that curves A and B are separable from curve C. This separability was demonstrated by preelectrolyzing the $Fe(acac)_3$ solution prior to adding the 1-octyl bromide, Figure 16. Curves A and B are related to the electrochemical activity of the iron

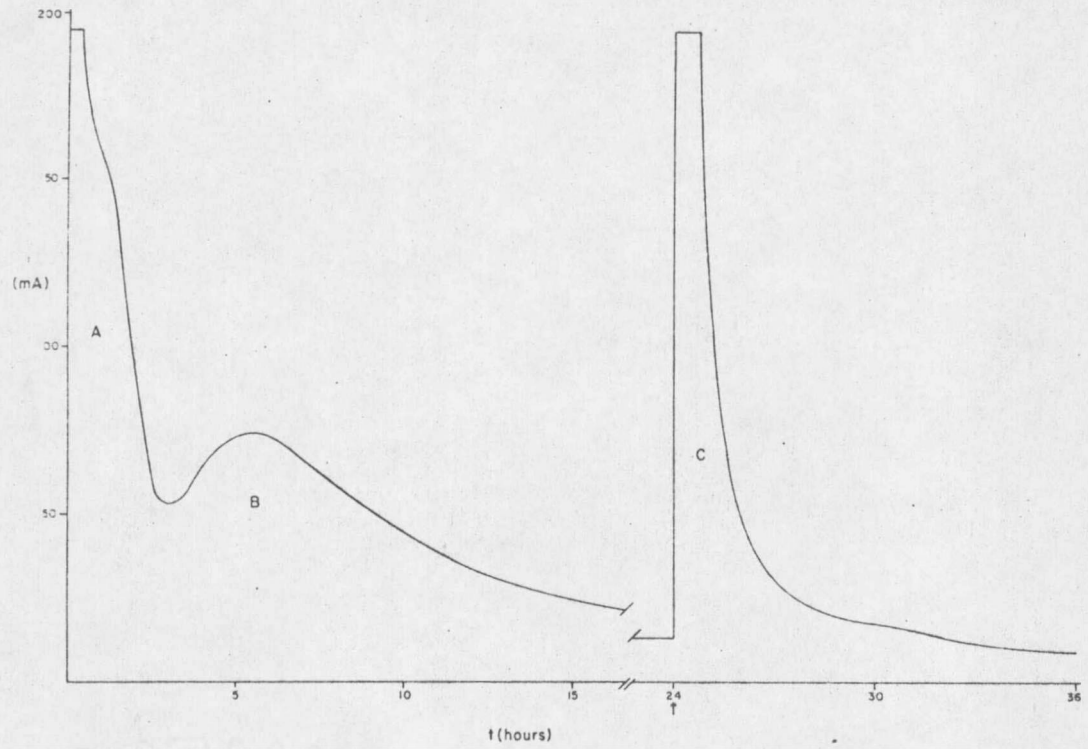

Figure 16. Separability of Current Transients. Preelectrolyzed $Fe(acac)_3$ for 24 hours. Arrow indicates addition of $1\text{-}C_8H_{17}Br$ to electrolysis cell. Aluminum electrodes with E_{ref} = -0.90V vs Cd(Hg).

salt while curve C involves the organic substrate. The rapid rise in current corresponding to the addition of 1-octyl bromide to the pre-electrolyzed solution suggest the process responsible for this rapid current surge is very facile. This may reflect the direct reduction of the organic substrate or suggests the active form of the metal responsible for our intended organometallic reaction reacts very rapidly leading to an electroactive organometallic complex. This separability of curves allows for the examination of the components of the electrolysis cell.

The current-time behavior may be dependent on the nature of the inorganic salt used to provide the iron (III). Such a dependence is easily tested by substituting another ferric salt for $Fe(acac)_3$. The reduction of iron (III) bromide was performed under the same conditions that established the separability of the current transients. Figure 17 displays these results. Again, three curves were obtained but this time curve B is more intense than before. A reasonable possibility for these first two curves is the independent reduction of Fe(III) → Fe(II) followed by a subsequent reduction of Fe(II) → Fe(I or 0). The metal ion may not be free, i.e. solvated, in solution therefore the current transient as seen in curve B could show some dependence on the metal salt used in the system if a chemical dissociation of the charged ligands about the iron (II) center must precede further reduction of iron (II) to iron (I or 0). This dissociation may be more facile for

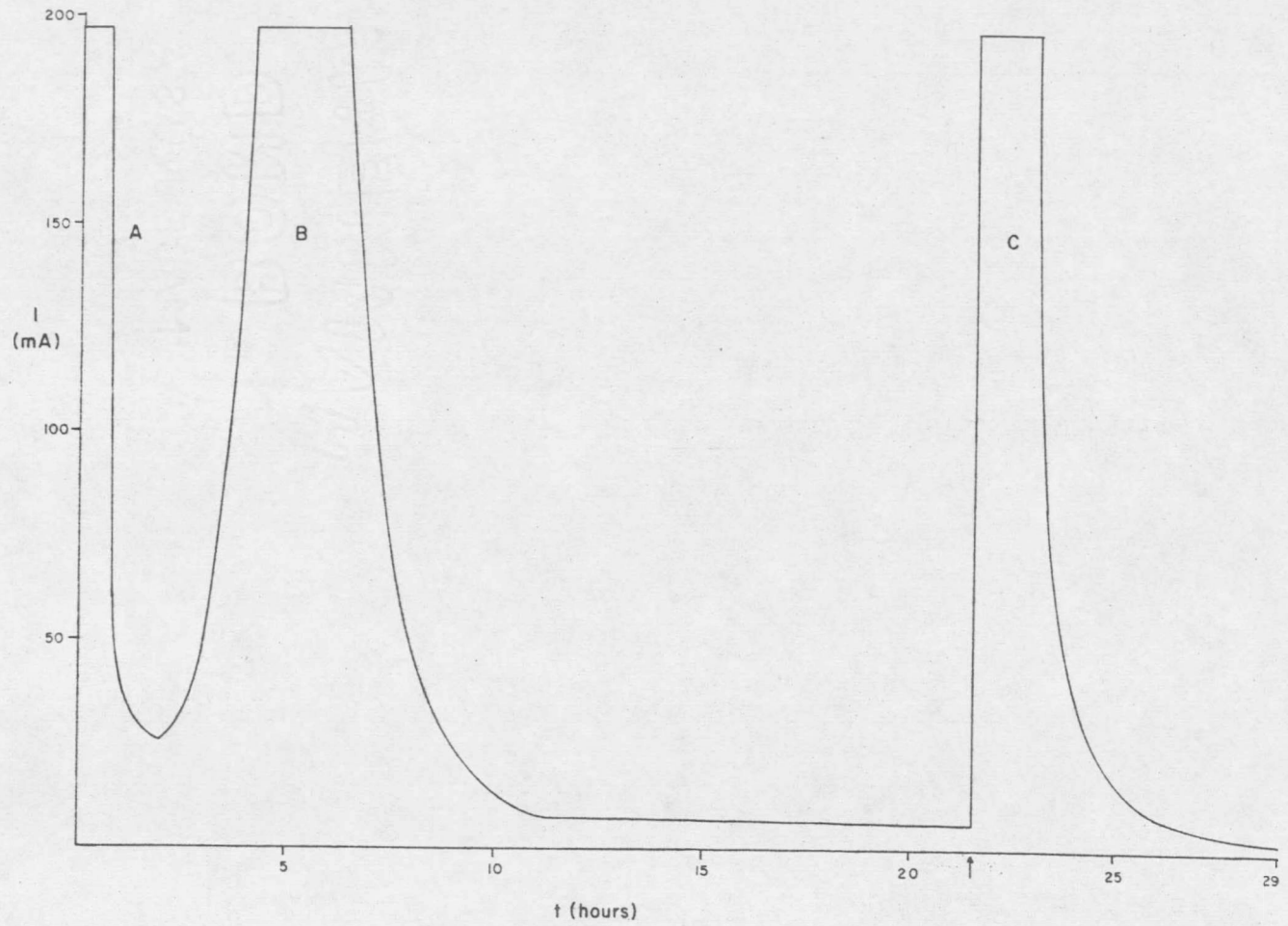

Figure 17. Cell Current versus Time Behavior for $FeBr_3$. Conditions the same as in Figure 16.

a monodentate ligand than a bidentate ligand which could be enhanced by a greater increase in current for curve B when a monodentate ligand is used.

An examination into the reduction potentials of the solution species may shed more light onto the problem. The reported reduction of $Fe(acac)_3$ in acetonitrile, CH_3CN, leads only to the iron (II) salt, $Fe(acac)_2$, when the potential was scanned to -0.3V vs Cd(Hg) (131). At -0.9V, the working electrode potential in the electrolysis cell, the reduction of Fe(II) to Fe (I or O) may be possible. Experimental examination of the half-wave potential of $Fe(acac)_3$ in a polarographic cell showed that the iron (III) to iron (II) conversion occurred at +0.18V. A second wave was observed as noted below.

DME: $E_{1/2}$, V corrected to Cd(Hg) reference

$Fe(acac)_3$	+0.18V	
	-1.29V	
$Fe(DMF)_6^{2+}$	-0.7V	(132)
$FeBr_4^{2-}$	-1.9V	(132)

Al : E_B, V vs Cd(Hg) in a stirred solution

$Fe(acac)_3$	+0.1 to -0.2V
$FeBr_3$	-0.2V

This wave had a half-wave reduction potential at -1.29V. The electrophore responsible for this wave was not identified. This wave, however,

is more cathodic than the -0.9V working electrode potential so that even if it corresponds to the reduction of iron (II) to iron (I or 0), the reduction would not occur in the macro-electrolysis cell.

The effects the ligands attached to the metal center have on the reduction of the metal complex have been noted (133). These effects on iron have been observed in the chemical transformations of alkenyl halides with Grignard reagents in the presence of various iron (III) salts (45) as well as the electrochemical reducibility of ionic iron (132,134-137). A particularly lucid examination of the effects of excess halide ion was performed by Ciana and Furlani (132) using iron (II) complexes. The half-wave potential of ferrous perchlorate in the presence of varying concentrations of haloquaternary salts were studied in DMF. For octahedrally coordinated iron (II), the $E_{1/2}$ is -0.7V which is anodic of the working electrode potential used in the electrolysis of both $Fe(acac)_3$ and $FeBr_3$. Therefore, $Fe(DMF)_6^{2+}$ is a possible electrophore for the system. Halide appears to shift the reduction potential of the iron (II) to more cathodic potentials as the tetrahedrally coordinated iron (II) complexes form making them cathodically insulated from further reduction at -0.9V. For the tetrahedral complex, $FeBr_4^{2-}$, the ratio of Br^- to Fe(II) must be greater than 25:1 in order to insure complete formation of this complex. In the electrolysis reaction using $Fe(acac)_3$, the ratio of Br^- to Fe(III) is 0.5 to 1, while in the $FeBr_3$ case, the ratio becomes 7:1. These latter

ratios are based on the iron (III) content of the electrolysis solution; the ratio of Br^- to Fe(II) will be significantly larger during the initial stages of the reduction for both systems. As the electrolysis continues, more iron (II) is generated which in turn reduces this ratio of Br^- to Fe(II). The identity of the iron salt influences the height of the curve by controlling the available concentration of iron (II) via a complexation reaction with the Br^- present in the cell from the base electrolyte as well as through the tenacity of a bidentate ligand over a monodentate ligand. The time delay between curves A and B may be associated with the initial successful competition of tetrahedral complexing versus electron reduction.

The literature has suggested that aluminum metal sites, Al^o, are exposed on an aluminum electrode when sufficiently cathodic potentials are reached (138). If such sites are available in the above systems, a galvanic cell may be established between the aluminum metal and the ferrous ions or the ferric ions. The original surface of the aluminum electrode is aluminum oxide, Al_2O_3, indicated in the following drawing, Figure 18, by a solid line. The electron transfer across this surface may expose these aluminum metal sites to the solution. The electropositive aluminum (0) may be more cathodic than the biased potential of the working electrode and could successfully displace iron ions from the solution, forming the galvanic cell, and reducing the iron (II) and iron (III) to iron (I) or iron (0). If the oxidation and reduction

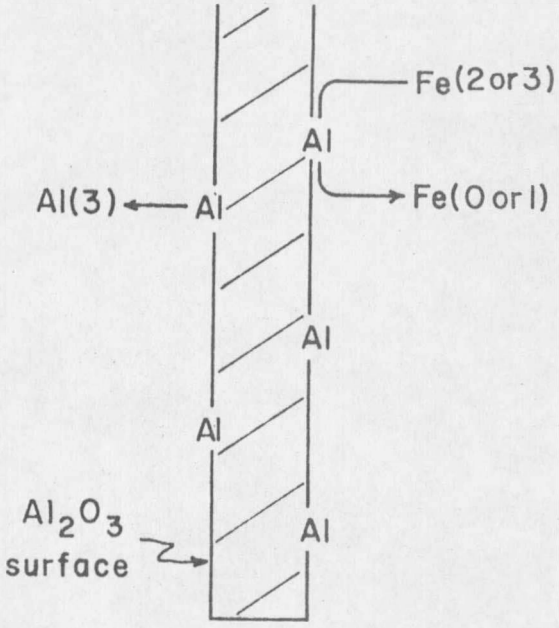

Figure 18. Exploded View of Aluminum Working Electrode Illustrating Possible Galvanic Cell Between Al(0) and Fe (ions).

sites occur at different places on the working electrode, iron could be reduced at one face of the electrode and aluminum ions discharged at the other face as demonstrated in Figure 18. Occasional pitting is observed on the reference side of the working electrode which is in agreement with this prediction. This system could be used to explain the increase in current since the reduction of iron (II) at Al_2O_3 to iron (I or 0) would not occur until the aluminum metal sites are exposed and of sufficient density to allow for a monitorable increase in the current. The argument dealing with the loss of the coordinated ligand would still be usable, i.e., the equilibrium concentration of iron (II) from a salt with a monodentate ligand would be greater than the concentration of iron (II) from a salt with a bidentate ligand.

These arguments are immediately testable. Working electrodes prepared from other materials besides aluminum should show no current transients corresponding to curve B if the aluminum metal sites are necessary for the reduction. On the other hand, if a preequilibrium step is required to establish a reducible iron (II) concentration which is only possible once the ratio of Br^- to iron (II) reaches a critical value, the current transient representing curve B should be present no matter what electrode material is used. The aluminum working electrode was replaced by a stainless steel working electrode and the only curve observed during the reduction of $Fe(acac)_3$ was curve A. This is supportive of the aluminum metal site proposition. However, when a

platinum foil working electrode was used, both curves A and B were present during the reduction of $Fe(acac)_3$. The platinum foil is without aluminum metal sites, therefore this explanation was abandoned. The absence of curve B during the reduction of $Fe(acac)_3$ at the stainless steel working electrode suggests that the preequilibrium argument is also suspect.

Other metal salts were examined using the platinum foil working electrode. The reduction of $Cu(acac)_2$ and $FeBr_3$ both generated current transients. The reduction of $Ni(acac)_2$ produced such small currents that no distinct curves were observable. Copper and iron plated onto the platinum foil working electrode. This plating was also noted to occur for the reduction of both $Fe(acac)_3$ and $FeBr_3$ when the aluminum working electrode was used. The current-time behavior for the reduction of these metal ions may be associated with the change in the average character of the working electrode's surface. For both the platinum and the aluminum working electrodes, some of the surface of the electrode will change from that of the original electrode material to that of the new plated material. Using iron as an example, the surface activity of the iron increases from zero initially to near unity during the plating process on either aluminum or platinum. The reference electrode monitors the average electrode potential of the surface. The surface is undergoing a change as the metal ion begins to plate. It is possible to imagine that these local islands of the new metal deposit

will not contribute to the average electrode potential until some critical surface coverage is reached. During the interim, the potential of this new surface may be more cathodic than the working electrode potential and hence generate a current transient until the average potential of the working electrode as seen by the reference electrode is that of the new metal surface. Figure 19 argues against a rest potential of the newly plated iron surface as being more cathodic than the biased potential of -0.90V for the electrolysis cell. If an iron electrode was that effective at reducing the $Fe(acac)_3$ or the iron (III), one would expect that simply introducing the iron electrode into a solution of $Fe(acac)_3$ would spontaneously (galvanic cell) lead to an appreciable current. Although a stainless steel electrode has only about 70 to 75% iron, the stainless steel electrode did not produce a galvanic reaction. Using the macroscopic electrolysis cell with a stainless steel working electrode, a potential of -0.1V must be imposed onto the working electrode before the reduction of $Fe(acac)_3$ is observed.

The nature of curve B is associated with the plating process. This curve is only observed in those cases where (1) the electrode material and the metal ion are not identical and (2) where plating was observed. This plating may cause the rise in current. The overpotential for the discharge of hydrogen from an aqueous solution at an aluminum electrode is greater than the overpotential for the same

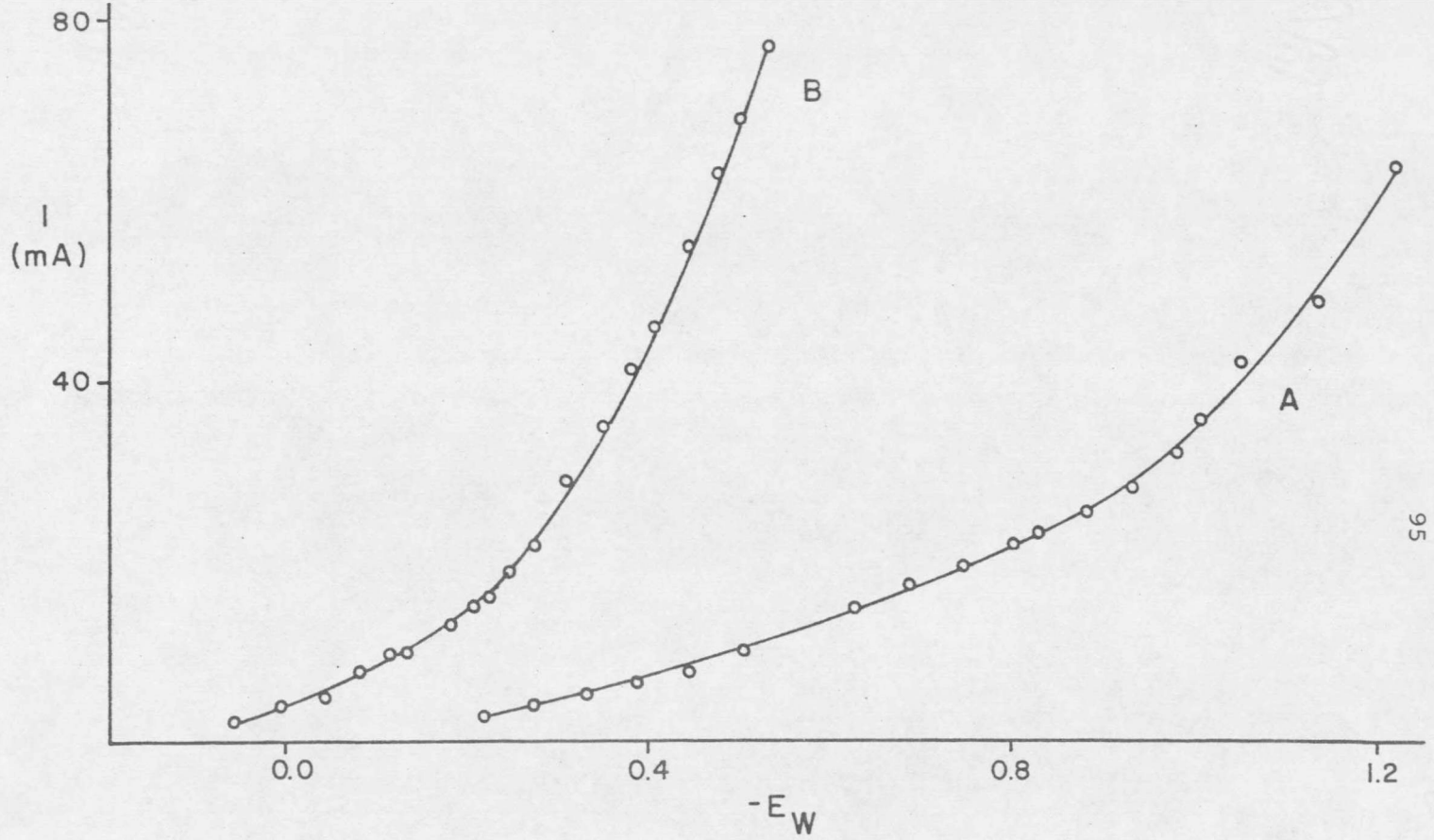

Figure 19. Cell Current versus Working Electrode Potential for $Fe(acac)_3$ at Aluminum, A, and Stainless Steel, B, Electrodes in Macro-electrolysis Cell.

process at copper, nickel, or iron electrodes, Table V, indicating that different cathode materials can catalyze the same reaction differently (107). This overpotential phenomena may also be applicable for plating an ion out of the solution onto a heterogeneous versus homogeneous suface. The rate of heterogeneous election transfer across the solid electrode-solution interface may be more facile with an electrode which has an activity of the plating ion already on the surface compared to an electrode which does not have this activity. Thus, the rate of election transfer would be faster across an iron surface than across an Al_2O_3 surface for the reduction of iron ions. If the electrons can be exchanged faster, the current density increases, i.e., more current flows. Although Table V shows that the overpotential for hydrogen evolution is greater for the copper electrode or iron electrode than for a platinum electrode, this is of course reaction and solvent dependent. The roles may reverse for the reduction and plating of copper or iron at a platinum cathode in DMF.

If the reduction potential for all the iron salts were the same and the currents generated for these potentials would be the same, the rate of heterogeneous electron transfer would be independent of the salt used. This may be true for the initial reduction of iron (III) to iron (II) which appears to have very nearly the same breaking potential at the aluminum working electrode for $Fe(acac)_3$ and $FeBr_3$ as well as similar currents.

$Fe(acac)_3$ +0.1 to -0.2V

$FeBr_3$ -0.2V

Dependence on the nature of the salt may only arise when plating occurs. The higher current for monodentate ligands may reflect the greater reservoir of iron (II) available for reduction than is established with a bidentate ligand. Thus, the current rise would be ascribable to the increased ease of electron transfer across an interface of Fe(0)/Fe(ion) than Al_2O_3/Fe(ion). The magnitude of the current rise would be associated with the availability of iron (II) in the electrolysis solution. Once the rapid electron transfer begins to occur across this new surface of plated metal, the electrophore is consumed and a more classical decay in current ensues. As the iron (II) is removed from the solution and plated onto the working electrode, the formation of the halo-tetrahedral complex can increase because the ratio of Br^- to Fe(II) increases and this may insulate the remaining reduced iron (II) from further reduction.

A change in electrode material can change the nature of the current-time trace (139). The electrochemical reduction of alkyl esters of p-toluene sulfonic acid at a glassy carbon electrode gave normal current-time curves while the same reduction at a mercury cathode gave a current transient. Changing the working electrode in the iron (III) electrolysis from aluminum to stainless steel also

changed the current-time curve. The literature example attributed the change in the current-time behavior to a double layer effect. The change in the current-time behavior in the electrolysis of iron (III) can be explained in terms of the model already suggested. Curve B would not be present with stainless steel because the surface activity of iron is already established in the iron alloy. Iron plating onto the stainless steel may modify the surface of the stainless steel working electrode, but the current density of the new iron surface versus the old iron alloy surface would not be distinguishable. If this argument has merit, although curve B would not observed during the preelectrolysis of $Fe(acac)_3$ with stainless steel working electrodes, curve C should appear when 1-octyl bromide is added. The results of such an experiment are presented in Figure 20. The electrode area of the stainless steel electrodes were reduced to half the size of the aluminum electrodes in order to observe the current decay. Addition of 1-octyl bromide to the preelectrolyzed solution of $Fe(acac)_3$ demonstrated that curve C was present, in agreement with the model.

The model that has been extended to explain the nature of curves A and B can be classified as an ECE-type mechanism with the following steps:

$$Fe(III)L_n + 1e^- \rightarrow Fe(II)L_n \qquad E$$

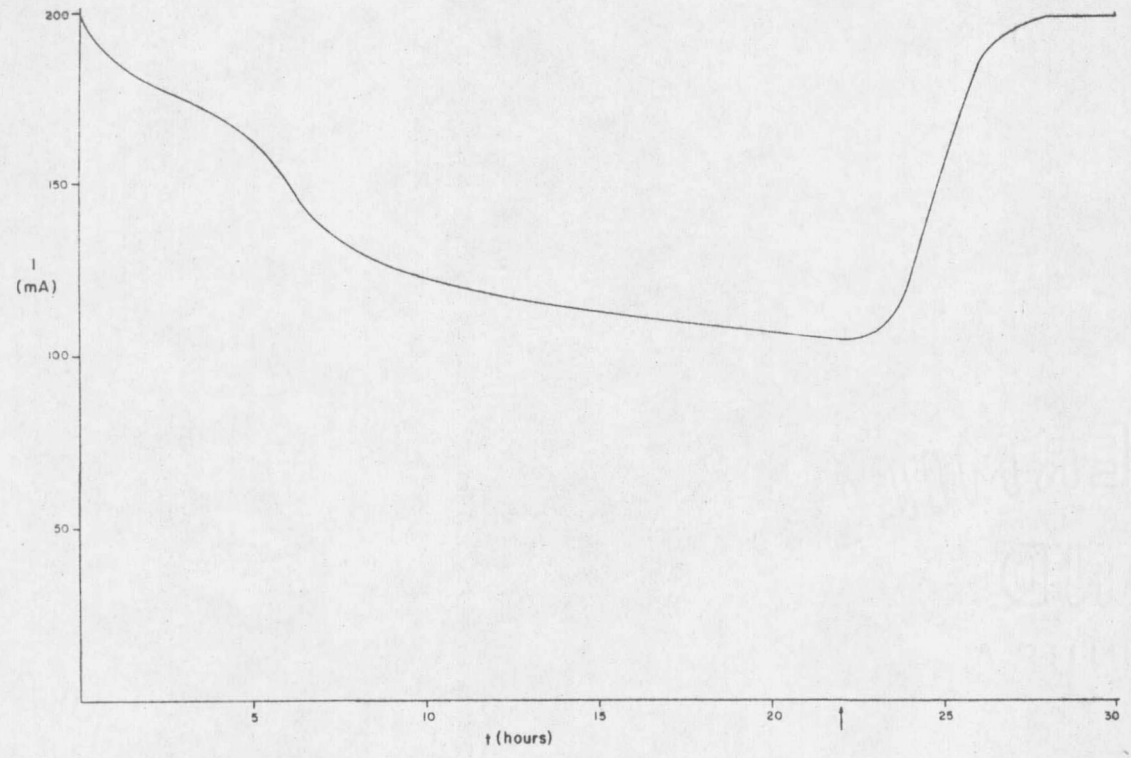

Figure 20. Cell Current versus Time Behavior of $Fe(acac)_3$ at a Stainless Steel Working Electrode. Working electrode one-half normal size of aluminum electrode. Arrow indicates the addition of $1\text{-}C_8H_{17}Br$. E_{ref} = -0.90V vs Cd(Hg).

$$Fe(II)L_n \overset{L'}{\rightleftharpoons} Fe(II)L'_4$$

$$Fe(II)L'_4 \overset{DMF}{\rightleftharpoons} Fe(DMF)_6^{2+} \quad \Big\} \text{ C}$$

$$Fe(DMF)_6^{2+} + 2e^- \rightarrow Fe(0) \qquad \text{E}$$

The chemical steps proposed are simply offered to reflect various equilibria that may be proceeding to generate the solvated iron (II) electrophore. These may indicate mixed complexation by Br^- and $acac^-$, complete dissociative steps to generate iron (II) solvated, etc. They must precede the generation of the solution electrode, $Fe(DMF)_6^{2+}$. The last step gains credibility when noting the formation of iron pentacarbonyl, an iron (0) complex, from the electrolysis of $Fe(acac)_3$ at a stainless steel cathode and an aluminum anode (140) and the observed plating in the three-electrode electrolysis cells discussed above. A discussion of the characteristics of curve C will be presented later in this dissertation.

Components of the Electrolysis Cell

The components of an electrolysis cell include the electrodes, the base electrolyte, the organic substrate, the metal salt, the supporting ligand and the solvent. The solvent that has been selected for this work is N,N'-dimethylformamide, DMF. Since the reference electrode was prepared for this particular solvent, other solvents

were not investigated. The overvoltage effects noted above, catalytic effects, adsorption of the substrate or components of the base electolyte onto the surface of the electrode, the nature of impurities and added components in the electrode material, the physical state and even the history of the electrode can influence the electrode process (101). Most of these effects are only monitorable through empirical observation and thus require independent optimization without much reliance on theoretical considerations. Each of the components of the electrolysis cell will be examined using the optimization of the coupled product as a measure of the success of a particular perturbation.

Electrodes and Cell Design

The electrolysis cell that was used throughout this work is an undivided cell. This selection was felt appropriate since our interest was to (1) maintain the convenience of a simple design which could be easily assembled and (2) eliminate the difficulties of the large iR drop across a salt bridge. Generally this latter problem decreased the net current flowing through the system thereby increasing the reaction time. The large iR drop across a salt bridge also increased the required applied potential which usually demanded more output from the power pack than was available. For most of the work presented in this dissertation, aluminum electrodes were used for both the working

electrode (cathode) and counter electrode (anode) in this undivided cell.

The choice of electrode material is critical to the outcome of the reaction. The selection of aluminum was partly coincidental with the ease of preparing the appropriate size electrodes and partly a response to the demonstrated increase in coupling observed for benzyl radicals (138,141-143) generated at an aluminum cathode. The general effect of electrode material on the overall product distribution is adequately demonstrated in Table X (141,143). The indicated products were prepared from the reduction of benzyl triethylammonium nitrate in

Table X. Effect of Cathode Material on Reduction of $(C_6H_5CH_2)(C_2H_5)_3NNO_3$ in DMF (141,143)

Cathode Material	Mol% $C_6H_5CH_3$	Mol% $C_6H_5CH_2CH_2C_6H_5$
Al	55	45
Mg	64	36
Ta	76	34
C	100	0
Hg	100	0
Pt	100	0

DMF. The coupled product, bibenzyl, arises from the benzyl radical, $C_6H_5CH_2^{\bullet}$, while toluene is generated from a carbanion (141). The effect of current density was also noted, but no clear indication of its subtleties has yet been established (138,141). The first three electrodes would be expected to have oxide films on their surface

which, in the case of aluminum, has been suggested to promote coupling (138).

The purity of the electrode material is also important in governing the course of the electrochemical reaction. Impurities in the electrode material modify the material's properties and hence influence the electrochemical response (101). Two aluminum alloys have been used as electrode material in this examination. One alloy was used for all of the two-electrode constant applied potential work. This alloy was of unknown composition. Another alloy, the 6061T6, was used for nearly all of the three-electrode reactions. The composition of this alloy is given in the experimental section. The three-electrode cell was used to examine the effects of the two aluminum alloys on the nature of the coupling reaction of 1-octyl bromide with reduced $Fe(acac)_3$. Table XI lists the results. Two potentiostats were used in this analysis. The modified Heathkit, mHK, was noted to be oscillatory about the control potential, the average reference electrode potential used to control the system reported as E_{ref}. The solid state device built by Dr. R. Geer, GP, was used for most of the 3-electrode work. For this device, E_{ref} did not oscillate. In order to insure that oscillation about the control potential for the modified Heathkit did not influence the yields of recovered products, both aluminum alloys were used at different control potentials.

Table XI. Three-electrode Cell Examination of the Aluminum Alloys[a]

Reaction No	NII106	NII108	NII124	NII117	NII121	NII139
Base Electrolyte	TEAB	TEAB	TEAB	TEAB	TEAB	TEAB
Working Electrode	Al(unk)	Al(unk)	Al(unk)	606IT6(Al)	606IT6(Al)	606IT6(Al)
Counter Electrode	Al(unk)	Al(unk)	Al(unk)	606IT6(Al)	606IT6(Al)	606IT6(Al)
E_{ref}, V vs Cd(Hg)	-1.0	-0.95	-0.86	-0.95	-0.75	-0.80
% $C_{16}H_{34}$	29.3	16.8	28.6	12.8	25.1	21.1
% C_8H_{18}	12.3	23.2	30.7	15.6	29.0	39.7
% C_8H_{16}	3.9	5.6	14.0	6.7	15.5	8.2
% reaction	93.5	38.8	65.8	34.9	75.0	76.3
I_{max}(mA)	120	40	180	50	410	200
Potentiostat	mHK	mHK	mHK	mHK	mHK	GP

Reaction No	NII141	NII157
Base Electrolyte	TEAB	TEAB
Working Electrode	606IT6(Al)	606IT6(Al)
Counter Electrode	606IT6(Al)	606IT6(Al)
E_{ref}, V vs Cd(Hg)	-0.80	-0.90
% $C_{16}H_{34}$	24.4	30.8
% C_8H_{18}	45.8	24.7
% C_8H_{16}	17.6	7.7
% reaction	76.2	36.1
I_{max}(mA)	200	200
Potentiostat	GP	GP

(a) See text for explanation of terms

The results in Table XI do not indicate any pronounced dependence on the aluminum alloy used for the electrodes. This is particularly gratifying since most of the early work, although well scattered in yields, was done with the unknown alloy of aluminum. The distribution of products has not improved with the greater control of the working electrode potential. Although this observation is discouraging, it refutes the arguments posed earlier that suggested the widely changing product distributions were a result of changes in the cathodic potential when the two-electrode constant applied potential cell was used. Finally, fluctuations in the control potential of the three-electrode cell appear to be ineffective in disturbing the yields of coupled products.

Other electrode material was also examined in the three-electrode cell. Table XII presents the results of this examination. The vitreous carbon electrodes were ineffective in converting substrate to coupled and disproportionated products. A probable cause for this lack of conversion resides with the low current obtained in this cell. The electrodes were small diameter cylinders with an effective surface area of 7.1 mm^2. The electrochemical rate constant, β, is a function of several parameters as noted above. The ratio of surface area of the vitreous carbon working electrode to the solution

volume is very small compared with the normal sized aluminum electrodes used in this study, 1.18×10^2 mm^2/liter versus 4.66×10^4 mm^2/liter.

A stainless steel alloy numbered 302 (SS302) appears to be more effective in generating coupled product than is the aluminum alloy. The composition of this stainless steel alloy is given in the experimental section. The working electrode potential for the stainless steel was selected to correspond to the working electrode potential of the aluminum in the series using the aluminum alloy. The particular

Table XII. Three-Electrode Cell Examination of Other Electrode Materials

Reaction No	NII104	NII176D	NII180
Base Electrolyte	TEAB	TEAB	TEAB
Working Electrode	Vitreous Carbon	SS302	SS302
Counter Electrode	Vitreous Carbon	SS302	SS302
E_{ref}, V vs Cd(Hg)	-0.90	-0.90	-0.90
% $C_{16}H_{34}$	--	39.2	50.2
% C_8H_{18}	--	20.5	10.6
% C_8H_{16}	--	11.7	3.2
% reaction	--	98.7	97.4
I_{max}(mA)	5	200	200
Potentiostat	mHK	GP	GP
Comments	Surface area too small	Preelectrolyzed $Fe(acac)_3$	Preelectrolyzed $Fe(acac)_3$; 1/2 the surface area of NII176D

effectiveness of the stainless steel to generate coupled product is appreciated when the surface area available for the reduction at the stainless steel working electrode was reduced to half that used for the aluminum electrodes, NII180. This is the first clue that the electrode surface itself may participate in the generation of products. If a reduced form of iron in the solution was responsible for coupled product formation, there should be no dependence on the electrode's surface area as long as the reduction of either iron ions or organometallic can occur at a reasonable rate. The comparison between reactions NII176D and NII180 demonstrates that perhaps the same scatter in yields of recovered products as noted to occur with aluminum electrodes will occur with stainless steel electrodes. In both the reported stainless steel reactions, the $Fe(acac)_3$ was pre-electrolyzed and for both the current increased with the addition of 1-octyl bromide, Figure 20.

The generation of coupled product may be occurring via the direct reduction of organic substrate and thus be independent of the reduction of iron. Although the half wave potential of 1-octyl bromide was approximately -1.5V at a dme which is more cathodic than the working electrode potential of -0.90V, the effects of the electrode material may be such that the overpotential for the direct reduction of 1-octyl bromide at stainless steel or aluminum is shifted anodically, falling within the domain of the electrolysis. Several methods of

examination were attempted in order to address this problem. A stirred solution of the 1-octyl bromide in the three-electrode electrolysis cell containing everything except $Fe(acac)_3$ was used to generate the appropriate current-working electrode potential curve for the two metal alloys. The breaking potential for the direct reduction of 1-octyl bromide is given in Table XIII. Although an anodic shift in the breaking potential was observed on changing the electrode material from aluminum to stainless steel, this shift should not be sufficient to allow the direct reduction of 1-octyl bromide since the

Table XIII. Macroelectrolysis Cell Breaking Potentials for $1\text{-}C_8H_{17}Br$

Metal Working Electrode	E_B, V vs Cd(Hg)
606IT6 (Al)	-1.8
SS302	-1.6

working electrode potential in both macroscopic cells is -0.90V. The counter electrode for both working electrodes was the 606IT6 alloy of aluminum.

These current potential scans represent a short-term electrolysis. The long-term electrolysis in the three-electrode cell at -0.90V may lead to some generation of products originating from the direct reduction of 1-octyl bromide since the reduction of this alkyl

halide is an irreversible process (68). Exploring this possibility, the electrolysis cell was prepared with all of the components except $Fe(acac)_3$. A series of these blank reactions are reported in Table XIV. The aluminum alloy of unknown composition gave no products after 48 hours of electrolysis at -0.9V. Traces of octane and 1-octene were observed after 48 hours of electrolysis at -2.0V but no coupled product was observed. If the direct reduction of 1-octyl bromide leads to the generation of coupled products, product formation should have been observed in reaction NII126C.

The blank determinations with stainless steel electrodes were more interesting. The stainless steel counter electrode is capable of discharging iron ions into solution. Of course, this discharge represents half of the net cell reaction and will only occur if the current can flow through the cell. Reaction NII178 indicates sufficient current can flow to discharge iron ions into the electrolysis solution. These ions are then reducible at the working electrode. The current-time behavior for reaction NII178 is shown in Figure 21. As the iron ions are reduced, more will be discharged and the current will begin to rise. This argument is pleasing, but it is incorrect in that it attempts to attribute the current increase to the reduction of iron (III) alone. The two half reactions for iron discharge and iron plating are:

Table XIV. Blank Reactions with the Three-Electrode Cell

Reaction No	NII126A	NII126C	NII178	NII181	NII182A	NII182B
Base Electrolyte	TEAB	TEAB	TEAB	TEAB	TEAB	TEAB
Working Electrode	Al(unk)	Al(unk)	SS302	SS302	Pt-foil	606IT6(Al)
Counter Electrode	Al(unk)	Al(unk)	SS302	606IT6(Al)	606IT6(Al)	SS302
E_{ref} V vs Cd(Hg)	-1.0	-2.0	-0.90	-0.90	-0.90	-0.90
% $C_{16}H_{34}$	none	none	15.1	0.1 mmole	none	none
% C_8H_{18}	none	0.7 mmoles	26.7	0.7 mmole	none	none
% C_8H_{16}	none	0.2 mmole	10.7	0.3 mmole	none	none
% reaction	none	--	100%	--	none	none
I_{max}(mA)	1	4	200	4	1	1
Potentiostat	mHK	mHK	GP	GP	GP	GP
Comments	48 hours of electrolysis	48 hours of electrolysis				

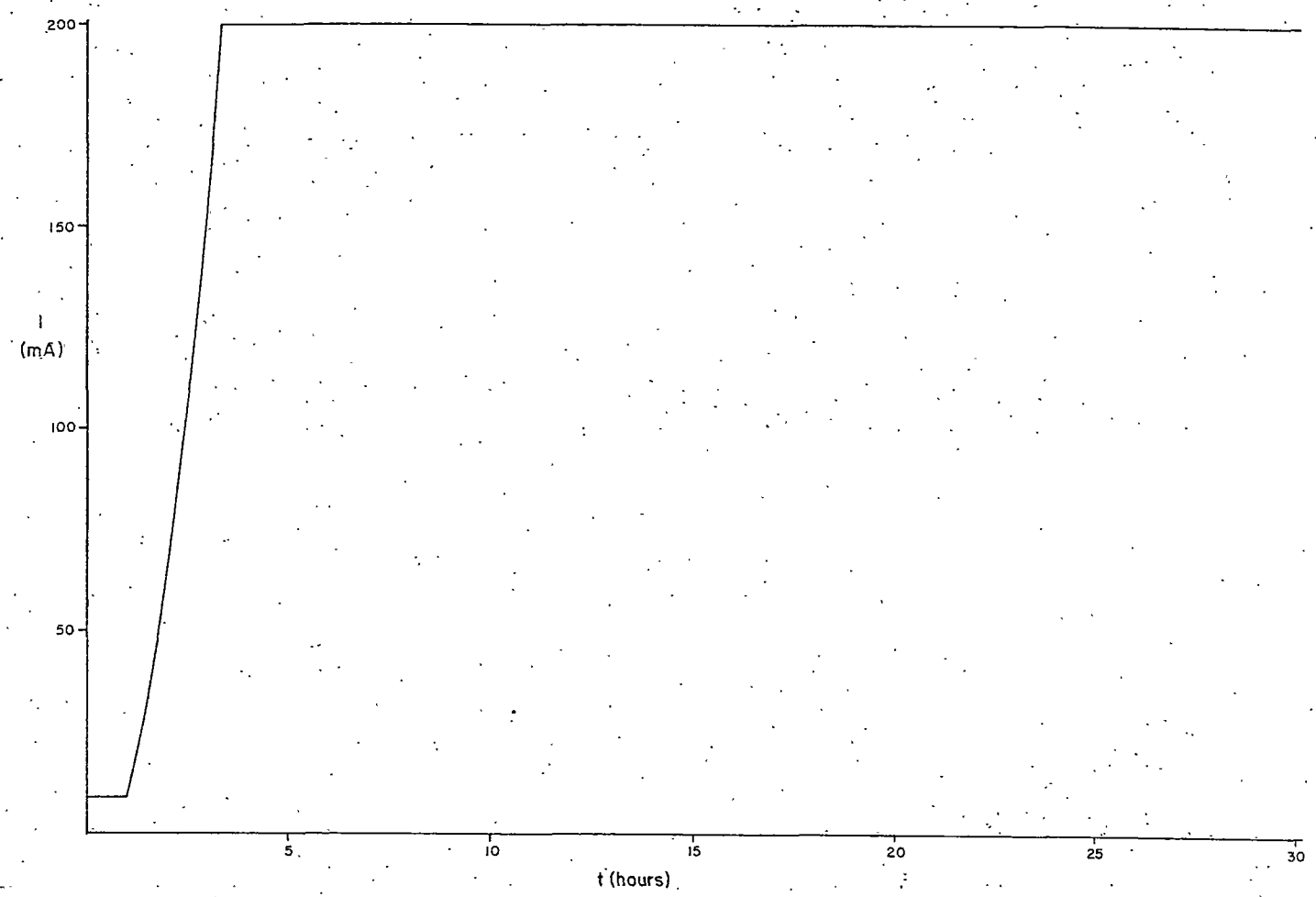

Figure 21. Cell Current versus Time Behavior for Blank Reaction NII178. E_{ref} = -0.90V vs Cd(Hg). Stainless steel electrodes with $1\text{-}C_8H_{17}Br$.

$Fe(III) + 3e^- \rightarrow Fe(0)$ working electrode

$\underline{Fe(0) \rightarrow Fe(III) + 3e^-}$ counter electrode

No net reaction

There is no net reaction for iron reduction and iron plating, therefore there should be no current increase, but rather a flat, constant steady-state current. If current is initially flowing in the cell, the current must represent an electron transfer process occurring at the working electrode. The initial half reactions for this system are:

$Ox + ne^- \rightarrow Red$ $n = ?$ working electrode

$Fe(0) \rightarrow Fe(+m) + me^-$ $m = 2$ or 3 counter electrode

followed by

$Fe(+m) + me^- \rightarrow Fe^o$ working electrode

The initial current may reflect the reduction of a solution contaminant or an organometallic formed at the stainless steel working electrode between surface iron (or nickel or chromium of the alloy) and 1-octyl bromide which is itself reducible. As the reduction of this substrate occurs, some iron ions will be discharged into the solution. These ions are then reducible. Should the initial reduction correspond to the reduction of a solution containment, its concentration would be anticipated to be small. Once the complete electrolysis of this contaminant occurs, the current should level off for now the net

reaction again corresponds to the steady-state transfer of iron from the counter electrode to the working electrode. The current-time behavior illustrated in Figure 21 is noted to maximize at 200 mA, the limiting value for Geer's potentiostat. This sizable increase in current from near zero to 200 mA suggests, of course, that the solution component responsible for this increase in current has a respectable concentration. The electrophore available in reasonable concentrations is 1-octyl bromide. The breaking potential for its reduction is -1.6 V at stainless steel. If it is to contribute to the cell current, the reduction at -0.9V must be facile. If the reduction is facile, the current should have started at some high value and dropped. This is not demonstrated in Figure 21. Two explanations are advanceable. One, the stainless steel electrode is passive and the observed current rise represents the direct reduction of 1-octyl bromide as the stainless steel is rendered active. As this process occurs, iron ions are discharged from the counter electrode and contribute to the total current. A second alternative is that some organometallic of iron is formed initially with the surface of the stainless steel working electrode which is easily reduced. The organometallic is electrode active and reduced at -0.9V, generating products. During this process, iron ions are discharged from the counter electrode which are, in turn, reduced at the working electrode. The reduced form of iron may be in solution or on the surface.

1-octyl bromide reacts with this reduced form of iron and forms more reducible organometallic. Two reducible species are available, both reducible at or below -0.9V, therefore the current increases. The process becomes autocatalytic (electrocatalytic (130)). This process would continue until all the 1-octyl bromide is consumed after which time the large steady-state current represents only the transfer of iron from the anode to the cathode. Iron (0) would be expected to plate onto the working electrode at this juncture in order to maintain solution charge neutrality. This proposed process again suggests the possible intermediacy of a surface species.

To eliminate the discharge of iron into the electrolysis cell solution from the stainless steel counter electrode, this electrode was replaced with an aluminum electrode, reaction NII181. Traces of the three products were observed, the yields being respectably smaller than those for the two stainless steel electrodes. That some products formed at this potential may also suggest the intermediacy of iron organometallics, but the production is not particularly facile. The activation of an initially passive electrode seems less convincing an argument for reaction NII178 since the activational process would presumably occur in both reaction NII178 and NII181. However, one can argue that the reduction of iron ions and hence current passage across the working electrodes surface is required for activating the system.

That some products are formed suggests that the electrode is activated for reduction.

To eliminate the possible contribution the stainless steel working electrode may have had in generating products in these blank reactions, a platinum-foil working electrode was used in place of the stainless steel. As indicated in Table XIV, no products were formed for reaction NII182A. The products formed in reactions NII126C and NII181 were not formed from the anodically discharged aluminum ions or aluminum alloy components since they should have influenced reaction NII182A. The products formed in reaction NII181 are suspiciously associated with the presence of a stainless steel working electrode.

Finally, switching the working and counter electrodes in reactions NII181 so that the aluminum alloy is the working electrode and the stainless steel alloy is the counter electrode produced no products. Certainly this is in harmony with the discourse concerning the discharge and reduction of iron ions. Without current flowing in the cell, the iron ions cannot be discharged from the counter electrode, therefore these ions are not available for reduction at the working electrode. Thus, the current remains constant at a very low value. If the reduction suspected of occurring at the stainless steel electrode in reaction NII178 is due to a solution contaminant, this reduction should also occur at the aluminum working electrode in reaction NII182B and the current should have increased. Since the current

did not increase, and assuming that the containments in the two electrolysis cells are identical, the proposition that organometallics of iron are responsible for the current-time behavior in reaction NII178, Figure 21, gains support.

The effect that $Fe(acac)_3$ has on the electrolysis cells using mixed electrodes is adequately demonstrated in Table XV which also reports the two blank reactions with identical mixed electrode combinations. The reduction of $Fe(acac)_3$ is critical for the overall conversion of 1-octyl bromide to products.

The effects of the electrode material on the generation of coupled product have been explored from the viewpoint of changes in the working electrode material. Overall, the effect of the working electrode material is seen to increase the production of dimer on going from an aluminum alloy to the stainless steel alloy. However, the current-time behavior for the reduction of $Fe(acac)_3$ and the conversion of 1-octyl bromide to product is sacrificed when stainless steel is used for the working electrode since curve B is not present. The diagnostic value of this curve with an aluminum working electrode results in considerable time savings. When curve B is present, the electrolysis cell will generate products. When curve B is not present, no products are formed. In most reactions, curve B appears within the first eight hours of the electrolysis. Thus, only a maximum of eight hours are spent when using the three-electrode cell

Table XV. Reduction of $Fe(acac)_3$ at Mixed Electrodes with Three-Electrode Cell

Reaction No.	NII182B	NII143	NII181	NII173
Reaction Type	Blank	$Fe(acac)_3$	Blank	$Fe(acac)_3$
Base Electrolyte	TEAB	TEAB	TEAB	TEAB
Working Electrode	606IT6(Al)	606IT6(Al)	SS302	SS302
Counter Electrode	SS302	SS302	606IT6(Al)	606IT6(Al)
E_{ref}, V vs Cd(Hg)	-0.90	-0.90	-0.90	-0.90
% $C_{16}H_{34}$	none	16.5	0.1 mmole	19.1
% C_8H_{18}	none	30.6	0.7 mmole	30.1
% C_8H_{16}	none	12.1	0.3 mmole	17.1
% reaction	--	100	--	100
I_{max} (mA)	1	200	4	150
Potentiostat	GP	GP	GP	mHK

and aluminum electrodes. Without this diagnostic tool, the usual 24 hours of electrolysis are consumed plus additional time required to work up the reaction in order to establish the isolated yields. Therefore, to maintain a continuity of approach from the two-electrode constant applied potential cell to the three-electrode cell, to maintain the ease of preparing an aluminum electrode versus a stainless steel electrode, and to continue the advantageous use of the appearance of curve B, aluminum remained the working electrode throughout the optimization procedure.

The effect the counter electrode has on the nature of this reaction is important to consider. The electrolysis cell is an undivided cell, therefore several systems can be envisioned as occurring within the electrolysis compartment. The reduced solution species generated at the working electrode may migrate to the counter electrode and be oxidized. This system is quite unlikely for in all cases that used an aluminum counter electrode, the cell current fell with time. This reduction in cell current would not be expected for such a reduction-oxidation sequence, but rather a constant current situation much like that with iron ions and a stainless steel counter electrode is expected until all the 1-octyl bromide is consumed. Alternatively, the discharge of ions from the sacrificial counter electrode can influence the nature of the reaction as seen with the stainless steel counter electrode in reaction NII178 of Table XIV. Finally, the oxidation

product formed at a nonsacrificial counter electrode may attack either the working electrode via a chemical or electrochemical process or attack the organic substrate and/or products.

Aluminum anodes have been noted to assist in the generation of polymeric material through the release of aluminum ions into a solution containing organic substrate (144,145). It is worthy to note that in the presence of transition metals, the identify of the product varied (145). The effect of added aluminum ions in certain chemical transformations has also been described. The compound, $AlCl_3$, is

$$>=< \xrightarrow[\text{Cr, Ti, V, Al anode}]{\text{Al cathode}} \text{polyethylene + branded chain polymers}$$

suggested to be a cocatalyst in the preparation of cyclic ketones by coordinating with a tricarbonyl iron complex through the carbonyl oxygen (146). Although Cl^- is not present in the electrolysis cell used in this study, the cell does contain the bromide ion which may scavenge the discharged Al(III) from the counter electrode and form a potential cocatalyst in the electrolysis solution. The bromide ion is not well solvated in DMF (96), therefore its ability to participate in complexing the discharged Al(III) or cathodically formed Fe(II) is reasonable. Aluminum (III) has been observed to complex directly with Fe(II) when the former was the bromide salt, $(Me_2NAlBr_2)_2$ (147). Such

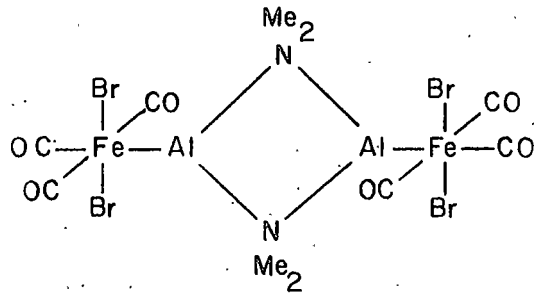

complexation may alter the reactivity of the iron in the electrolysis cell toward reactions with 1-octyl bromide, i.e., the Al(III) may function as a cocatalyst. Alkyl aluminum species may form which have been demonstrated to be particulatly effective cocatalysts in the condensation of two olefins using an $Fe(acac)_3$ catalyst (148), a system reminiscent of the oligomerization catalysts of the Ziegler type (149,150). The reaction of the alkyl aluminum species,

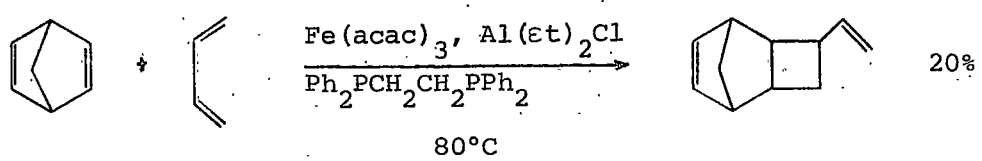

Me_2AlOEt, with $Fe(acac)_3$ lead directly to a dialkyl iron species which generated a 2.5 to 1 ratio of ethane to methane (151,152). This is of particular interest in the electrolysis cells used in this study since alkyl aluminum compounds were reported to form in the system using two aluminum electrodes (145). The aluminum (III) generated from the

discharge reaction of the aluminum counter electrode has been suggested to be activated for further reaction by complexation with DMF (66). A 1:1 adduct of $AlCl_3$ to DMF was reported to form a very strong adduct via coordination through the carbonyl oxygen of the DMF, which subsequently attacks an organometallic complex to ultimately yield an aldehyde. This is peculiar in that $AlCl_3$ is reported to react with DMF presumably leading to decomposition products (153). Thus, aluminum ions, discharged from the counter electrode, may be influential in product formation in the electrolysis cell.

A separated electrolysis cell is best suited to test the importance of the aluminum counter electrode in the generation of products as well as the importance of oxidizing any organometallic compounds formed at the working electrode. Such a cell was prepared using a methyl cellulose bridge. Both compartments were identical except that $Fe(acac)_3$ was only present in the cathode compartment. The cell was operated using a constant applied potential of 1.5V. Traces of octane, 1-octene, and n-hexadecane were found in the cathode compartment while the anode compartment appeared to have no products formed. Attempts at reproducing the separated cell reaction using a three-electrode design and modified salt bridges generally failed because of the low current available.

The separated cell was not particularly helpful in evaluating the effect of the aluminum as either an anode or as a classical reagent

in the solvent. The next procedure was to substitute another electrode material for the aluminum counter electrode. The results have already been presented in Table XV. The blanks establish that no reaction occurs when $Fe(acac)_3$ is not present. Switching the aluminum and stainless steel electrodes indicates that the discharged aluminum ions are not participating as a cocatalyst in the generation of product since the product distributions are nearly identical for reactions NII143 and NII173.

Finally, the three major products generated in this reaction are octane, 1-octene, and hexadecane. If the DMF-aluminum complex provided a facile route for the generation of aldehydes, this product should have been identified during the reaction work up as one of the major products. Not all of the carbon from the organic substrate is recoverable, therefore the possibility of forming some aldehyde is reasonable, but the concentration is not very large. In particular, if this aluminum reagent is present in the electrolysis solution, the yields of octane, octene, and hexadecane should be less when an aluminum counter electrode is used than when a stainless steel counter electrode is used assuming, of course, that the overall reaction for both systems is identical. Reaction NII173 used on aluminum counter electrode and the yields of products <u>increased</u> rather than <u>decreased</u> over those generated using a stainless steel counter electrode. The effect of the discharged aluminum ions from an aluminum counter electrode is

inconsequential to the overall conversion of octyl bromide to coupled product.

The problem of other electrochemical oxidations occurring at the anode must also be considered. For the two electrode systems presented so far, both use sacrificial counter electrodes, that is, both discharge metal ions into the electrolysis solution. A noble metal such as platinum, Pt, cannot perform the same as the aluminum or stainless steel counter electrodes. If the oxidation of a solution organometallic electrophore is important in product formation, this oxidation should proceed at all the counter electrodes. However, if the discharge of the metal ion of the counter electrode is the important attribute of this electrode, the reaction using Pt should proceed differently than those using aluminum or stainless steel. The results of this investigation are presented in Table XVI.

The oxidation potential for the couple Br^-/Br_2 is reported to be +0.65V vs SCE which, in terms of the Cd(Hg) reference electrode is -0.05V, at a platinum anode in DMF (154). This potential corresponds to the potential at the quarter wave, $E_{1/4}$. The overpotential for this reaction at aluminum and stainless steel electrodes is directly observed in the macroscopic scans of the current versus working electrode potential curves for the three-electrode electrolysis cell. No current is observed to follow from approximately +0.25V vs Cd(Hg) to -0.10V vs Cd(Hg) when tetraethylammonium bromide, TEAB, and $Fe(acac)_3$

Table XVI. Platinum Counter Electrodes in Three-Electrode Cell

Reaction No.	NII151	NII153A	NII153B	NII129
Base Electrolyte	TEAB	TEAB	TEAB	TEAB
Working Electrode	SS302	SS302	SS302	SS302
Counter Electrode	Pt	Pt	Pt	SS302
E_{ref}, V vs Cd(Hg)	-0.11	-0.13	-1.50	-0.1
% $C_{16}H_{34}$	6.1	none	18.3	none
% C_8H_{18}	30.5	none	38.7	none
% C_8H_{16}	trace	none	4.2	none
% reaction	30	none	65.5	none
I_{max} (mA)	200	2	220	194
Potentiostat	GP	GP	GP	mHk
Comments	At end of reaction E_W = +0.1V	no $Fe(acac)_3$	Back of cathode pitted, plated on front; E_W = +0.55V	

are present in the solution with either aluminum or stainless steel working electrodes. If Br^- was being oxidized at the same potential for the aluminum and stainless steel electrodes as is observed at platinum, a sizable current should have been observed between +0.25 and -0.1V. With a platinum counter electrode, the possibility of Br^- oxidation is reasonable.

The platinum counter electrode used in reactions NII151, 153A and 153B was a platinum spiral of 18-gauge wire. Figure 22 demonstrates the alignment of the stainless steel working electrode and the platinum counter electrode. This particular configuration generated a hot spot on the stainless steel working electrode. This hot spot had the dimensions of the platinum spiral, 4 mm x 15 mm. At this hot spot plating occurred as evidenced by a deposit of material in reaction NII151. This site must be more cathodic than the rest of the surface of the working electrode. Since maximum current was flowing through the cell, 200 mA, the current carriers were $Fe(acac)_3$, 1-octyl bromide, and Br^-. That the generation of this hot spot produced a surface that was more cathodic than the -0.1V control potential is demonstrated by comparing the results for reaction NII151 and reaction NII129 in which two stainless steel electrodes were used with a control potential of -0.1V. No products were formed in this latter case.

The generation of products in reaction NII151 is not due to the direct reduction of 1-octyl bromide. Assembling an identical

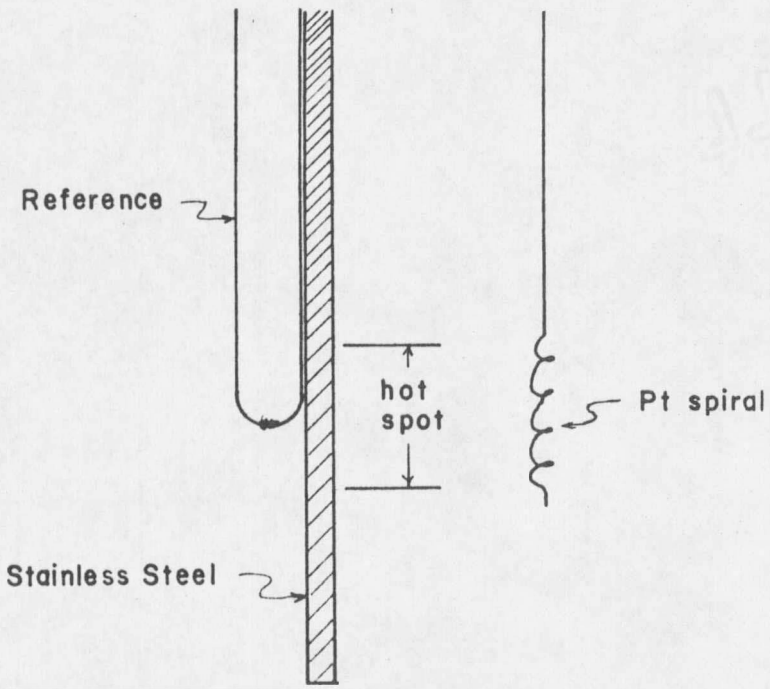

Figure 22. Three Electrode Alignment with Pt Counter Electrode.

electrolysis cell as used in reaction NII151 but eliminating the $Fe(acac)_3$ and running the electrolysis with a control potential of -0.13V, reaction NII153A, no products were generated. Maximum current in this cell was only 2 mA therefore the lack of products may be argued to reflect the lack of electrochemical action. The hot spot may only form at high current levels.

The solution for reaction NII153A was water clear. The control potential was increased to -1.5V. While the working electrode climbed to this value, the stirring of the electrolysis solution was momentarily halted. The solution around the platinum spiral was yellowing. Bubbles formed on both sides of the stainless steel counter electrode. The reaction proceeded for 24 hours but the working electrode potential never remained at -1.5V. The system was under current control with the working electrode potential, E_W, at +0.55V vs Cd(Hg). After 24 hours the electrodes were removed from the electrolysis solution. The cathode was consumed on the backside (the reference electrode side) and plated on the front side. The plating on the front side was irregular with high ridges of material. The plated material appeared blue in the valleys and copper on the ridges. The hot spot was again present, but this time the area was clear. The platinum counter electrode appeared to be yellow. The reaction that occurred in the initially metal ion free solution must have been able to generate metal ions via a chemical attack on the working electrode. The average

potential for the backside of the working electrode measured by the reference electrode would be different than the front side which faced the thin spiralled counter electrode that created the hot spot. The physical appearance of the working electrode attests to this. Since oxidation of Br^- can occur at a platinum electrode well within the potentials attained in this system, the oxidant that is suggested to attack the cathode in Br_3^{1-}. The yellowing of the solution around the platinum counter electrode would also support this interpretation. This oxidant generated at the platinum counter electrode could attack and solubilize the working electrode. Plating would occur on the more cathodic front face of the working electrode while chemical attack proceeded on the back side. Either the plated surface or a solution species would be responsible for the formation of product. The direct reduction of 1-octyl bromide is suggested to also occur and is responsible for the observed evolution of gas about the stainless steel working electrode. The bubbles are suggested to be ethylene formed from the Hoffman elimination reaction involving the carbanion generated by the direct reduction of 1-octyl bromide, R_8^-.

$$R_8^- + CH_3CH_2\overset{(+)}{N}(CH_2CH_3)_3 \rightarrow R_8H + CH_2CH_2 + (CH_3CH_2)_3N$$

The dissolution of the working electrode in reaction NII153B is further supported with uv-vis spectral data. Comparison of spectral scans for electrolysis cells hosting two stainless steel electrodes

with spectral scans for aliquots of solution removed from the electrolysis cell of reaction NII153B demonstrate the presence of the same chromophores. The former cell discharges material from the stainless steel counter electrode therefore the stainless steel working electrode of reaction NII153B must have done the same.

The use of sacrificial counter electrodes precludes the complexation associated with Br^- oxidation. The function of the counter electrode in this electrolysis reaction is simply to circumvent the noxious reaction of Br^- oxidation by discharging metal ions into the electrolysis solution. The stainless steel electrode provides iron ions for further reduction. The aluminum electrode discharges aluminum ions which are passive to chemical or electrochemical processes.

Electrode History

An oxide coating on aluminum is present no matter what grade of aluminum or pretreatment of aluminum is used (138). The oxide coating on aluminum insulates it to current passage and also prohibits its ready dissolution as an anode since aluminum (III) cannot migrate through this oxide film (107). Protons, however, can migrate through this oxide film, therefore the aluminum can function as a cathode. Cl^-, Br^-, and NO_3^- can also penetrate this surface oxide allowing the aluminum to function as an anode in solutions containing these ions (107).

The history of the electrode has been suggested to have an effect on the nature of the electrolysis reaction (101) and, given the characteristics of the aluminum surface, may be expected to be important for aluminum electrodes. Such effects should be demonstrable by observing the current-time behavior for the reduction of the inorganic ion. Curve B is a diagnostic tool for monitoring the performance of the cell and hence is ideal for examining the effects of the working electrode's history. Secondly, changes in the breaking potential of the current versus working electrode potential curves would be expected to demonstrate the effects of the working electrode's history. This latter demonstrates changes in the electron transfer processes that generate the reduced solution ion while the former system might provide information concerning the effectiveness of plating. Figure 23 presents four curves for the current versus working electrode scans in the macroscopic electrolysis cell containing $Fe(acac)_3$ without 1-octyl bromide being present. A considerable shift in the breaking potential is observed. All the aluminum electrodes will have an oxide layer on them even after the acid pretreatment. The harsh surface treatment using steel wool as an abrasive followed by acid cleaning may increase the surface area of the aluminum electrode over that of a simple acid washed electrode, curves I and IV, which results in an increase in current for the electrode with the greater surface area. The breaking potential is also a function of the surface

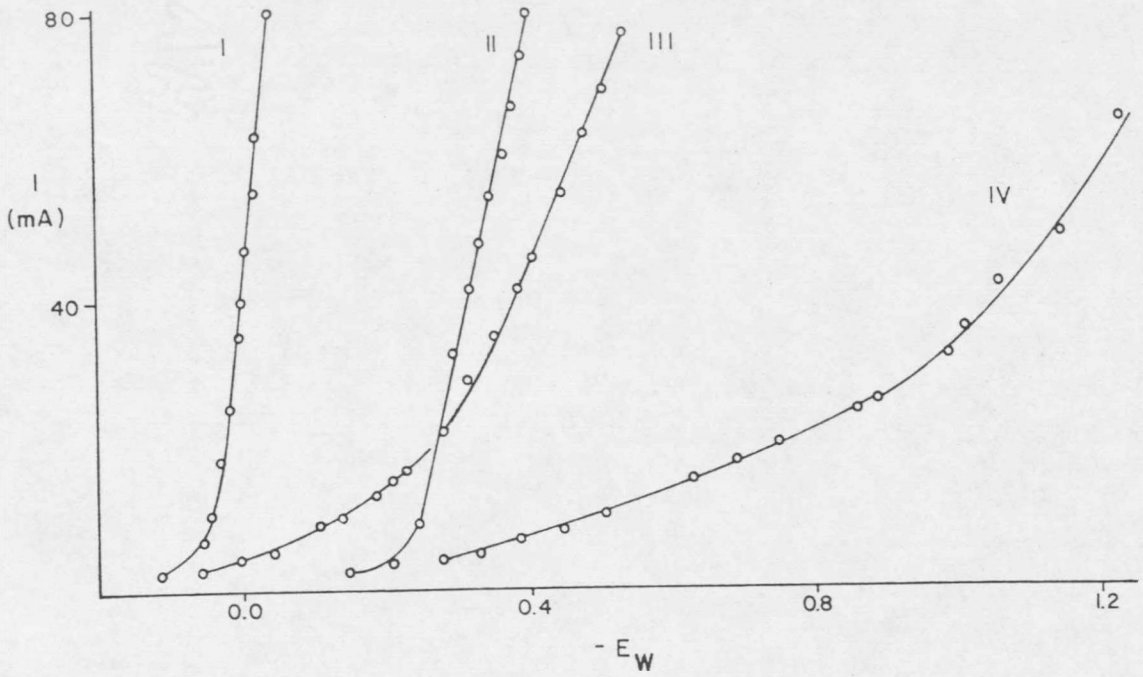

Figure 23. Cell Current versus Working Electrode Potential for Different Aluminum Pretreatments.

Treatment	E_B, V vs Cd(Hg)
(I) Al, steel wool, pH 0.5	+0.1
(II) I exposed to air for 2-3/4 hours	-0.2
(III) Stainless steel	-0.05
(IV) Al, pH 0.5	-0.2

characteristics. Aluminum oxide was noted to be an insulating film with limited penetrability. As an oxide layer is formed over the aluminum surface, a greater (more cathodic) potential would be required to get electrons to transfer across this surface oxide. This is nicely demonstrated with curves I and II. The electrodes used to generate curve I were exposed to the air after being thoroughly dried. Exposure time was 2-3/4 hours. During this time the surface of the aluminum is expected to be oxidized. Returning this oxidized electrode to the electrolysis cell, the breaking potential for the reduction of $Fe(acac)_3$ is offset by 300 mV, from +0.1V originally to -0.2V. This overpotential reflects the difficulty of passing an electron across an insulting layer. This history of the aluminum electrode is important in producing reproducible curves.

Curve III of Figure 23 is that for reducing $Fe(acac)_3$ with a stainless steel working electrode. This curve is not adversely affected by the previous history of the stainless steel electrode since working electrodes pretreated with acid and with no pretreatment at all gave nearly indistinguishable curves.

The second phase of the examination was to observe the current-time behavior for aluminum electrodes during the reduction of $Fe(acac)_3$ as a function of pretreatment. Figure 24 demonstrates the current-time behavior for the reduction of $Fe(acac)_3$ at various pretreated aluminum working electrodes. Both the magnitude and the duration of

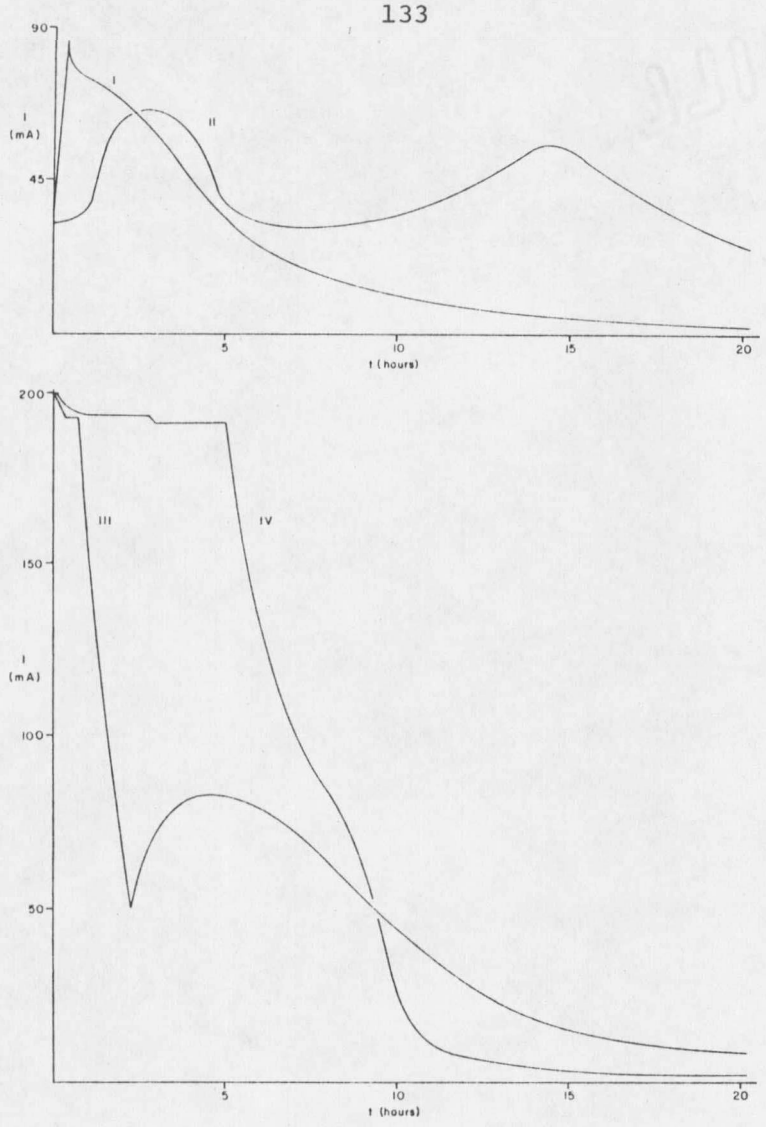

Figure 24. Cell Current versus Time Behavior for Reduction of $Fe(acac)_3$ at Various Pretreated Aluminum Working Electrodes. E_{ref} = -0.9V vs Cd(Hg). (I) no pretreatment; (II) 0.03N HCl for 15 min.; (III) 0.3N HCl for 15 min.; (IV) 3N HCl for 15 min.

the current reflect the effectiveness of acid washing. The untreated working aluminum electrode required initial activation before electrons crossed the solid/solution interface. No curve B was observed. Even a mild acid pretreatment improved the situation. Again, an apparent activational process occurred before the current reached its initial peak. Curve B also appeared suggesting that the second electron transfer could occur to form enough plated iron so that a current increase was observable. Curve 3 represents the standard pretreatment procedures used throughout most of this work on the three-electrode system. The 3N HCl pretreatment provided a sufficient amount of working electrode area to maintain a high current. Curve B may be partially concealed beneath this high sustained current appearing as a shoulder in this figure. The history of the electrode affects the solution reduction of iron (III) to iron (II) and the plating process as evidenced by curve B.

Base Electrolyte

The effects a base electrolyte has on the solvent medium have been classified by Sawyer and Roberts into the following categories (96):

(a) It regulates the cell resistance and mass transport by electrical migration.

(b) It may control or "buffer" the level of hydrogen ion activity in solution.

(c) It may associate with the electroactive solute such as complexing with the metal ion before or after electron transfer.

(d) It may form ion-pairs or micellar aggregates with the electroactive species.

(e) It determines the structure of the double layer.

(f) It may impose positive or negative potential limits on the system due to its own redox properties.

Each of these categories are discussed by Sawyer and Roberts and will not be elaborated on here. The iR effect, specific adsorption, and association phenomena are of interest for this report.

For most organic solvents, quaternary ammonium salts are used to reduce the high incipient resistance of the organic solvent. This reduction of the internal resistance is improved with reasonably high concentrations of the base electrolyte. Table XVII gives the solubility of various quaternary salts in DMF as well as the specific resistance of the solvent for a particular concentration. The choice of conditions for an electrolysis cell is to reduce the internal resistance of the solvent as much as possible. Tetraethylammonium bromide, TEAB, was used as the base electrolyte for all the preparative electrolysis cells except where otherwise indicated. To increase the

anodic potentials available for oxidation scans with the polarographic cell, the perchlorate salt was used in place of the more readily oxidized bromide (143).

Table XVII. Solubility and Specific Resistances for R_4NX salts in DMF (96)

R_4NX	Solubility g/100 ml of soln (concn, F)	Specific Resistance Ω cm (concn, F)
Et_4NClO_4	23(1.00)	52(0.60)
$n\text{-}Bu_4NClO_4$	79(2.29)	77(0.60)
Et_4NBF_4	27(1.24)	38(1.0)
$n\text{-}Bu_4NBF_4$	75(2.34)	69(1.0)
Et_4NBr	4.1(0.19)	--
$n\text{-}Bu_4NBr$	52(1.57)	106(0.60)

The alkyl ammonium salts have been noted to directly affect the nature of the electron transfer process (155-159). Meites (156) has noted that the quaternary ammonium cation adsorbs onto the surface of the mercury drop from a dme over a wide range of potentials, changing the halfwave potentials, the diffusion currents, and even the mechanism of the reaction. The effects depend on both the size and the concentration of the ammonium salt. Generally, as the size of the

tetraalkyl ammonium cation increases, the polarographic waves move to more negative potentials (157,159) and changes in the reversibility of the electron transfer step occur (158). This phenomenon has been attributed to the decrease in electron transfer rate constants as the electrolyte cation increases (157). Similar adsorption charactertistics are associated with the halide ion particularly at mercury (68). Even the toluene-p-sulfate anion is noted to influence the rate of electron transfer due to adsorption phenomena (160). A study of these interfacial characteristics of the supporting electrolyte on stainless steel or aluminum is beyond the scope of this dissertation.

The base electrolyte can also intercept products of the electron transfer process. Two specific reactions will be briefly considered. Carbanions generated in an electrolysis cell generally abstract a proton from the solvent to generate the saturated system. This route is particularly favorable when quaternary ammonium salts are available. The strong base, R^-, abstracts a proton from the quaternary salt and generates an olefin plus tertiary amine. This is the Hoffman elimination. This process is not possible for the tetramethylammonium cation, $Me_4N^{(+)}$. Several experiments were performed in which the concentration of TEAB was varied in order to observe any changes in octane production. An experiment was also performed in which Me_4NBr was used in a concentration equal to the concentration of TEAB in a standard

electrolysis cell. If octane formed via a Hoffman elimination process, a reduced amount of octane should be obtained with Me_4NBr. Furthermore, if a double layer phenomena existed and influenced the nature of the reaction, the change from ethyl to methyl quaternary salts should demonstrate these effects (159). Results for these experiments are given in Table XVIII. The percent reaction is seen to drop dramatically for a solution that is essentially saturated with TEAB and a solution that has no TEAB. This latter solution was still capable of conducting some current because of the high concentration of metal salt present in the electrolysis cell.

Reactions NII184 and NII188 are identically assembled reactions included with this table to demonstrate the fluctuations in the yields for identical reactions. Comparing the yields of products for reactions NII184, NII188, and those for reaction NII196 in which Me_4NBr was used as the base electrolyte, it is tempting to suggest that (1) the generation of coupled product may be influenced by specific adsorption effects of the tetraethyl ammonium salt and (2) the generation of octane is independent of the availability of a Hoffman elimination route. The first claim is not supported by the evidence since an adsorption effect by TEAB would be expected to increase with the concentration of this quaternary ammonium salt. At some critical surface coverage, the effect of adsorption on the generation of coupled product should be constant so that a constant yield of coupled

Table XVIII. Effects of Base Electrolytes

Reaction No	NII184	NII188	NII190	NII192	NII193	NII194	NII196
Base Electrolyte (Concn, F)	TEAB (0.08)	TEAB (0.08)	TEAB (0.16)	TEAB (0.24)	TEAB (0.04)	No TEAB	TMAB (0.08)
Working Electrode	606IT6(Al)	606IT6(Al)	606IT6(Al)	606IT6(Al)	606IT6(Al)	606IT6(Al)	606IT6(Al)
Counter Electrode	606IT6(Al)	606IT6(Al)	606IT6(Al)	606IT6(Al)	606IT6(Al)	606IT6(Al)	606IT6(Al)
E_{ref} (V vs Cd(Hg))	-0.90	-0.90	-0.90	-0.90	-0.90	-0.90	-0.90
% $C_{16}H_{34}$	59.0	35.9	22.1	60.8	24.6	2.45 mmoles	24.9
% C_8H_{18}	23.8	33.1	39.0	50.9	35.2	3.69 mmoles	40.5
% C_8H_{16}	10.9	15.5	21.1	12.5	19.6	1.52 mmole	12.9
% reaction	57.5	81.3	95.2	19.6	94.2	?	68.6
I_{max} (mA)	70	70	70	70	1	12	12
Resistor (ohms)	12	12	12	12	12	GP	GP
Potentiostat	GP	GP	GP	GP	GP		

product is obtained. However, the results indicate that at half the original concentration of TEAB and at twice the original concentration of TEAB, the effect of the concentration of the base electrolyte on the yield of coupled product is the same. A maximum in the yield of coupled product occurs in between these two concentration limits. This is not expected for an absorption effect.

The second claim is substantiated by the results. The generation of octane is independent of the availability of the Hoffman elimination pathway. However, the quaternary salt is important in the overall reaction since the lack of a base electrolyte sabotaged the generation of product, reaction NII194.

Another effect the base electrolyte may have on the system is associated with a coordinative relaxation process available for the reduction of $Fe(acac)_3$ in the presence of lithium salts (161,162). The general scheme for coordinative relaxation has been worked out by Murray et al. (161). The proposed reaction for this process with reduced $Fe(acac)_3$ and lithium ions was presented by Heineman (162).

$$Fe(acac)_3^{1-} + 2Li^+ \rightarrow Fe(acac)_2 + Li_2(acac)^+$$

Such a process may increase the concentration of $Fe(acac)_2$ which may establish a higher concentration of reducible Fe(II) ions. Table XIX

Table XIX. Added Inorganic Base Electrolytes

Reaction No	NII198	NI273	NI289
Base Electrolyte	TEAB + $LiNO_3$	TEAB + NaBr	TEAB + KBr
Working Electrode	606IT6(Al)	Al(unk)	Al(unk)
Counter Electrode	606IT6(Al)	Al(unk)	Al(unk)
E_r, V vs Cd(Hg)	-0.90	1.5 E_{APP}	1.5 E_{APP}
% $C_{16}H_{34}$	44.4	29.5	14.3
% C_8H_{18}	26.0	15.0	17.2
% C_8H_{16}	15.2	5.2	3.9
% reaction	81.0	95.3	43.8
I_{max} (mA)	70	53	40
Resistor (ohms)	12	--	--
Potentiostat	GP	HK	HK

gives the results for added cations. Sodium bromide, NaBr, and potassium bromide, KBr, were added to a two-electrode constant applied potential electrolysis cell. The yields are within the range of yields usually recorded for such cells, see Table VI. The lithium nitrate, $LiNO_3$, may have influenced the electrolysis reaction. Considering reaction NII188 of Table XVIII which is identical to reaction NII198 of the above table except that LiBr has been added to the latter, the yields of products between these two cells are different. This comparison can be made because the percent reaction for both systems are the same. The coupled product is seen to increase with added LiBr at the expense of the monomeric alkane. Unfortunately, the range of yields established for this system without added LiBr is sufficiently great to reduce this observation to elements of conjecture and interpretation. Therefore, the lithium ion, although affecting the reduction of $Fe(acac)_3$ does not affect the production of organic product.

Solution Components

The concentration of the other solution components was varied with the intent of optimizing the yield of dimer. Only two other components fall into this category, the stabilizing ligand triphenylphosphine, Ph_3P, and the organic substrate, 1-octyl bromide. Results of experiments in which these components have been varied are given in Table XX. Triphenylphosphine appears to have no effect on the nature

Table XX. Effects of Varying the Concentration of Ph_3P and n-$C_8H_{17}Br$

Reaction No	NII184	NII186	NII187	NII188	NII195
Component	Ph_3P (0.095)	Ph_3P (0.00)	Ph_3P (0.191)	Ph_3P (0.095)	$C_8H_{17}Br$ (0.409)
Base Electrolyte	TEAB	TEAB	TEAB	TEAB	TEAB
Working Electrode	606IT6(Al)	606IT6(Al)	606IT6(Al)	606IT6(Al)	606IT6(Al)
Counter Electrode	606IT6(Al)	606IT6(Al)	606IT6(Al)	606IT6(Al)	606IT6(Al)
E_r, V vs Cd(Hg)	-0.90	-0.90	-0.90	-0.90	-0.90
% $C_{16}H_{34}$	59.0	34.4	42.2	35.9	18.0
% C_8H_{18}	23.8	32.1	28.8	33.1	46.0
% C_8H_{16}	10.9	17.1	11.8	15.5	11.9
% reaction	57.5	90.9	48.0	81.3	100
Resistor (ohms)	12	12	12	12	12
I_{max} (mA)	70	70	70	70	70

of the reaction. Reactions NII184 and NII188 are identical and therefore represent possible limits for the yields of coupled product. Removing all of the supporting ligand or doubling its concentration gave yields of coupled product that fell within the range established by reactions NII184 and NII188.

1-octyl bromide does appear to have an effect on the yield of dimeric product. Halving the standard concentration of 1-octyl bromide resulted in a decrease of hexadecane and an increase in octane production. This effect may offer some mechanistic evidence that suggests the generation of coupled product may represent the decomposition of a dialkyl iron species, the disproportionation of two performed organoiron species, or an attack by an organoiron intermediate on starting material. Increasing the available 1-octyl bromide would be expected to generate more coupled product. Unfortunately, doubling the concentration of 1-octyl bromide produced a heterogeneous solution. No further investigations were performed.

Total Current

The total current of the electrolysis cell can influence the product distribution. Low current densities were claimed to favor the production of $C_6H_5CH_3$ during the reduction of $C_6H_5CH_2\overset{+}{N}(CH_2CH_3)_3NO_3$ (138) although others claim there is no effect (141) when the reduction proceeds at a aluminum cathode. In the Kolbe oxidation, increased

current density favors coupling, while other coupling reactions are independent of the current density (143).

Of necessity, the total current becomes the diagnostic tool used in this system. If hot spots corresponding to exposed aluminum are generated which carry most of the current, the number of these hot spots remains undetermined. Secondly, plating is observed to occur with iron being deposited on the surface, the surface area of this new deposit also remains undetermined. The total current can be used as a measure of the effectiveness of a reaction as long as the same experimental set-up and electrode pretreatment is used (143).

The three-electrode potentiostat prepared by Dr. Geer can adjust the limiting current of the electrolysis cell by simply replacing two resistors of the potentiostat. This represents the easiest method of controlling the limiting current and was adopted to generate the data recorded in Table XXI. A general trend appears in that optimum coupling occurs when the total current is limited to approximately 70 mA, coupling being suppressed at either higher or lower total current levels. The pattern suggests that perhaps adsorbed alkyl species, presumably octyl radicals, are important to coupled product formation. Alternatively, the deposition of iron may be affecting the distribution of products. Perhaps a certain current density is required for a particular type of iron deposit which, when present, optimizes the conversion of coupled product. Both of these possibilities indicate

Table XXI. Total Current Effects on Three-Electrode Cell

Reaction No	NII121	NII139	NII167C	NII171	NII172
Base Electrolyte	TEAB	TEAB	TEAB	TEAB	TEAB
Working Electrode	606IT6(Al)	606IT6(Al)	606IT6(Al)	606IT6(Al)	606IT6(Al)
Counter Electrode	606IT6(Al)	606IT6(Al)	606IT6(Al)	606IT6(Al)	606IT6(Al)
E_e, V vs Cd(Hg)	-0.75	-0.80	-0.90	-0.90	-0.90
% $C_{16}H_{34}$	25.1	21.1	21.8	17.3	29.1
% C_8H_{18}	29.0	39.7	35.1	31.8	31.7
%C_8H_{16}	15.5	8.2	9.2	17.3	15.9
% reaction	75.0	76.3	100	100	100
Potentiostat	mHK	GP	GP	GP	GP
Resistor	--	3.3	3.3	4.7	6.8
I_{max} (mA)	410	200	200	145	98
HCl pretreatment	pH 0.5	pH 0.5	3N	pH 0.5	pH 0.5

	NII184	NII188	NII185
	TEAB	TEAB	TEAB
	606IT6(Al)	606IT6(Al)	606IT6(Al)
	606IT6(Al)	606IT6(Al)	606IT6(Al)
	-0.90	-0.90	-0.90
	59.0	35.9	25.9
	23.8	33.1	39.7
	10.9	15.5	13.1
	57.5	81.3	51.1
	GP	GP	GP
	12	12	27
	70	70	25
	pH 0.5	pH 0.5	pH 0.5

a contribution to coupled product formation this is essentially a heterogeneous mechanism.

Spectroscopic Studies

The discussion has developed about the theme of understanding the electrochemical consequences of the proposed synthetic reaction. The scatter in product yields associated with the early two-electrode constant applied potential work suggested the need for a three-electrode system. The components of the electrolysis cell were examined in hopes of optimizing the yield of coupled product generated in this synthetic scheme but, unfortunately, the wide scatter of results for seemingly duplicate reactions in both the two- and three-electrode cells reduced the value of this attempt. The solution components had less of an effect than did the electrode material, the history of the electrode, and the total current flowing through the cell. This problem of reproducibility is elusive. For all of the reactions examined, the reaction leads to the same isolated products in widely varying distributions. This facet of the problem suggests that whatever mechanism is postulated, a common intermediate exists in all the systems in order to generate the same products. This is a convenient hypothesis for it provides a reasonable argument concerning the product distribution. As the concentration of this intermediate changes, so will the distribution of the products.

The theme for the majority of this work has been the generation of a solution organometallic which proceeds to generate the indicated products. The assumption of a homogeneous species was reinforced by observing a new solution chromophore during the reduction of $Fe(acac)_3$ in the presence of 1-octyl bromide using a two-electrode constant applied potential electrolysis cell. Figure 25 demonstrates the transition from a solution of $Fe(acac)_3$ at the onset of the electrolysis to a solution hosting the new chromophore at the termination of the electrolysis. The absorbance maximum for $Fe(acac)_3$ in DMF occurs at two wavelengths, 353 nm and 435 nm. The literature reports these maxima to occur at 353 nm and 437 nm in chloroform (163). The agreement for the system under investigation with the literature values for $Fe(acac)_3$ is quite satisfactory.

The new solution chromophore was observed to have its absorbance maximum at 367 nm. The observance of this solution chromophore offered encouragement to suggesting that it represents a possible homogeneous reagent that was postulated to form in this system. The formation of this chromophore was independent of the Ph_3P in that it appeared in a reaction using a two-electrode electrolysis cell that was not charged with Ph_3P. If the chromophore represents an organoiron species, its stability is not a function of the Ph_3P also present in the system. Secondly, two aluminum electrodes were used, but the alloy was not known. Using the 606IT6 aluminum alloy for electrode material resulted

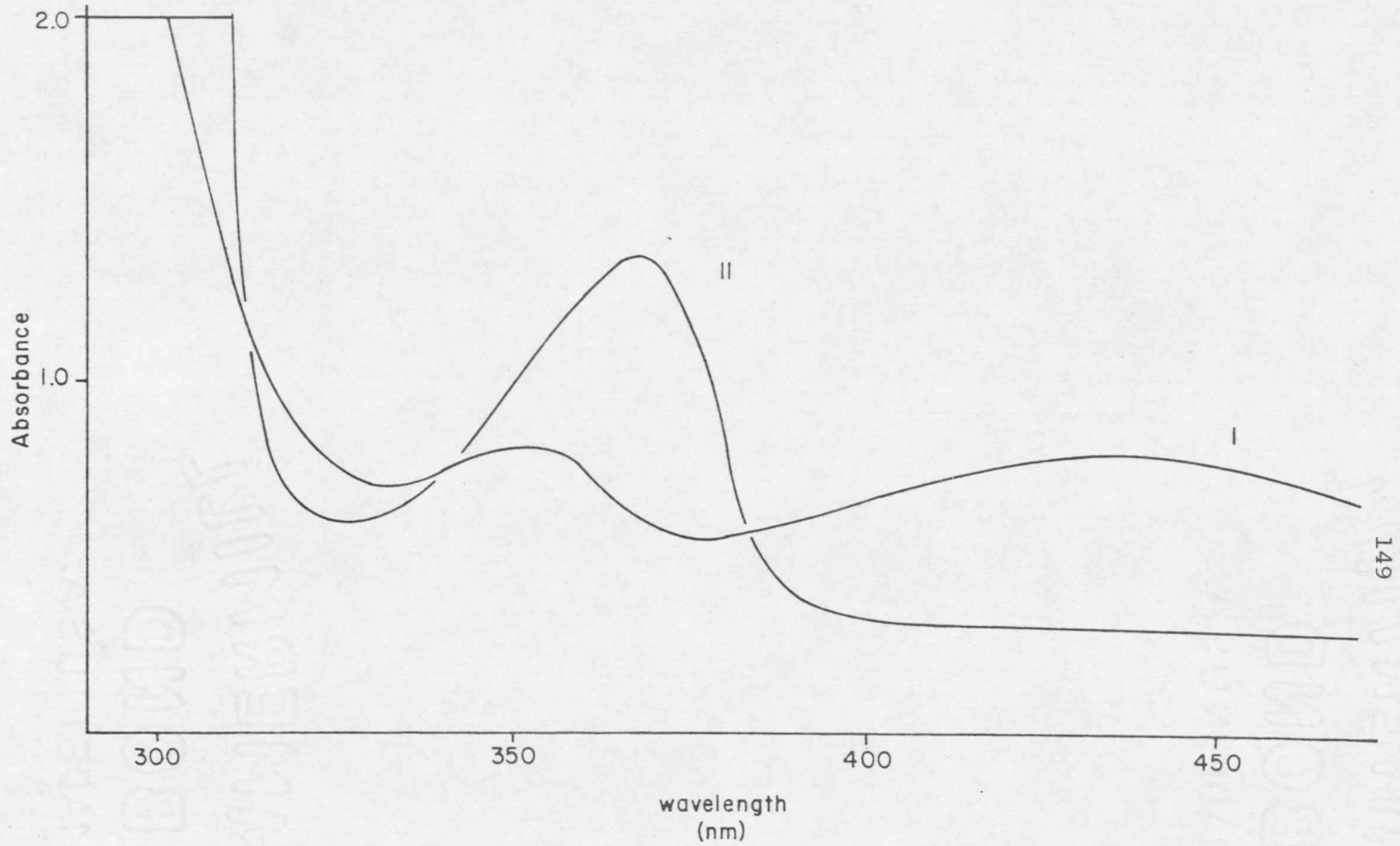

Figure 25. Absorbance Spectra Before (I) and After (II) Electrolysis of $Fe(acac)_3$ with $1\text{-}C_8H_{17}Br$ at Aluminum Electrodes in Two-Electrode Constant Applied Potential Electrolysis Cell.

in a decrease in the absorbance spectrum of this new chromophore suggesting that it may originate with the counter electrode.

The chromophore at 367 nm may be a simple salt of reduced $Fe(acac)_3$. Heineman et al. (162) have reported the spectral properties for the reduced forms of $Fe(acac)_3$ generated at optically transparent thin electrodes (solvent: CH_3CN, 0.1M in both $LiClO_4$ and TEAP). The wavelengths at which absorbance maxima occurred for the various forms of $Fe(acac)_3$ are given in Table XXII. The shorter

Table XXII. λ_{max} for $Fe(acac)_3$ and Reduced Forms (162)

Species	λ
$Fe(acac)_3$	353 nm, 430 nm
$Fe(acac)_2^{1+}$	352 nm, 485 nm
$Fe(acac)^{2+}$	353 nm, 540 nm
$Fe(acac)_3^{1-}$	346 nm, 470 nm
$Fe(acac)_2$	335 nm, 412 nm

wavelengths were read from a figure included in the paper and may be in error by as much as ±10 nm. Two absorbance maxima occur for each species. The general characteristics of these curves is that the absolute absorbance of both wavelengths are nearly identical. The solution chromophore at 367 nm in the electrolysis cell, Figure 25, does not have another absorbance maximum at longer wavelengths, therefore

it is considered as being a solution species that is not one of those included in Table XXII.

Several three-electrode electrolysis cells have been used to examine the generation of the 367 nm chromophore and any other spectral changes associated with the electrolysis. A complete listing of these electrolysis cells and the observed spectral properties of the respective solutions are included in Appendix A. Those systems that are germain to the arguments presented here will be repeated in the accompanying tables.

The chromophore of 367 nm may be the proposed organoiron species that forms in the solution during electrolysis. This premise has been shown to be false. An 1-octyl bromide-free solution of $Fe(acac)_3$ with aluminum electrodes of the 606IT6-alloy was electrolyzed for 24 hours. After this time a solution aliquot was examined. Table XXIII lists the results of the UV-VIS work. The chromophore at 367 nm is present

Table XXIII. Spectral Properties of an Electrolyzed 1-Octyl Bromide-Free Solution. Reaction NII157, 606IT6(Al)/606IT6(Al) Electrodes

Time	No R_8X 24 hours	R_8X added 36 hours
λ_1 (O.D.)	350 nm (0.48)	357 nm (0.50)
λ_2 (O.D.)	366 nm (0.43)	367 nm (0.51)

in the solution even when 1-octyl bromide is absent, therefore the chromophore cannot be the organometallic reagent. The addition of 1-octyl bromide to the solution appears to red shift the absorbance at the shorter wavelength, but for the moment, this spectral shift will not be considered.

The suggestion that the chromophore responsible for the 367 nm absorbance might be an Al-Fe adduct can be tested using other electrode material. If this adduct is responsible for product formation, its absence should limit or halt any generation of products. Stainless steel electrodes have already been used to establish improved reaction yields over similar electrolysis solutions using aluminum electrodes. These experimental observations have been used to rule out any contribution to product formation by such an aluminum-iron complex. However, spectral examinations of electrolysis solutions from cells having used stainless steel electrodes will support or refute the intermediary of the 367 nm chromophore in product formation. If this chromophore is not present in those electrolysis cells using stainless steel electrodes, it cannot be a participant in product formation. Figure 26 presents the uv-vis spectrum of a reduced solution of $Fe(acac)_3$ prepared using stainless steel electrodes. No chromophore having an absorbance maximum at 367 nm is present in the solution.

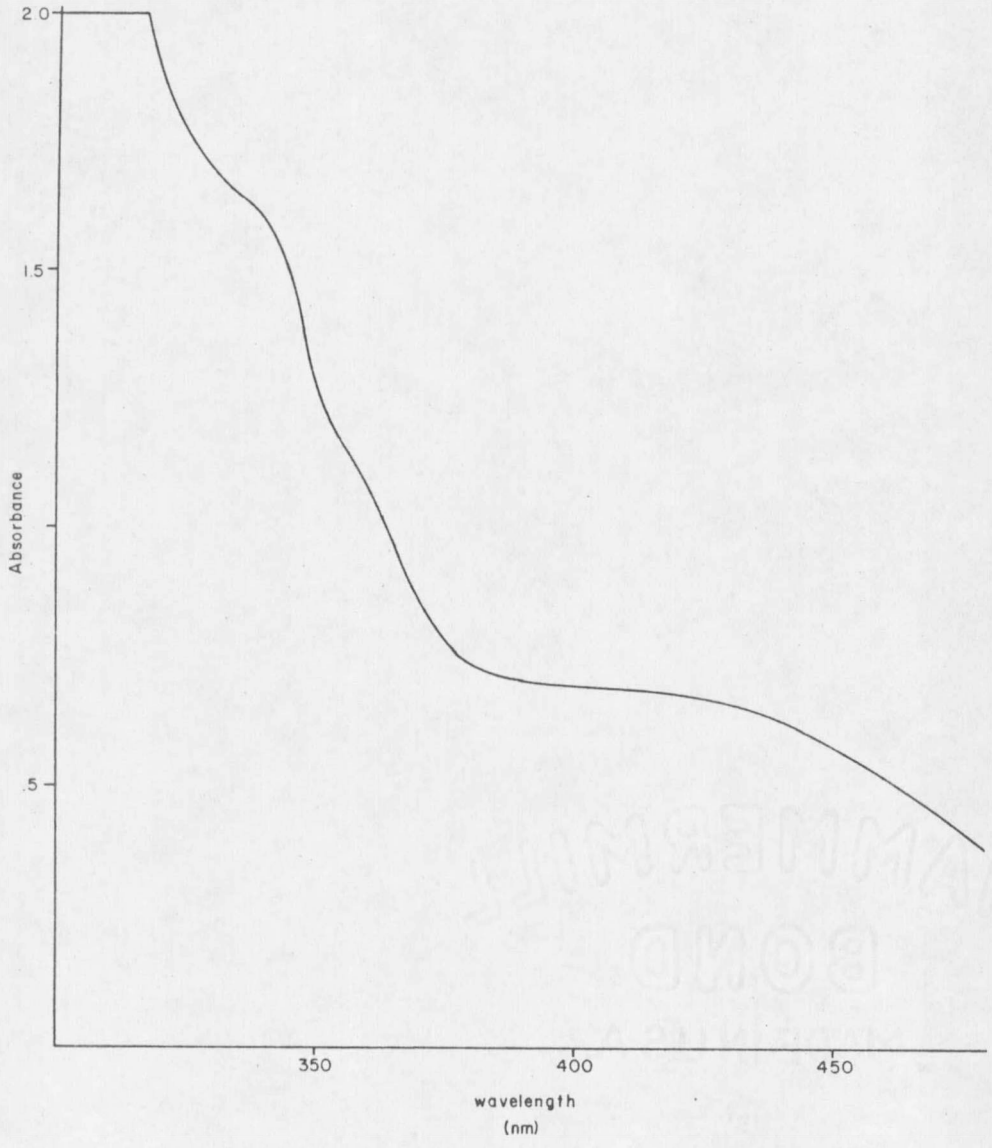

Figure 26. Absorbance Spectrum for Reaction NII146. Stainless steel electrodes used to reduce $Fe(acac)_3$ at E_{ref} = -0.9V vs Cd(Hg).

Two electrolysis reactions were performed using the mixed electrode system of aluminum and stainless steel. In one instance, the aluminum was the working electrode and in the other the stainless steel was the working electrode. Figure 27 displays the absorbance curves for these two cells after approximately twenty-one hours of electrolysis. A chromophore at 370 nm was found when the counter electrode was aluminum but not when the counter electrode was stainless steel.

Other attempts to discharge the proposition that the 367 nm chromophore was an Al-Fe adduct were not particularly successful. A solution free of both $Fe(acac)_3$ and 1-octyl bromide produce no current therefore there was no discharge of material from the counter electrode. The uv-vis spectrum was without distinction. Another cell was assembled which used an iron plated aluminum working electrode in an iron-free solution containing 1-octyl bromide. Some current did flow under these conditions, discharging ions from the counter electrode into the solution. A uv-vis spectrum of an aliquot of this solution showed that a chromophore at 377 nm appears, Figure 28. This peak is but a ripple on an absorbtion band and hence not very useful. Since the current in the cell was small, the discharge of material from the counter electrode would not be great.

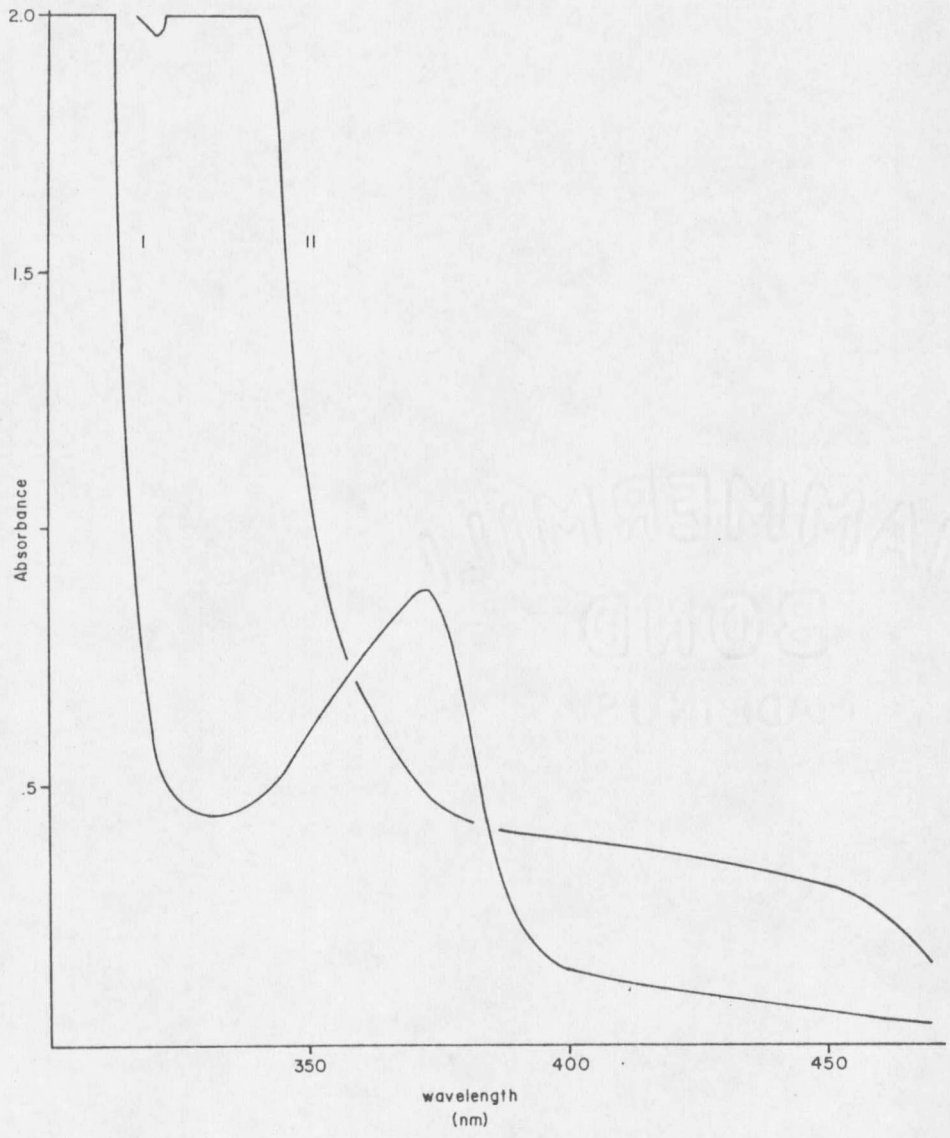

Figure 27. Absorbance Spectra for Reduction of $Fe(acac)_3$ with Mixed Electrode Systems. (I) Stainless steel working electrode, aluminum counter electrode of reaction NII173, (II) Aluminum working electrode, stainless steel counter electrode of reaction NII168A.

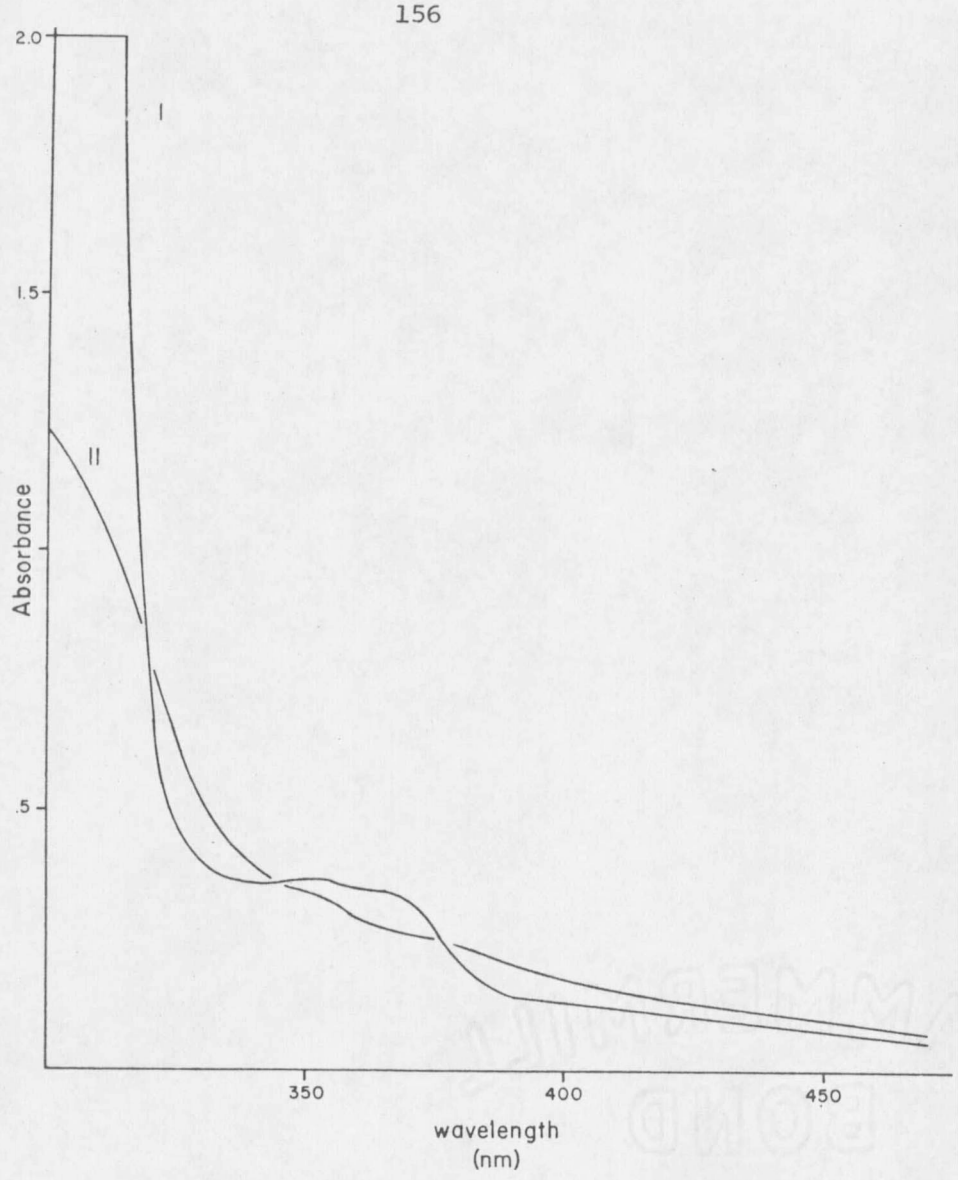

Figure 28. Absorbance Spectra of (I) An Electrolyzed $Fe(acac)_3$ Solution and (II) an Iron-Free Solution after Electrolysis Using an Fe-Plated Aluminum Electrode, Working Electrode and an Aluminum Counter Electrode.

The spectral characteristics of the two solutions using stainless steel counter electrodes, Figures 26 and 27, are very similar and independent of the working electrode material. This suggests, of course, a common origin to the chromophores. The spectral properties of these solutions are different than those for solutions using an aluminum counter electrode. An attempt at eliminating the effects of the dissolving metal electrode failed. A platinum counter electrode with a stainless steel working electrode was used in two electrolysis cells, one involving TEAP as the base electrolyte, the other TEAB. Table XXIV gives the spectral properties of these solutions. The spectral

Table XXIV. Spectral Properties of Solutions with a Pt Counter Electrode

Reaction No.	Base Electrolyte	Time	Absorbance	
			λ_1 (O.D.)	λ_2 (O.D.)
NII147	TEAP	6	354 (0.76)	438 (0.71)
		24	351 (0.70)	444 (0.60)
NII149	TEAB	24	354 (0.70)	437 (0.67)
		48	354 (0.63)	437 (0.60)

characteristics are sufficiently identical to suggest that the reduction of $Fe(acac)_3$ is being followed by its oxidation either chemically, NII149, or electrochemically, NII147.

The evidence to rule out an iron-aluminum adduct is not compelling. However, notice of the experimental conditions used in

obtaining these spectra indicate that no provisions have been established to eliminate traces of moisture or dissolved oxygen. The stability of an iron-aluminum adduct to water and air has not been reported although it may be assumed that it would be sensitive to air oxidation. The spectral properties of the solution containing the 367 nm chromophore are not time dependent even after exposure to air. This suggests that an air-sensitive chromophore is not present. Secondly, the absolute absorbance of this chromophore depends on the aluminum alloy used as the counter electrode. Since both alloys would be expected to discharge aluminum ions, this observation suggests that the chromophore is a trace constituent of the aluminum alloy. Finally, the near identical spectral properties for the two solutions using the stainless steel counter electrode which were different for solutions using aluminum counter electrodes also suggest that the chromophore originates from the counter electrode.

The spectral examination of the electrolysis solutions has established the following conclusions:

(1) $Fe(acac)_3$ is consumed during the electrolysis.

(2) The chromophore at 367 nm is not an organoiron species. The peak appears with or without Ph_3P, with or without 1-octyl bromide, and does not appear when a stainless steel counter electrode is substituted for the aluminum counter electrode.

(3) The stainless steel counter electrode changes the electrolysis solution spectrum in a way that is different from the aluminum counter electrode and independent of the working electrode.

(4) The 367 nm chromophore is due to the aluminum counter electrode and is dependent on the alloy.

(5) The 367 nm chromophore is not sensitive to air oxidation.

These conclusions suggest that the chromophore at 367 nm is generated from material that is being discharged into the solution from the sacrificial aluminum counter electrode. The material is a constituent of the aluminum alloy, but is not aluminum ions.

Homogeneous vs Heterogeneous

The spectral examinations of the electrolysis solutions have not established the presence of a chromophore in solution which may be critical to product formation. This does not refute the possibility that a solution species is respondible for product generation since this species may (1) have no absorbance throughout the examined electromagnetic spectrum or (2) be in such low concentration that even if it could adsorb in the wavelength region explored, it was too dilute to establish its presence. Therefore, the homogeneous reagent is not eliminated. From Table XVI, reaction NII129, we are assured that the solution species that may lead to product formation is not an iron (II)

complex. The working electrode potential was just cathodic of the breaking potential for $Fe(acac)_3$ at stainless steel electrodes. The current in this reaction fell smoothly with time, but no products were isolated. The working electrode potential was not cathodic enough to further reduce iron (II), therefore the solution ion, iron (II), is not capable of product formation.

Some very interesting clues have been established that suggest a heterogeneous system may be operative in product formation. The dependence of product formation on the nature of the electrode material suggests that the electrode may participate in the reaction with stainless steel working electrodes improving the yield of coupled product over identical reactions using aluminum electrodes. Secondly, when the surface area of the stainless steel electrodes was reduced to half the normal area, more effective coupling, as evidence by increased dimer production, prevailed. This may be appreciated for a system involving adsorbed surface radicals since bimolecular formation of coupled product has been noted to be favored with high current density and high surface coverage (143). Finally, the electrolytic behavior of two stainless steel electrodes without $Fe(acac)_3$ resulted in apparent autocatalytic behavior of the current, Figure 21 and Table XIV, reaction NII178. This current time behavior suggested that possible organoiron surface species were formed on the stainless steel working electrode which was readily reduced and in so doing,

caused the current to flow through the cell. This is further supported by the formation of products at a stainless steel working electrode and aluminum counter electrode, but not the reverse combination, Table XIV.

A critical test is required to establish whether or not a reduced form of the metal exists in the solution and is responsible for the production of products. Such a test was designed by preelectrolyzing an $Fe(acac)_3$ solution with aluminum electrodes in a solution that did not contain 1-octyl bromide. The three-electrode electrolysis cell was used and operated at -0.90V as the control potential. Spectral examinations of this solution, reaction NII160, after 48 hours demonstrated the presence of the 367 chromophore.

NII160	24 hours	350 (0.48)	367 (0.30)
	48 hours	351 (0.37)	367 (0.34)
$n\text{-}C_8H_{17}Br$	48 hours	362 (0.34)	367 (0.31)
NII161	48 hours	351 (0.34)	377 (0.25)

1-Octyl bromide was added to this preelectrolyzed $Fe(acac)_3$ solution after the electrodes were removed, and the solution stirred for 48 hours. The iron-plated aluminum working electrode, counter electrode, and reference electrode were placed in an iron-free solution containing 1-octyl bromide. This solution was electrolyzed for 48 hours and is designated reaction NII161. The yields of the two reactions are

reported in Table XXV. The product distribution is quite dramatic. Products were only obtained in the solution that had the iron-plated working electrode. No products were available in the solution stirred with the 367 nm chromophore. This chromophore was present in both reaction vessels at the end of the reaction.

Table XXV. Homogeneous vs Heterogeneous Reaction

Reaction No	NII160	NII161
Description	$1\text{-}C_8H_{17}Br$ stirred with preelectrolyzed $Fe(acac)_3$	Fe-plated Al electrodes in Fe-free solution of $1\text{-}C_8H_{17}Br$
% $C_{16}H_{34}$	none	48.8
% C_8H_{18}	<0.04 mmoles	27.0
% C_8H_{16}	<0.06 mmoles	8.4
% reaction	--	37.0

Two attempts at plating iron onto a platinum foil electrode were attempted. The difficulty of plating iron on to the platinum surface was associated with the poor adhesion of the plated material onto the platinum. The results of these two attempts are given in Table XXVI. These results are encouraging. The plated iron surface was effective in generating products albeit in very low yields. The plating of the iron onto the surface of the platinum foil was not extensive, therefore the reaction was limited. The difficulty, as noted, is the generation of a

plated surface on the support that will be sufficiently cohesive to allow for further plating. Platinum was not this surface.

Table XXVI. Fe-Plated Platinum Working Electrode

Reaction No	NII179	NII183
E_r, V vs Cd(Hg)	-0.90	-0.90
% $C_{16}H_{34}$	0.96 mmoles	20.1
% C_8H_{18}	1.46 mmoles	--
% C_8H_{16}	0.36 mmoles	--
% reaction	∿4.5%	∿3.7%

A heterogeneous reaction is supportive of an interpretation alluding to the need for a common intermediate. If a plated surface is necessary, then the lack of uniform generation of this surface is associated with the wide distribution of products for seemingly identical reactions. Allmand (107) has noted that different metals can be deposited in very different conditions of aggregation and satisfactory correlation of the experimental changes in the electrolysis conditions with the type of surface generated does not exist. High concentrations were associated with improved plating. High current densities cause the solution in the immediate vicinity of the working electrode to have lower ionic strength than in the bulk solution and this condition generally leads to poorer deposits. The observation that the total current attained in the electrolysis cell had an effect on the distribution of products is in agreement with this statement,

i.e., lower current densities (limiting current) gave better plating and hence higher product yields, particularly dimeric product. The importance of a uniform iron surface has been demonstrated in the literature during examinations of the redox couple $Fe(CN)_6^{3-}/Fe(CN)_6^{4-}$ at an iron electrode (164). Olmedo et al. (164) observed that reproducibility and self-consistency of results were only possible after extreme care was taken to prepare an iron surface.

The iron plated aluminum working electrode was examined using the scanning electron microscope. Figures 29 and 30 are micrographs of the surface of two different plated electrodes obtained under identical electrolysis conditions. Figure 29 shows that this surface of the electrode is covered by platelets of deposited material. The yields for this reaction, NII184, are given in Table XXVII. The coupled product was formed in high yields. Figure 30 shows the micrographs of another plated working electrode obtained from reaction NII188 supposedly run under identical conditions as reaction NII184. Although platelets of deposit are also available, the majority of the surface is covered by a grandular material. The yields for this reaction are also given in Table XVII. For this latter reaction, the yield of coupled product is reduced. Thus, a correlation appears to exist between the yields of coupled products and the nature of the surface deposit. The deposit has been identified by x-ray

Figure 29. Scanning Electron Micrograph of the Iron-Plated Aluminum Working Electrode for Reaction NII184. (A) 700x; (B) 2000x.

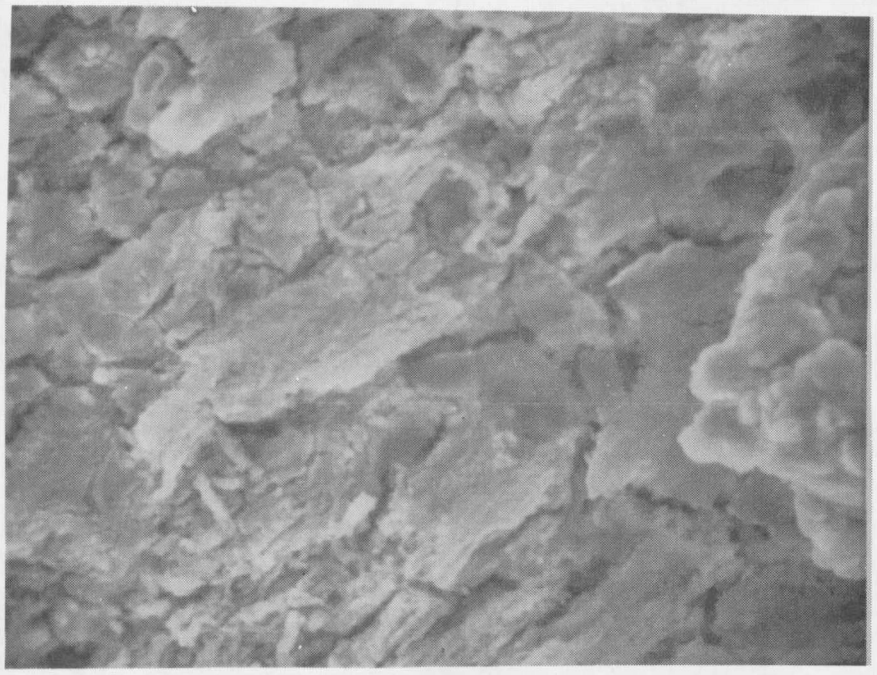

A

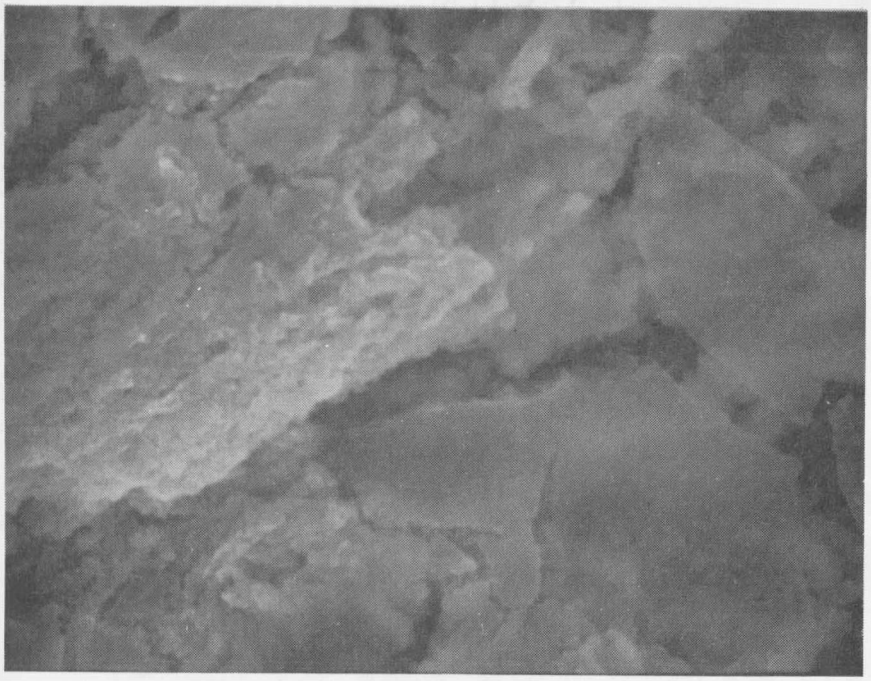

B

Figure 30. Scanning Electron Micrograph of the Iron-Plated Aluminum Working Electrode for Reaction NII188. (A) 700x; (B) 1000x.

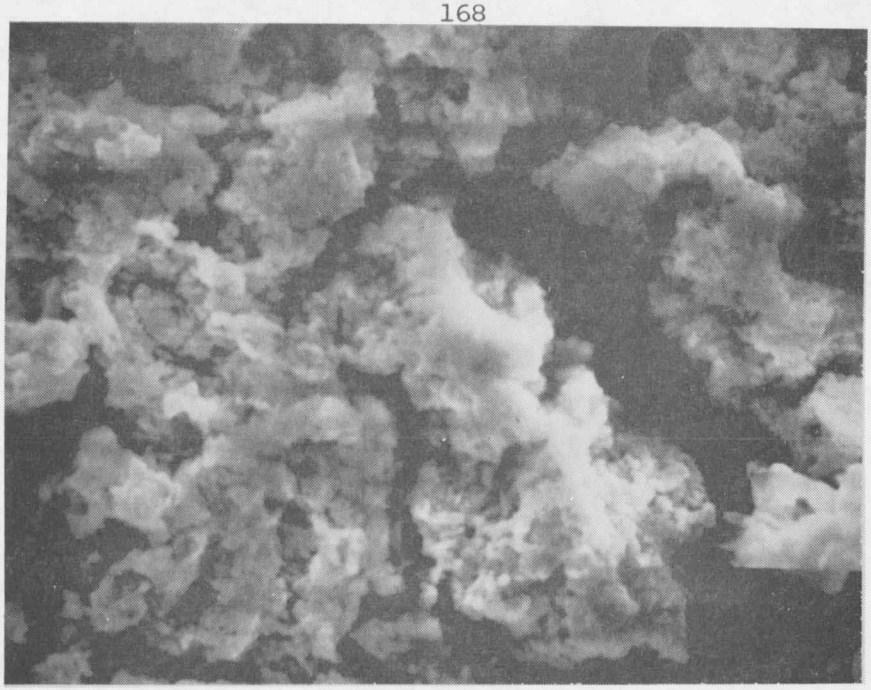

A

B

Table XXVII. Product Distribution for SEM Examined Electrodes

Reaction No	NII184	NII188
Base Electrolyte	TEAB	TEAB
Working Electrode	606IT6(Al)	606IT6(Al)
Counter Electrode	606IT6(Al)	606IT6(Al)
E_{ref}, V vs Cd(Hg)	-0.90	-0.90
% $C_{16}H_{34}$	59.0	35.9
% C_8H_{18}	23.8	33.1
% C_8H_{16}	10.9	15.5
% reaction	57.5	81.3
I_{max} (mA)	70	70.

fluorescence to be mainly iron with bromine present at reasonable levels and some copper, probably from the material discharged by the aluminum counter electrode.

A brief survey of the problem of metal-solution interfaces (electrodics) will be presented to establish the complexity of this problem which can influence the product yield. West (165) has summarized much of this information. For an anode, dissolution normally occurs at chemically active sites that are associated with crystallographic dislocations at the surface as well as general discontinuities from severing a crystallographic plane at the solid surface. The latter is responsible for steps and kinks on the surface. Cathodic deposition is not so straightforward. The incoming metal ion is complexed by either ligands or solvent molecules as it exists in the solution. The ions may be totally reduced at the chemically active sites that are analogous to those for dissolution, or the ions may be only partially reduced. In the latter instance, the ion can be reduced anywhere at random on the surface and then wander about on the surface until it reaches a suitable discontinuity such as a step or a kink. The initial reduction appears to generate an adatom with surface mobility. In both cases, metal crystal growth will most likely occur along growth edges. Thus, it is possible for the original electrode surface to exert an epitaxial effect on the nature of

the deposit. If random deposition is preferred during the electrolysis and surface migration eliminated, new crystal grains can be established from the nucleation initiated by the adatom. Such surface growth generates grains of no particular orientation to those previously deposited resulting in small grain size. Direct deposition or indirect deposition with surface migration to a crystallographic plane are important processes in growing a smooth surface. As noted above, high current densities and/or high overpotentials limit the crystallographic nature of the deposits and growth becomes nodular. If an electrolyte is surface active, the material generally adsorbs at growth edges affecting the deposition of the solution ion even at low overpotentials. Thus, although the investigation of electrolysis conditions appeared to be uninfluential in determining the distribution of products, other reagents may sufficiently perturb the surface deposition of iron that no products are found.

Generally, "non-crystallographic" deposits of a plated metal, i.e., one that allows for surface migration, usually results in a bright deposit. Although other complicating factors in the electrolysis cell may change the nature of the deposit, all of the iron plated electrodes appeared black to dark brown. This suggests that epitaxial effects of the supporting electrode are possible. Such a proposition agrees favorably with the observed effects of electrode history, pretreatment, and material. The aluminum oxide surface is an insulating

surface although electron transfer may proceed through pores or fractures in thin spots of this oxide coating. The high overpotential of this surface to iron ion reduction precludes the deposition of iron at -0.9V. When the electrode is treated in acid, the chemical etching can clean the surface. The reduction of the proton to hydrogen gas is readily observed as bubbles of gas form on the surface of the aluminum. The extent of this chemical degradation of the surface influences the magnitude of the total current and the deposition of iron. The former increases due to the increased surface area of the electrode which is active to electron transfer. This activity is increased by degradation of the oxide layer. The influence of chemical cleaning of the surface on the deposition of iron is found in the appearance of curve B during the reduction of $Fe(acac)_3$ at an aluminum electrode. Only if the surface is clean will curve B and hence iron deposition occur.

Electrolytic deposition of iron is difficult due to its inertness (165), therefore adherent electrodeposits are formidable to prepare. The history of the aluminum surface affects the nature of the deposit, epitaxial or non-crystallographic. The deposition of iron is difficult. These two statements are suggested to be the governing problems in the formation of coupled product. The control of the surface, cited earlier to be of prime importance in establishing reproducibility and self-consistency in the results, was not

carefully established. Identical electrolysis solutions gave different product distributions because the surface of the aluminum electrode and hence the nature of the iron deposit was not properly controlled.

Can these different surface structures affect the product distribution? Somorjai (165-169) has demonstrated that for platinum single crystals with varying surface structures such as terraces, steps, kinks, and adatoms, the chemistry of bond making and bond breaking varies. Atomic steps appear to be preferred surface sites for breaking hydrogen-hydrogen or carbon-hydrogen bonds. Kinks are also good for carbon-carbon bond breaking. Terraces are essentially the idealized smooth surfaces and very little occurs on these surfaces at moderate temperatures and pressures. If the surface structure of the iron deposit changes from one electrolysis cell to another, a different density of these surface species, i.e., kinks, steps, terraces, and adatoms, can occur which will change the distribution of products. Since steps and kinks and adatoms represent surface species with fewer nearest neighbors than terrace atoms, they can be classified as coordinatively unsaturated d^8 iron (0) centers and thus can intercept reactive organic substrates.

The picture that emerges involves a heterogeneous transformation of 1-octyl bromide to coupled and disproportionated products. The product formation process is preceded by the electrochemical

deposition of iron onto the working electrode as evidenced by the presence of curves A, B and C in the macroelectrolysis using aluminum electrodes. The nature of this surface establishes the distribution of product; the presence of this surface establishes the formation of products. The optimization of coupled product yields was inappropriately examined by adjusting gross solution parameters rather than exploring the subtitles of surface conditions.

Product Formation vs Time

Work performed with the two-electrode cell run with constant applied potential demonstrated that the product formation followed the current-time curve, i.e., octane, octene, and hexadecane were produced in greater quantities as the current increased. All of the work performed with three-electrode electrolysis cells involved isolation of the products to assess the yields using an internal standard procedure. This technique was used to monitor the production of product versus time for a three-electrode cell using aluminum electrodes. Figure 31 demonstrates such a plot for reaction NII203. The disappearance of 1-octyl bromide is initially very slow but after an hour its consumption increases. This hour delay fits well within the framework of a heterogeneous reaction. The time delay may correspond to time required for forming the iron deposit on the working electrode. As this deposit increases, the turnover of starting material increases.

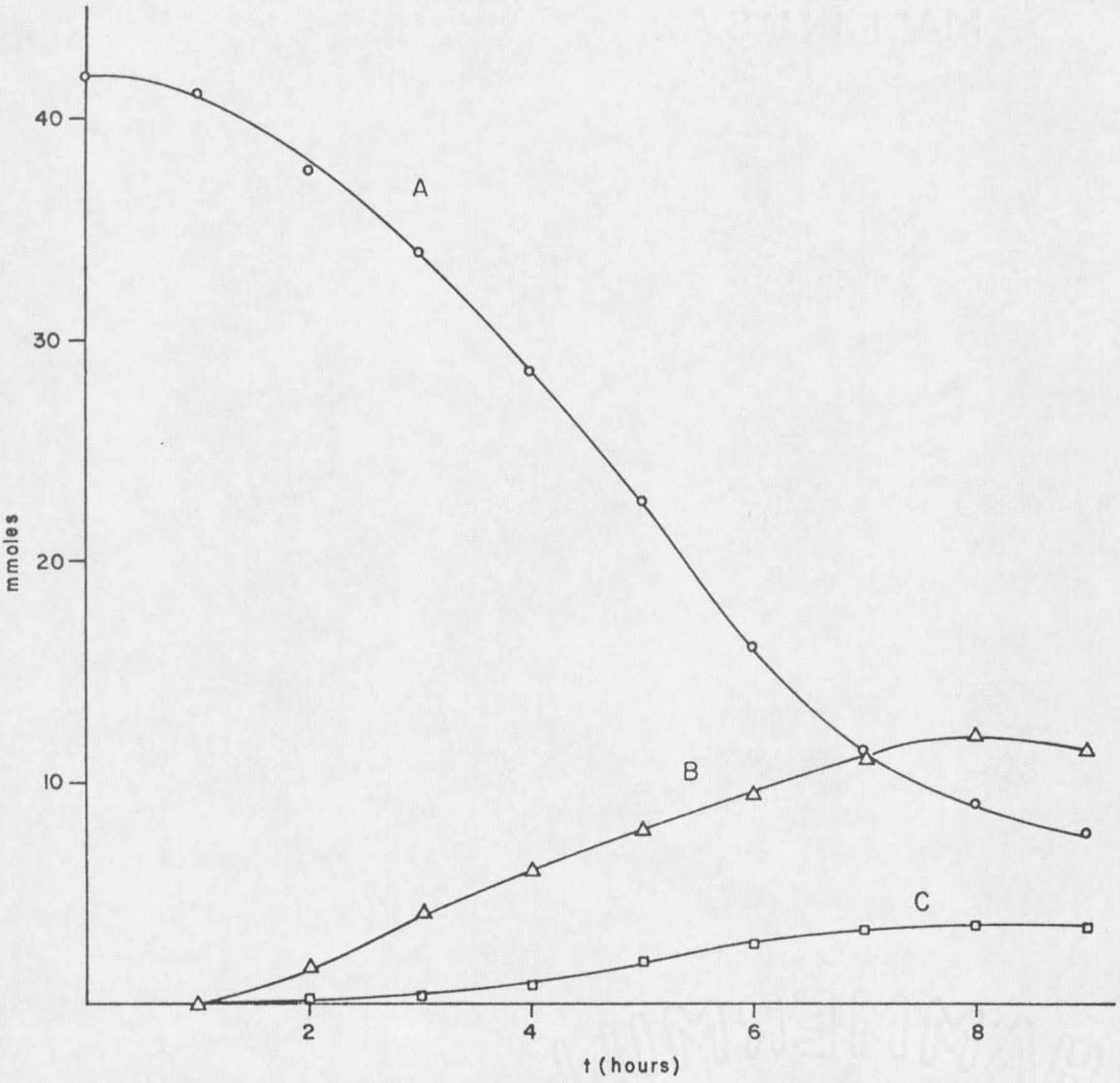

Figure 31. Formation of Products versus Time. (A) Loss of 1-$C_8H_{17}Br$; (B) Production of C_8H_{18}; (C) Production of C_8H_{16} and $C_{16}H_{34}$.

Octane is formed independently of 1-octene and hexadecane, these latter two being almost indistinguishable. The yield of products never equals the amount of consumed 1-octyl bromide, a phenomenon that has plagued much of this work. Peters (159) has noted that the presence of trace amounts of N-methyl formamide are effective radical traps for the consumption of any alkyl radical. This could lead to the 'loss' of starting material, since no products associated with dimer formation between N-methyl formamide and octyl radicals were sought.

Water can react with electrochemical intermediates causing the reduction of an organic substrate to be irreversible although in strictly anhydrous solvents electron transfer to the organic substrate is reversible (170). Water may influence the nature of the electrode deposit or intercept organometallic intermediates. Zuman has noted that traces of water in DMF do not act as proton donors (171) suggesting that the effects of any water are not due to the presence of the proton. Peters (159) noted that DMF stored over 4A molecular sieves, the same size used for the DMF in this work, contains about 130 ppm of water. If the water does not act as a strong acid in DMF, it may still affect the chemistry within the electrical double layer. Peters (159) felt that an alcohol was formed during the reduction of

alkyl halide at mercury in DMF. The formation of ROH from RX was via an S_N2-type reaction activated by the electric field of the mercury cathode. The loss of 1-octyl bromide may be associated with the generation of an alcohol from the dissolved water.

The independent formation of octane may be partially accounted for by several processes.

$$R\cdot + CH_3NHCH(=O) \rightarrow RH + CH_3\dot{N}COH \qquad (1)$$

$$R\cdot + H_{\text{Fe Soln.}} \rightarrow RH \qquad (2)$$

$$R\cdot_{ads} + H\cdot_{ads} \rightarrow RH \qquad (3)$$

$$R^- + Et_4N^+ \rightarrow RH + CH_2CH_2 + Et_3N \qquad (4)$$

The free radical attack of an alkly radical on traces of N-methyl formamide was noted by Peters (159). Reaction 2 can occur in this system if it is recalled that the overpotential for hydrogen evolution is greater at aluminum than at iron, Table V. With an iron deposit, protons from the available water can be reduced. This is

$$2H^+ + 2e^- \rightarrow H_2$$

particularly convenient if the hydroxide ion forms an alcohol with the starting material within the electrical double layer. However, at iron, hydrogen dissociatively adsorbs and forms a solid gas

solution of hydrogen atoms. Because the reaction is surface sensitive, the alkyl halide must migrate through the diffuse layer

$$H_2 \rightarrow 2H^{\bullet}_{\text{Fe-soln}}$$

and through the electrical double layer perhaps becoming dissociatively adsorbed onto the iron surface and therefore the surface effect (172). The adsorbed alkyl radical can now react with the solid solution hydrogen atom from the hydrogen discharge and form octane. Alternatively, an olefin can be formed by β-hydride migration forming an iron hydride

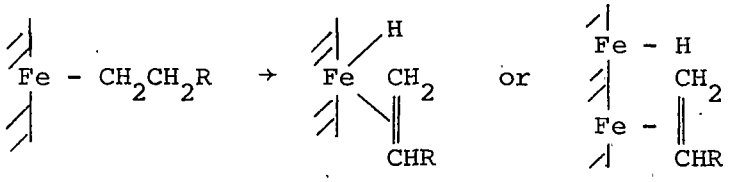

Homolytic cleavage of the iron-hydrogen bond can generate an adsorbed hydrogen atom which can subsequently react with the adsorbed alkyl species. Alternatively, the two systems, R-Fe and H-Fe, can disproportiate. Iron-hydrides are known making this a reasonable step (173-175). Fe(0) is also known to insert into a C-H bond via an oxidative addition reaction (47,176,177) again supporting the β-hydride elimination pathway. The Hoffman elimination process has been discussed and appears not to be important.

The formation of olefin and hexadecane at almost the same rate and quantity suggests some similarities in method of formation. One possible route is the two-site concept required to β-hydride eliminate or to couple two alkyl radicals. That is, octane can form by processes that only require the initial site of adsorption. On the other hand, a vacancy must be available on the metal center on which adsorption has taken place, or on a nearest neighbor such that β-elimination can occur. Similarly, coupling requires that either both alkyl radicals are on one metal center or occupy two metal centers of nearest neighbors. Again, two sites are related to the formation of dimer. Assuming all other rates of reaction are similar--a vast assumption indeed--the rate of formation of olefin and hexadecane will be different than the rate of formation of octane. Depending on the surface structure of the iron deposit the rate of production of olefin and dimer may be the same or different, as a comparison of the yields of hexadecane and 1-octene throughout this dissertation demonstrate.

The current increased rapidly when 1-octyl bromide was added to a preelectrolyzed solution of $Fe(acac)_3$ or $FeBr_3$. Examining the breaking potential of 1-octyl bromide at both a stainless steel working electrode and an aluminum working electrode, Figure 14 and Table XIII, indicated that the direct reduction of 1-octyl bromide occurred at potentials more cathodic than -1.5V. Therefore, with a working electrode potential of -0.9V, 1-octyl bromide is not directly reducible.

If 1-octyl bromide oxidatively adds to an iron atom in the iron-plated matrix, the oxidation number of the iron is increased by two, i.e., the d^8 iron (0) becomes the d^6 iron (II). A one electron reduction of this organometallic would lead to the formation of a σ-bonded alkyl-iron (I) species and a halide ion. This process, the electrochemical reduction of an alkyl-iron-halide surface species could account for the current associated with curve C. The alkyl-iron species can proceed to generate products. In the preelectrolyzed electrochemical cells, the active iron-plated surface is prepared before the organic substrate is added. The rapid rise in current within the first minutes after the addition of 1-octyl bromide, attests to the rapid oxidative addition process to the low valent, coordinately unsaturated (kinks, steps, and adatoms) iron sites. This model requires that the integrated area beneath the current-time curve should correspond to a one-electron transfer process.

The integrated areas beneath curve C in reactions NII157, $Fe(acac)_3$, and NII158, $FeBr_3$, are given in Table XXVIII. The expected number of equivalents are generated as the sum of the moles of recovered products assuming the number of equivalents per mole is one. This assumption requires the following reaction to have occurred

$$RX + 1e^- \rightarrow R\cdot + X^-$$

Table XXVIII. Integrated Areas Beneath Curve C for Preelectrolyzed Reactions of Iron Salts

Reaction No	NII157	NII158
Integrated Areas (Faradays)*	1.50×10^{-2}	1.54×10^{-2}
Expected Equivalents	1.12×10^{-2}	1.20×10^{-2}
Per Cent Equivalents Recovered	74%	78%
Iron Salt	$Fe(acac)_3$	$FeBr_3$
n (Assumed)	1	1

*Integration used Simpson's Rule

which is exactly the reaction postulated for the surface model. The nearly 25% loss in the number of equivalents recovered probably reflects reactions such as equation one given above as occurring, i.e., a free radical is discharged into solution where it is converted into unrecoverable material, as well as loss due to experimental work up.

Intermediates

The generation of product has been suggested to be a free radical process that occurs on the surface of the active iron. The adsorbed radicals can combine on the surface or may be discharged into the electrical double layer where they can react to generate coupled and disproportionated products. The radicals, particularly those in the electrical double layer may be intercepted with appropriate free radical scavengers. Cumene was used as a free radical trap in the

two-electrode constant applied potential electrolysis cell. Results of this investigation are given in Table XXIX. The problems of

Table XXIX. Effects of Cumene on Product Production in Two-Electrode Cell at Constant Applied Potential, 1.5V

Reaction No	NI144	NI158	NI167	NI220
Mole ratio Cumene:n-$C_8H_{17}Br$	1:1	4.9:1	10:1	benzene 10:1
% $C_{16}H_{34}$	19.9	7.0	3.9	10.4
% C_8H_{18}	29.2	42.3	29.1	20.5
% C_8H_{16}	10.4	21.8	7.1	6.8
% reaction	100	100	73.9	67.7

reproducing the active surface were not appreciated during most of this work, therefore these results are susceptible to the same scatter as was observed for other electrolysis cells. Noteworthy in this scheme is the systematic reduction of the yield of recovered coupled product. This indicates a free radical component to the coupling reaction is present. The coupling reaction must be surface mediated since concentration ratios of cumene to 1-octyl bromide as high as 10:1 failed to inhibit the coupling reaction. If the radical was a free solution radical, normal scavenger concentrations on the order of one to one scavenger to substrate should have quenched the coupling (178). The yield of octane should increase while the yield of coupled product decreases. This trend was not observed and may

indicate once again the problems of generating the active iron surface. Benzene was added to a standard electrolysis reaction in order to examine the dilution effect cumene, in a ratio of 10 to 1, had on the product formation. Cumene appears to actively suppress the yield of coupled product.

Carbanions were tested for using the base electrolyte TEAB and Me_4NBr. Varying the concentrations of the TEAB or substituting the tetramethyl salt which is incapable of Hoffman elimination reactions had no effect on the octane formation, Table XVIII. Indicating the absence of a carbanion mechanism

Phenol is a reasonably good proton source that is also used to test for the presence of carbanions in an electrolytic reduction (68). A reaction run in a three-electrode electrolysis cell with the concentrations of phenol equal to the concentration of 1-octyl bromide generated the following results:

% $C_{16}H_{34}$	0.5
% C_8H_{18}	49.0
% C_8H_{16}	3.1
% reaction	60.5

The quaternary ammonium salts indicated that no carbanion formed in this electrolysis. These results for inhibition of coupling by phenol can be interpreted as surface effects. The phenol may lose its

proton in the electrical double layer or the working electrode. The proton can be reduced at the plated iron surface and the generated hydrogen gas can dissociatively absorb onto the iron forming the iron-hydrogen solution. The hydrogen atom in solution is available to react with the surface radicals and in so doing generate octane. Since this scheme postulates extended proton reduction, the generation of hydrogen gas may be detrimental to the deposition of a proper iron surface. Therefore, the reduced per cent yield of hexadecane may also reflect the low quality surface that was formed.

These sorties into possible intermediate formation are instructive, but not necessarily definitive. Ultimately, this work must be reexamined only after the surface is properly and reproducibly prepared.

Other Substrates

Table XXX gives the results obtained for several other substrates tested in the electrolysis cell. The effect of changing the halide was examined by performing the standard reaction using primary octyl chloride rather than 1-octyl bromide, reaction NII199. The highest yield of octane was obtained with the chloride substrate, while the coupled product was severely repressed. This may reflect specific surface interactions or may be attributed to a poor surface formation due to the improved complexation of Cl^- with iron (II) and

Table XXX. Other Organic Substrates Examined with $Fe(acac)_3$ in Three-Electrode Cell

Reaction No	Substrate	E_{ref}	Products*
NII110	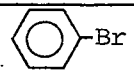	-1.0V	None
NII111	$BrCH_2CH_2COOEt$	-0.95V	diethyladipate (7%)
NII131	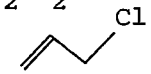	-0.95V	1,5-hexadiene (98%)
NII133	$ClCH_2COOEt$	-0.70V	$EtOCCH_2CH_2COEt$ (41%)
NII135	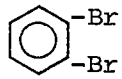	-1.0V	None
NII199	$1\text{-}C_8H_{17}Cl$	-0.90V	$C_{16}H_{34}$, 4.5% C_8H_{18}, 68.4% C_8H_{16}, 15.1%
NII200	$2\text{-}C_8H_{17}Br$	-0.90V	$2,1\text{-}C_{16}H_{34}$, 1.3% $2,2\text{-}C_{16}H_{34}$, 10.0% C_8H_{18}, 39.6% $1\text{-}C_8H_{16}$, 6.9% $2\text{-}C_8H_{16}$, 5.4% $1\text{-}C_8H_{16}$ Br, 2.5%
NII201	t-BuBr	-0.90	highly volatile product (23.5%) no coupled product

*vpc yield in parenthesis; isolated yield is not enclosed in parenthesis

hence the removal of iron (II) from further reduction (132). Mole ratios of 4:1 in Cl^- to iron (II) are sufficient to drive the equilibrium well to the cathodically insulated tetrahedral complex.

The series of 1°, 2°, and 3° halides was also briefly examined. Mixed coupling was noted to occur with the secondary octyl bromide. This is possible if the dissociative adsorption (oxidative addition) is a reversible process. An olefin would have to form by β-hydride migration. This olefin would be either 1-octene or 2-octene. If this step is at all reversible, the hydride can reattach at the secondary carbon for the coordinated 1-octene thus generating a primary surface radical. Two possible reaction pathways are available at this juncture. The primary surface could react with a secondary radical to lead to the mixed coupled product. Alternatively, a bromine atom could reattach and for primary octyl bromide, also observed in this reaction. Both 1-octene and 2-octene are capable of forming. Statistically, carbon one has more hydrogen than carbon three therefore more 1-octene should have formed. The slight preference may not be significant.

Tertiary halides did not couple although a reasonable concentration of volatile product was formed, probably t-butane. The trend of reactivities towards coupling qualitatively appears to be $1^o > 2^o > 3^o$ and $Br^- > Cl^-$. This is the expected order for a free radical process. The ease of homolytic cleavage of the C-Br bond is greater than a C-Cl bond and this appears to be the reactivity

pattern. The stability of free radicals is $3^{o} > 2^{o} > 1^{o}$ which is expected to be the order of alkane production. The iron-plated surface may be considered to stabilize incipient free radicals. The greater the stabilization, the longer the residence time on the surface, and the greater the probability of bimolecular encounters which should favor coupling.

SUMMARY

A two-electrode electrolysis cell was initially used to examine the effectiveness of electrolytically reducing a transition metal salt in the presence of an organic halide. The postulated strategy for the cell was the direct solution reaction of the electrolytically reduced metal and the organic substrate according to accepted homogeneous organometallic reaction processes. Decomposition of this homogeneous organometallic would lead to an oxidized metal center and organic products. The oxidized metal center is again reducible at the cathode of the electrolysis cell and the cycle can continue until the organic substrate is consumed.

The constant current two-electrode electrolysis cell used by Pillsbury (66) was, in principle, unsatisfactory for selective reduction of the inorganic ion. The two-electrode electrolysis cell was then operated under constant applied potential. Much work was done using this electrolysis cell with iron (III) acetylacetonate, $Fe(acac)_3$, and 1-octyl bromide. The results for the production of the coupled product, hexadecane, were unsatisfactory. Identically assembled two-electrode cells gave yields of coupled products that ranged from 0 to 33%. This scatter was felt to reflect the problems associated with a two-electrode cell. Particularly, the potential of the cathode can drift during the electrolysis which, if the drift is sufficiently cathodic, may result in the direct reduction of the organic halide.

A three-electrode electrolysis cell operates under a constant working electrode potential. This configuration eliminates the problem of a drifting cathode potential and therefore would lead to presumably more desirable precision in the yields of organic products for duplicate reactions. The three-electrode configuration requires a reference electrode that is stable in the nonaqueous solvent, N,N'-dimethylformamide used throughout this research effort. Such a reference electrode was prepared using an electrolytic method to reproducibly generate the cadmium-amalgam required as part of the internal standard half-cell for the reference electrode (124). An in-house manufactured potentiostat designed and built by R. D. Geer controlled the working electrode potential. The intended increase in the precision of the yields of organic products for duplicate reactions was not experimentally observed.

The current-time curves for both the two-electrode constant applied potential electrolysis cell and the three-electrode constant working electrode potential electrolysis cell provided much information concerning the nature of the electrolysis reaction. The two-electrode constant applied potential electrolysis cell was unusual in that the current slowly increased for many hours before dropping to near zero values during the reduction of $Fe(acac)_3$ in the presence of $1\text{-}C_8H_{17}Br$. This is unexpected for a simple reduction of inorganic material. Although the current behavior is interpretable in terms of

a drifting cathode potential, it also suggests the possibility of an ECE mechanism.

The current-time behavior for the three-electrode constant working electrode potential electrolysis cell in which $Fe(acac)_3$ was reduced in the presence of $1\text{-}C_8H_{17}Br$ was even more exceptional. After an initial current decay, two current transients appeared each associated with an increase followed by a decrease in current. Further experiments noted that these current transients were separable. At aluminum electrodes, the initial current decay and the first current transient were associated with the reduction of $Fe(acac)_3$. The second current transient required the first two curves to be present and only formed when the 1-octyl bromide was present in the electrolysis solution. This second current transient is associated with the reduction of an organometallic. The first two current curves also appeared during the electrolytic reduction of $Fe(acac)_3$, $FeBr_3$, and $Cu(acac)_3$ at a platinum-foil working electrode. Only a slow current decay appeared during the electrolytic reduction of $Fe(acac)_3$ at a stainless steel working electrode.

The first current transient was ascribed to the difference in overpotential for the reduction of iron ions in the nonaqueous solution at an iron electrode compared to the same reduction at an aluminum or platinum-foil electrode. The overpotential for this reduction at an iron electrode is assumed to be less than the overpotential for

the same reduction at aluminum or platinum-foil electrodes. Since the potential of the working electrode is not changed, this reduction in overpotential causes the current to increase. As the reduction of iron ions in solution continues at the plated iron surface, the concentration of the available electrophores drops and the current decreases. The height of this current transient was noted to be dependent on the identity of the iron (III) salt used during the electrolysis. This observation was interpreted to reflect the chelate effect of a bidentate ligand such as the acetylacetonate anion. The solution species that is susceptible to further reduction is the solvated iron (II) complex, $Fe(DMF)_6^{2+}$. The concentration of this electrophore would be higher for a monodentate complex in equilibrium with this solvated iron (II) than for a bidentate complex. This current transcient is not present at stainless steel electrodes because iron centers are already available on the surface of this electrode material.

The history of the aluminum electrodes changes the nature of the first two current curves. The first current transient is not observed when the aluminum electrodes are not previously cleaned in an acid solution. Furthermore, the initial current for untreated aluminum electrodes is not high and rapidly decays to background levels. As the strength of the acid wash changes, the first two curves also change, increasing in total current with increased acid strength.

These results are interpreted in light of the aluminum oxide layer present on the surface of the aluminum electrode. The oxide is an insulating layer, therefore it hinders electron transfer between the electrode and the electrolyte solution. The removal of this oxide coating or a reduction in its thickness by acid washing the electrodes before use facilitates electron transfer. This increase in the rate of electron transfer across the electrode-solution interface is demonstrated by an increase in the cell's current.

The total current flowing through the cell affects the yield of coupled product while changing the concentration of the bulk solution components has no observable effect on the yield of coupled products. This effect of the total current was originally considered to be associated with the presence of surface alkyl radicals. However, as the total current decreased, the production of coupled product, envisioned to be formed by a bimolecular process between two surface radicals, increased. This inverse relationship is unexpected for surface radicals since the concentration of these radicals should decrease with a decrease in current. The observed trend is in harmony with plating technology. High currents remove the metal ion electrophore from the electrical double layer. This reduction of the double layer concentration generally leads to a flaky metal deposit. Lower current levels produce a smoother electrochemically plated surface.

The correlation of the type of metal deposit on the surface of the electrode and the yield of coupled product suggests that the reaction is heterogeneous and not homogeneous as previously postulated. Several experimental results substantiate the heterogeneous nature of this reaction. First, the generation of coupled product was demonstrated to occur only at an iron-plated aluminum electrode rather than in a prereduced iron solution. Similarly, coupled product was also obtained at an iron-plated platinum electrode, but not at a platinum-foil electrode in an iron-free solution of 1-octyl bromide. Finally, electron micrographs of the surface of two iron-plated aluminum electrodes demonstrated that high yields of coupled product were obtained with an iron deposit composed of platelets of material rather than a grainy deposit. This correspondence was observed for electrolysis cells that were identically assembled and operated. An epitaxial effect by the surface of the aluminum working electrode is suggested to account for the difference in the physical appearance of the iron deposit, the wide scatter in yields of coupled products for supposedly identical reactions, and the noted effect of the electrode's history.

The rapid current increase on the addition of 1-octyl bromide to a preelectrolyzed solution of $Fe(acac)_3$ is reconcilable in terms of the heterogeneous nature of the reaction. An active iron deposit is available on the surface of the working electrode after the

preelectrolysis. The 1-octyl bromide rapidly reacts with this plated-iron surface in an oxidative addition type process leading to the alkyl iron (II) halide or an alkyl iron (I) and iron (I) halide surface complex. The rapid current increase corresponding to the second current transient demonstrates that this oxidative addition is very rapid. This current increase corresponds to the reduction of an alkyl-iron (II) halide center or to an iron (I) halide center leading to the formation of X^- in solution and a reduced iron center. The adsorbed surface alkyl radical can couple or disproportionate with another surface radical either on the surface of the working electrode or in the electrical double layer. This process corresponds to a net one-electron transfer per mole of alkyl halide. Integrating the area beneath this last current transient supports the one-electron transfer process. Thus, the production of organic products is heterogeneous and electrocatalytic. This latter conclusion follows from the generation of an iron ion during the chemical transformation leading to the surface species which is then subsequently reduced.

EXPERIMENTAL

Tetraethylammonium Bromide (TEAB)

An equal molar (1.5 M) mixture of triethylammine and ethyl bromide was refluxed for 24 hours in toluene. The precipitated ammonium salt was filtered, washed with toluene, and recrystallized from a benzene-ethanol mixture. The resulting crystals were dried in a vacuum desiccator at 60°C. After drying, the crystals were stored in an ambient dessicator.

Tetraethylammonium Perchlorate (TEAP)

A saturated aqueous solution of 26.5 g (125 mmoles) of TEAB in about 40 ml of water was treated with 10.5 ml (about 130 mmoles) of aqueous 70 to 72% perchloric acid. The crude insoluble perchlorate salt so formed was cooled and then filtered. The salt was washed several times with cold water and then recrystallized from water. The resulting pure crystals were dried at 100°C in a vacuum desiccator. After drying, the crystals were stored in an ambient desiccator.

Iron (III) acetylacetonate [$Fe(acac)_3$]

$Fe(acac)_3$ was prepared by mixing stoichiometric amounts of $FeCl_3$ and ammonium acetylacetonate in an aqueous solution. The latter was prepared by adding equal molar solutions of 2,4-pentanedione and concentrated ammonium hydroxide. A dark red precipitate formed. The precipitate was filtered and washed several times with cold water. The

precipitate was air dried prior to recrystallization from a hot methanol-water solution. The recrystallized $Fe(acac)_3$ was again collected and allowed to air dry followed by vacuum drying at 60°C. The $Fe(acac)_3$ prepared by this method decomposed at 184°C (uncorrected).

N,N'-Dimethylformamide (DMF)

'Baker Analyzed' reagent grade DMF was atmospherically distilled. The middle fraction (bp 144°C) was collected and stored in a brown bottle over Linde 4A molecular sieves. The solvent was used within fourteen days of the distillation.

Other Reagents

The n-octyl bromide used in this study was purchased from Aldrich Chemical Company as was the triphenyl phosphine, Ph_3P. The internal standard used for the gas chromatographic analysis was "gold label" n-decane also purchased from Aldrich Chemical Company.

Vanadium oxysulfate, $VOSO_4 \cdot xH_2O$, was obtained from Alfa Inorganics, Inc. This material was used to establish the reliability of the reference electrode.

Other organic substrates used in this work were obtained from various distributors. The n-octyl chloride and o-dibromobenzene were purchased from Aldrich Chemical Company. The 2-bromooctane was obtained from Eastman Kodak Company. Chem Services provided the acid halo esters used in the screening reactions. These latter substrates

were of technical grade and included ethyl bromoproprionate and ethyl chloroacetate. Bromobenzene, allyl chloride, and tertiary butyl bromide were also provided by Chem Services.

Equipment

A Heathkit Regulated L.V. Power Supply Model IP-27 was used as a constant applied potential source for all of the two-electrode electrolysis reactions. This power supply was slightly modified, mHK, to accommodate the three-electrode constant working electrode operation. The modification simply introduced an operational amplifier circuit into the control assembly. One input of the operational amplifier was the reference electrode. The output of the operational amplifier was then a signal for increasing or decreasing the applied potential.

The circuit for the potentiostat which R. D. Geer designed and assembled, GP, is presented in Figure 32. All of the components of this potentiostat are solid-state devices. The potentiostat is powered by a ±15V Hewlett-Packard Power Supply with 0.75A current output. The potential drop between the reference electrode and the working electrode is measured at E_W using a high impedance digital voltmeter. Since this is the output side of the operational amplifier, limited current is drawn through the reference electrode. The electrolysis current attained with this potentiostat was continuously recorded using a variable speed Heath Servo-Recorder Model EUW-20A. A 1.02 ohm resistor was

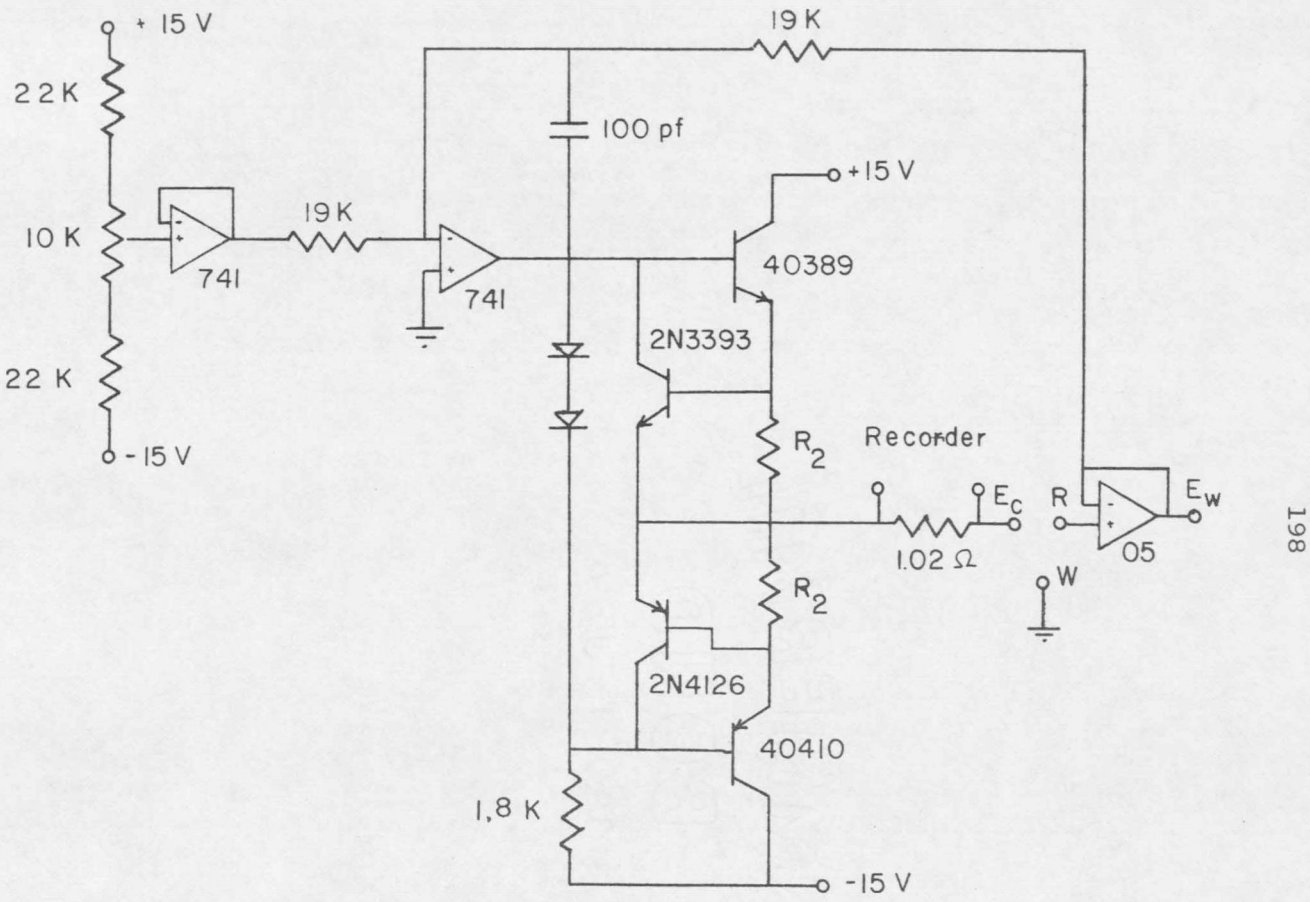

Figure 32. Geer's In-House Manufactured Potentiostat. R_2 resistors limit the total cell current; E_W is the monitored working electrode potential.

connected across the recorder's input and ground terminals in order to provide the potential drop necessary for the recorder to function. Maximum electrolysis currents were controlled by replacing the resistors labeled R_2 with appropriately sized resistors. Five resistors were used in this study. Table XXXI lists the size of the resistor and the maximum current obtained.

Table XXXI. Current Maximum for Appropriately Sized Resistors Used at R_2

R_2 (ohms)	Current Maximum (mA)
3.3	200
4.7	145
6.8	98
12	70
27	25

Potentiometric measurements were obtained using a Heath EU-401 series polarography system. The polarographic measurements were made with three-electrode potentiostatic control of the working electrode's potential. The electrode assembly consisted of an 18-guage platinum spiral counter electrode, the dropping mercury working electrode, and the appropriate reference electrode.

Reaction products and starting materials were analyzed using a Varian Aerograph Model 1740 gas chromatograph equipped with

temperature programming, flame ionization detector, and a Varian CH-5 mass spectrometer. Peak areas of gas chromatographed samples were analyzed using a Spectra-Physics Minigrator which was referenced to n-decane as an internal standard, and by mass spectral fragmentation patterns.

Spectroscopic analysis was performed using a Varian Cary-14 Spectrophotometer. The cell path length used for both the analyte compartment and the blank compartment was 1.0 mm. The cells were made of silica.

Reference Electrodes

The glassy carbon reference electrode was prepared by sliding a piece of glassy carbon rod, 3 mm in diameter, into an appropriately sized polypropylene sleeve that was approximately 150 mm long. Electrical contact between an external lead and the glassy carbon tip was made by extending a piece of single stranded wire down the central bore of the polypropylene and into a mercury pool placed on the glassy carbon insert.

The cadmium amalgam reference electrode was prepared by electrolyzing an aqueous solution of cadmium sulfate at a mercury cup cathode. Cadmium sulfate (12.0 g) was dissolved in 50 ml of distilled water acidified to a pH of 0.5 with concentrated sulfuric acid (1 ml). This solution was placed in the cathode compartment of the electrolysis

cell. The electrolysis cup was filled with 6.4 g of triply distilled mercury and immersed into this solution. The anode compartment consisted of a Pyrex test tube with a cracked glass junction, a piece of 18-gauge platinum wire, and a similarly acidified water solution less the $CdSO_4$. A SCE reference electrode was immersed into the cathode compartment. After purging the system with nitrogen, N_2, the potential of the cathode was maintained at approximately -1.0V vs SCE [$E^{\circ}_{1/2,Cd(II)/Cd(Hg)}$ = -0.594V vs SCE (179)]. Nitrogen was bubbled slowly through the cathode compartment during the full course of the reaction. The electrolysis was allowed to continue until the mercury cathode became a crystalline amalgam. The amalgam was removed, washed four times with distilled water followed by eight washes with DMF. Sodium chloride (0.30 g) and $CdCl_2 \cdot 2H_2O$ (0.15 g) were added to the amalgam. The amalgam and salts were ground with a glass rod until a uniform mixture was obtained. Triply distilled mercury was added as necessary to get the proper consistency. The amalgam was loaded into two reference electrode assemblies differing only in the nature of the liquid junction. One junction was prepared from porous Vycor (Corning Glassware, "thirsty glass") the other junction was a cracked glass junction. The reference electrode was assembled by placing a piece of glass wool above the junctions and then adding a small aliquot of a DMF solution saturated with NaCl and $CdCl_2 \cdot 2H_2O$. All air bubbles in the glass wool were removed. The cadmium amalgam was then placed

above the glass wool, forming a porous plug about 15 mm deep. More NaCl and $CdCl_2 \cdot 2H_2O$ saturated DMF was placed above the amalgam. Electrical contact was made with a piece of platinum wire sealed into a piece of soft glass tubing. The Pt was forced into the cadmium-amalgam slurry. Finally, a few drops of triply distilled mercury was poured down the soft-glass caning and external electrical contact was made by sliding a piece of singly stranded wire down the tubing and into the mercury pool.

The performance of a new reference electrode was evaluated using the half wave potential for the reduction of a metal ion in an appropriate solvent and comparing this potential against the results obtained with a known standard reference electrode or the reported literature values.

The glassy carbon reference electrode was used as the reference for the polarographic analysis of a 10^{-3} M and a 10^{-4} M nickel sulfate solution both in 1.0 M KCl. The solvent was water, therefore the half-wave potential for the Ni(II) was compared against that measured versus the SCE standard. The glassy carbon reference drifted while the SCE remained relatively stable.

The cadmium amalgam reference electrode was used to monitor the half-wave potential of the vanadyl ion in vanadium oxysulfate. The reduction potential was compared against the reported literature values (121,122). This method of examination was also used before and

after a macroscopic electrolysis to insure the integrity of the reference electrode during the course of the reduction.

Electrodes

Two aluminum alloys and one stainless steel alloy were used for electrodes in the two-electrode and three-electrode cells. The composition of one of the aluminum alloys was unknown. Table XXXII lists the composition of the known aluminum alloy, 606IT6, and the stainless steel alloy, 302. The dimensions of the surface of these electrodes normally exposed to the electrolysis solution was 35 mm x 40 mm x 0.9 mm.

The aluminum electrodes were pretreated using a hydrochloric acid bath. The acid bath was generally prepared by adding 1.6 ml of concentrated HCl to 60.0 ml of distilled water. The aluminum electrodes were immersed in this bath for 15 minutes prior to use in the electrolysis cell. Just before these electrodes were placed in the electrolysis cell, they were removed from the acid bath, rinsed with water, and dried by rinsing them in organic solvents. Stainless steel electrodes were also pretreated the same way.

The platinum foil electrode was donated by Dr. Eric Grimsrud. The dimensions of the foil were 34 mm x 12 mm.

The geometric surface of these electrodes changed during the electrolysis as a result of plating. Also, the counter electrode or

Table XXXII. Alloy Composition for Aluminum and Stainless Steel (180,181)

Element	Aluminum 606IT6 %	Stainless Steel 302 %
Si	0.4 to 0.8	1.00 max
Fe	0.7	67.8 to 71.8
Cu	0.15 to 0.40	--
Mn	0.15	2.00 max
Mg	0.8 to 1.2	--
Cr	0.04 to 0.35	17.0 to 19.0
Zn	0.25	--
Ti	0.15	--
Al	95.85 to 97.21	--
Ni	--	8.0 to 10.0
S	--	0.03
P	--	0.045
C	--	0.15
other	0.15	--

anode dissolved during the course of the reaction. Therefore, current densities were not calculated.

Electrolysis Reaction

In a typical reaction, to 60 ml of DMF in a 100-ml Berzelius beaker were added $Fe(acac)_3$ (4.4 g, 12.46 mmol), triphenylphosphine (1.5 g, 5.66 mmol), tetraethylammonium bromide (0.855 g, 4.07 mmol), and 1-octyl bromide (8.6 ml, 49.03 mmol). A rubber stopper fitted with cleaned aluminum electrodes was used to seal the beaker for all the two-electrode work. The rubber stopper was adapted to house the reference electrode for use in a three-electrode electrolysis cell. Nitrogen was bubbled through the stirred solution until all the solutes dissolved. The two-electrode constant applied potential electrolysis cell was generally operated at 1.5V applied potential. The three-electrode electrolysis cell was usually operated with a working electrode potential setting of -0.90V vs Cd(Hg). This three-electrode cell occasionally went into a current-limiting mode. During such times, the working electrode potential shifted to potentials anodic of -0.9V vs Cd(Hg). The two-electrode electrolysis cells normally were operated for 70 hours. The three-electrode electrolysis cells were operated for 24 hours.

Octane and octene were removed from the electrolyzed solution by vacuum distillation. These products were analyzed by gas

chromatography using n-decane as the internal standard. An 8-ft column packed with 20% Carbowax 20 M on 80-100 mesh Chromosorb W was used to separate octane from octene and a 6-ft column of 5% SE-30 on 80-100 mesh Chromosorb W was used to separate 1-octyl bromide from DMF.

The pot residue was treated with 100 ml of distilled water acidified with 2.0 ml concentrated HCl. This aqueous solution was extracted with five 50 ml aliquots of ether. The ether solution was dried over anhydrous magnesium sulfate, filtered, and evaporated by a rotoevaporator. Liquid chromatography on a 46x2 cm column of activated acidic aluminum oxide eluted with hexane was used to separate hexadecane and unreacted 1-octyl bromide from other residues contained in the ether extract. After solvent evaporation on a rotoevaporator, the products were analyzed by gas chromatography using n-decane as the internal standard. The same columns as used for the analysis of octane and 1-octene were used to analyze the recovered hexadecane and 1-octyl bromide. If there was no precipitate formed in the ether extract after rotoevaporation, the liquid chromatography step was omitted and this extract was analyzed directly.

The per cent yields were based on the amount of 1-octyl bromide which was unrecovered. The amount of 1-octyl bromide that was unrecovered was calculated from the known amount of 1-octyl bromide originally added to the electrolysis cell less the amount of 1-octyl bromide recovered after the electrolysis reaction. The per cent reaction

is the amount of unrecovered 1-octyl bromide divided by the original amount of 1-octyl bromide added to the electrolysis cell.

Perturbation on Standard Cell

Other organic halides were used in the electrolysis cell. The concentration of these substrates duplicated the concentration of n-octyl bromide in all cases. The concentration of other cell components remained unchanged.

The attempts to optimize the yield of coupled product by varying the concentration of the cell components was accomplished by independently varying the concentration of the desired constituent. All other solution components retained their concentration as given in the general reaction.

Spectroscopic Analysis

Blanks for the double beam instrument were prepared from the general electrolysis cell solution less the inorganic chromophore. A 0.1 ml aliquot of this colorless electrolysis cell solution was diluted to 10.0 ml with DMF. The $Fe(acac)_3$ was added to the electrolysis cell. Aliquots of 0.1 ml were periodically removed from the cell during electrolysis, diluted to 10.0 ml with DMF, and spectrophotometrically analyzed. Those solutions containing other inorganic ion chromophores were treated similarly.

Polarography

Polarographic cells were assembled using a 10^{-3} M to 10^{-4} M solution of the appropriate electrophore. The solvent was DMF containing either 0.10 M tetraethylammonium bromide or 0.10 M tetraethylammonium perchlorate. The latter quaternary base electrolyte was used for purposes of increasing the anodic window.

BIBLIOGRAPHY

BIBLIOGRAPHY

1. G. Wilkinson, Pure Appl. Chem., 30, 627 (1972).

2. P.S. Bratterman and R.J. Cross, J.C.S. Dalton Trans., 657 (1972).

3. P.S. Bratterman and R.J. Cross, Chem. Soc. Rev., 2, 271 (1973).

4. W. Mowat, A. Shortland, G. Yagupsky, N.J. Hill, M. Yagupsky, and G.W. Wilkinson, J.C.S. Dalton Trans., 533 (1972).

5. R.R. Schrock and G.W. Parshall, Chem. Rev., 76, 243 (1976).

6. P.J. Davidson, M.F. Lappert, and R. Pearce, Chem. Rev., 76, 219 (1976).

7. J. Halpern, Adva. Chem. Ser., No. 70, 1 (1968); J. Halpern, Accts. Chem. Res., 3, 386 (1970).

8. J.P. Collman, Accts. Chem. Res., 1, 136 (1968); J.P. Collman, private communication.

9. C.A. Tolman, Chem. Soc. Rev., 1, 337 (1972).

10. R.A. Howald and D.P. Keeton, Spectrochim. Acta, 22, 1211 (1966).

11. R.F. Heck, "Organotransition Metal Chemistry," Academic Press, New York, 1974.

12. J.P. Collman, Accts. Chem. Res., 8, 342 (1975).

13. J.P. Collman, S.R. Winter, and D.R. Clarke, J. Am. Chem. Soc., 94, 1788 (1972).

14. W.O. Siegel and J.P. Collman, J. Am. Chem. Soc., 94, 2516 (1972).

15. J.P. Collman, S.R. Winter, and A.G. Komoto, J. Am. Chem. Soc., 95, 249 (1973).

16. E.A. Sullivan and T.F. Jula, American Laboratory, 1974, 49 (1974).

17. D.F. Schriver, Accts. Chem. Res., 3, 231 (1970).

18. M.P. Cooke, Jr. and R.M. Parlman, J. Am. Chem. Soc., 97, 6863 (1975).

19. K. Sisido, Y. Udo, and H. Nozaki, J. Am. Chem. Soc., 82, 434 (1960).

20. Y. Ogata and H. Nakamura, J. Org. Chem., 21, 1170 (1956).

21. M.K. Al-Noori and J.M. Saleh, J.C.S. Faraday I, 69, 2140 (1973).

22. D.L. Williams-Smith, L.R. Wolf, and P.S. Skell, J. Am. Chem. Soc., 94, 4042 (1972).

23. H. Alper and E.C.H. Keung, J. Org. Chem., 37, 2566 (1972).

24. J. Mantzaris and E. Weissberger, J. Am. Chem. Soc., 96, 1873 (1974).

25. J. Mantzaris and E. Weissberger, J. Am. Chem. Soc., 96, 1880 (1974).

26. E. Weissberger and G. Page, J. Am. Chem. Soc., 99, 147 (1977).

27. M.A. Bennett, G.B. Robertson, I.B. Tomkins, and P.O. Whimp, J. Organometal. Chem., 32, C19 (1971).

28. A. Stockis and E. Weissberger, J. Am. Chem. Soc., 97, 4288 (1975).

29. G. Cardaci, Inorg. Chem., 13, 2974 (1974).

30. G. Cardaci, J. Organometall. Chem., 76, 385 (1974).

31. R. Baker, Chem. Rev., 73, 487 (1973).

32. G. Cardaci and A. Foffani, J.C.S. Dalton, 1808 (1974).

33. F.D. Mango, Coord. Chem. Rev., 15, 109 (1975).

34. M. Green and R.P. Hughes, Chem. Commun., 619 (1975).

35. G. Huttner and W. Gartzke, Chem. Ber., 108, 1373 (1975).

36. A. Cutler, D. Ehntholt, W.P. Giering, P. Lennon, S. Raghu, A. Rosan, M. Rosenblum, J. Tancrede, and D. Wells, J. Am. Chem. Soc., 98, 3495 (1976).

37. S. Ruei Su and A. Wojcicki, Inorg. Chem., 14, 89 (1975).

38. T.C. Flood, F.J. DiSanti, and D.L. Miles, Chem. Commun., 336 (1975).

39. M.S. Kharasch, L. Biritz, W. Nudenberg, A. Bhattacharya, and N.C. Yang, J. Am. Chem. Soc., 83, 3229 (1961).

40. M.S. Kharasch, M. Weiner, W. Nudenberg, A. Bhattacharya, T. Wang, and N.C. Yang, J. Am. Chem. Soc., 83, 3232 (1961).

41. M. Tamura and J.K. Kochi, Bull. Chem. Soc. Japan, 44, 3063 (1971).

42. M. Tamura and J.K. Kochi, J. Am. Chem. Soc., 93, 1487 (1971).

43. M. Tamura and J.K. Kochi, J. Organometall. Chem., 31, 289 (1971).

44. C.L. Kwan and J.K. Kochi, J. Am. Chem. Soc., 98, 4903 (1976).

45. S.M. Neumann and J.K. Kochi, J. Org. Chem., 40, 599 (1975).

46. R.S. Smith and J.K. Kochi, J. Org. Chem., 41, 502 (1976).

47. J. Allison and D.P. Ridge, J. Am. Chem. Soc., 98, 7445 (1976).

48. E.C. Ashby and T.L. Wiesemann, J. Am. Chem. Soc., 96, 7117 (1974).

49. E.C. Ashby, J.D. Buhler, I.G. Lopp, T.L. Weisemann, J.S. Bowers, Jr., and J.T. Laemule, J. Am. Chem. Soc., 98, 6561 (1976).

50. P.L. Bock, D.J. Boschetto, J.R. Rasmussen, J.P. Demers, and G.M. Whitesides, J. Am. Chem. Soc., 96, 2814 (1974).

51. D. Slack and M.C. Baird, Chem. Commun., 701 (1974).

52. T.C. Flood and F.J. DiSanti, Chem. Commun., 18 (1975).

53. P.L. Bock and G.M. Whitesides, J. Am. Chem. Soc., 96, 2826 (1974).

54. G.M. Whitesides and D.J. Boschetto, J. Am. Chem. Soc., 93, 1529 (1971).

55. D.L. Reger and E.C. Culbertson, J. Am. Chem. Soc., 98, 2789 (1976).

56. S.J. Okrasinski and J.R. Norton, J. Am. Chem. Soc., 99, 295 (1977).

57. A. Yamamoto, K. Morifuji, S. Ikeda, T. Saito, Y. Uchida, and A. Misono, J. Am. Chem. Soc., 90, 1878 (1968).

58. T. Yamamoto, A. Yamamoto, and S. Ikeda, Bull. Chem. Soc. Japan, 45, 1104 (1972).

59. J.K. Kochi and F.F. Rust, J. Am. Chem. Soc., 83, 2017 (1961).

60. J.T. Groves and M. van der Puy, J. Am. Chem. Soc., 96, 5274 (1974).

61. D.J. Mackinnon and W.A. Waters, J. Chem. Soc., 323 (1953).

62. M.S. Kharasch, F.S. Arimoto, and W. Nudenberg, J. Org. Chem., 16, 1556 (1951).

63. J. Kumamota, H.E. De La Mare, and F.F. Rust, J. Am. Chem. Soc., 82, 1935 (1960).

64. T.M. Hellman and G.A. Hamilton, J. Am. Chem. Soc., 96, 1530 (1974).

65. M.J. Gibian and R.C. Corky, Chem. Revs., 73, 441 (1973).

66. D. Pillsbury, Ph.D. Thesis, Montana State University, 1973.

67. S. Zecchin, G. Schiavon, G. Pilloni, and M. Martelli, J. Organometall. Chem., 110, C45 (1976).

68. A.J. Fry, "Synthetic Organic Electrochemistry," Harper and Row, Publishers, New York, 1972.

69. C.K. Mann and K.K. Barnes, "Electrochemical Reactions in Nonaqueous Systems," Marcel Dekker, Inc., New York, 1970.

70. M.M. Baizer, Ed., "Organic Electrochemistry," Marcel Dekker, Inc., New York, 1973.

71. M.R. Rifi in "Techniques of Chemistry," Vol. V, Part II, N.L. Weinberg, Ed., John Wiley and Sons, New York, 1975, p. 83.

72. M. von Strackelberg and W. Stracke, Z. Elektrochem., 53, 118 (1949).

73. P.J. Elving, Rec. Chem. Progress, 14, 99 (1953).

74. J.P. Petrovich and M.M. Baizer, Electrochim. Acta, 12, 1249 (1967).

75. R. Annino, R.E. Erickson, J. Michalovic, and B. McKay, J. Am. Chem. Soc., 88, 4424 (1966).

76. J.L. Webb, C.K. Mann, and H.M. Walborsky, J. Am. Chem. Soc., 92, 2042 (1970).

77. F.L. Lambert and K. Kobayashi, J. Am. Chem. Soc., 82, 5324 (1960).

78. F.L. Lambert, J. Org. Chem., 31, 4184 (1966).

79. L.W. Marple, L.E.I. Hummelstedt, and L.B. Rogers, J. Electrochem. Soc., 107, 437 (1960).

80. H.E. Ulery, J. Electrochem. Soc., 116, 1201 (1969).

81. J.W. Sease, P. Chang, and J.L. Groth, J. Am. Chem. Soc., 86, 3154 (1964).

82. F.L. Lambert, J. Am. Chem. Soc., 86, 3155 (1964).

83. A.K. Hoffmann, W.G. Hodgson, D.L. Maricle, and W.H. Jura, J. Am. Chem. Soc., 86, 631 (1964).

84. E.M. Marlett, Ann. N.Y. Acad. Sci., 125, 12 (1965).

85. O.R. Brown, H.R. Thirsk, and B. Thornton, Electrochim. Acta, 16, 495 (1971).

86. O.R. Brown and K. Taylor, J. Electroanal. Chem., 50, 211 (1974).

87. R. Galli, J. Electroanal. Chem., 22, 75 (1969).

88. M. Fleischmann, D. Pletcher, and C.J. Vance, J. Electroanal. Chem., 29, 325 (1971).

89. M. Fleischmann, G. Mengoli, and D. Pletcher, Electrochim. Acta, 18, 231 (1973).

90. H. Lehmkuhl in "Organic Electrochemistry," M.M. Baizer, Ed., Marcel Dekker, Inc., New York, 1973, p. 621.

91. W.J. Settineri and L.D. McKeever in "Techniques of Chemistry," Vol. 5, Part II, N.L. Weinberg, Ed., John Wiley and Sons, New York, 1975, p. 397.

92. H. Lehmkuhl, Synthesis, 377 (1973).

93. R.E. Dessy and L.A. Bares, Accts. Chem. Res., 5, 415 (1972).

94. R. Ercoli, M. Guainazzi, and G. Silvestri, Chem. Commun., 927 (1967).

95. J.B. Headridge, "Electrochemical Techniques for Inorganic Chemists," Academic Press, New York, 1969.

96. D.T. Sawyer and J.L. Roberts, Jr., "Experimental Electrochemistry for Chemists," John Wiley and Sons, New York, 1974.

97. G. Cauguis in "Organic Electrochemistry," M.M. Baizer, Ed., Marcel Dekker, Inc., New York, 1973, p. 13; G. Cauguis and V.D. Parker, ibid., p. 93.

98. L. Meites, "Polarographic Techniques," 2nd ed., John Wiley and Sons, 1965.

99. J. O'M. Bockris and A.K.N. Reddy, "Modern Electrochemistry," Vols. 1 and 2, Plenum Press, New York, 1970.

100. P. Zuman in "Organic Electrochemistry," M.M. Baizer, Ed., Marcel Dekker, Inc., New York, 1973, p. 155.

101. H. Lund and P. Iverson in "Organic Electrochemistry," M.M. Baizer, Ed., Marcel Dekker, Inc., New York, 1973, p. 165.

102. L. Meites in "Techniques of Chemistry," Vol. 1, A. Weissberger, Ed., John Wiley and Sons, New York, 1971, p. 645.

103. C.J. Pickett and D. Pletcher, J.C.S. Dalton Trans., 879 (1975).

104. R. Dietz and H. Lund in "Organic Electrochemistry," M.M. Baizer, Ed., Marcel Dekker, Inc., New York, 1973, p. 821.

105. P.W. Jennings, D.G. Pillsbury, J.L. Hall, and V.T. Brice, J. Org. Chem., 41, 719 (1976).

106. D.A. Skoog and D.M. West, "Principles of Instrumental Analysis," Holt, Rinehart, and Winston, Inc., New York, 1971, p. 517.

107. A.J. Allmand, "The Principles of Applied Electrochemistry," Longmans, Green and Co., London, 1920.

108. J.M. West, "Electrodeposition and Corrosion Processes," 2nd ed., Van Nostrand Reinhold Company, London, 1970.

109. W.W. Arbogast, Jr., Corrosion, 30, 179 (1974).

110. D.J.G. Ives and G.J. Janz in "Reference Electrodes, Theory and Practice," D.J.G. Ives and G.J. Janz, Eds., Academic Press, New York, 1961, p. 1.

111. G.J. Hills in "Reference Electrodes, Theory and Practice," D.J.G. Ives and G.J. Janz, Eds., Academic Press, New York, 1961, p. 433.

112. J.N. Butler in "Advances in Electrochemistry and Electrochemical Engineering," Vol. 7, P. Delahay and C.W. Tobias, Eds., John Wiley and Sons, New York, 1970, p. 77.

113. C.K. Mann in "Electroanalytical Chemistry," Vol. 3, A.J. Bard, Ed., Marcel Dekker, Inc., New York, 1969, p. 57.

114. N. Matsuura, K. Umenoto, M. Waki, Z. Jakeuchi, and M. Omoto, Bull. Chem. Soc. Japan, 47, 806 (1974).

115. T. Kakutani, S. Totsuka, and M. Senda, Bull. Chem. Soc. Japan, 46, 3652 (1973).

116. J.W. Diggle, A.J. Parker, and D.A. Owensby, Aust. J. Chem., 28, 237 (1975).

117. M. Saito and A. Kanamori, Bull. Chem. Soc. Japan, 48, 3021 (1975).

118. R.J. Taylor and A.A. Humffray, J. Electroanal. Chem., 64, 63 (1975).

119. D.L. McMasters, R.B. Dunlap, J.R. Kuempel, L.W. Kreider, and T.R. Shearer, Anal. Chem., 39, 103 (1967).

120. L.W. Marple, Anal. Chem., 39, 844 (1967).

121. C.W. Manning and W.C. Purdy, Anal. Chim. Acta, 51, 124 (1970).

122. C.W. Manning and W.C. Purdy, Anal. Chim. Acta, 51, 483 (1970).

123. J.C. Symott and J.N. Butler, Anal. Chem., 41, 1890 (1969).

124. J.L. Hall and P.W. Jennings, Anal. Chem., 48, 2026 (1976).

125. E.W. Washburn, Ed., "International Critical Tables," Vol. II, McGraw-Hill Book Co., Inc., New York, 1927, p. 429.

126. J.W. Mellor, "A Comprehensive Treatise on Inorganic and Theoretical Chemistry," Vol. IV, Longmans, Green and Co., London, 1923, p. 1042.

127. G. Lauer and R.A. Osteryoung, Anal. Chem., 38, 1106 (1966).

128. S.O. Farwell, Ph.D. Thesis, Montana State University, 1973.

129. R.C. Buchta and D.H. Evans, Anal. Chem., 40, 2181 (1968).

130. W.M. Moore and D.G. Peters, J. Am. Chem. Soc., 97, 139 (1975).

131. W.R. Heineman, J.N. Burnett, and R.W. Murray, Anal. Chem., 40, 1970 (1968).

132. A. Ciana and C. Furlani, Electrochim. Acta, 10, 1149 (1965).

133. G. Filardo, M. Galluzzo, B. Giannici, and R. Eroli, J.C.S. Dalton Trans., 1787 (1974).

134. T. Saji, T. Yamada, and S. Aoyagui, Bull Chem. Soc. Japan, 48, 1641 (1975).

135. T. Saji and S. Aoyagui, Bull. Chem. Soc. Japan, 49, 1399 (1976).

136. N.G. Connelly and K.R. Somers, J. Organometal. Chem., 113, C39 (1976).

137. M.C. Rakowski and D.H. Busch, J. Am. Chem. Soc., 97, 2570 (1975).

138. O.R. Brown and E.R. Gonzalez, J. Electroanal. Chem., 35, 13 (1972).

139. P. Yousefzadeh and C.K. Mann, J. Org. Chem., 33, 2716 (1968).

140. R. Ercoli, M. Guainazzi, and G. Silvestri, Chem. Commun., 927 (1967).

141. S.D. Ross, M. Finkelstein, and R.C. Petersen, J. Am. Chem. Soc., 92, 6003 (1970).

142. M. Finkelstein, R.C. Peterson, and S.D. Ross, Electrochim. Acta, 10, 465 (1965).

143. L. Eberson and K. Nyberg, Adv. Phys. Org. Chem., 12, 1 (1976).

144. M. Guianazzi, G. Filardo, G. Silvestri, S. Gambino, and R. Ercoli, Chem. Commun., 138 (1973).

145. G. Filardo and M. Guianazzi, J.C.S. Dalton Trans., 678 (1974).

146. B.F.G. Johnson, J. Lewis, D.J. Thompson, and B. Heil, J.C.S. Dalton Trans., 567 (1975).

147. J.A. McCleverty, J. Organometal. Chem., 68, 423 (1974).

148. P. Heimbach, Angew. Chem. internat. Edit., 12, 975 (1973).

149. M.F. Lappert, T.A. Nile, and S. Takashahi, J. Organometal. Chem., 72, 425 (1974).

150. K. Fischer, K. Jonas, P. Misbach, R. Stabba, and G. Wilke, Angew. Chem. internat. Edit., 12, 943 (1973).

151. J.A. McCleverty, J. Organometal. Chem., 119, 261 (1976).

152. T. Ikariya and A. Yamamoto, Chem. Commun., 720 (1974).

153. J.W. Vaughn in "The Chemistry of Nonaqueous Solvents," Vol. II, J.J. Lagowski, Ed., Academic Press, New York, 1967, p. 191.

154. N.L. Weinberg in "Techniques of Chemistry," Vol. 5, N.L. Weinberg, Ed., John Wiley and Sons, New York, 1975, p. 1.

155. W.H. Reinmuth, L.B. Rogers, and L.E.I. Humelstadt, J. Am. Chem. Soc., 81, 2947 (1959).

156. S.R. Missan, E.I. Becker, and L. Meites, J. Am. Chem. Soc., 83, 58 (1961).

157. A.J. Fry and R.L. Krieger, J. Org. Chem., 41, 54 (1976).

158. A.J. Fry, C.S. Hutchins, and L.L. Chung, J. Am. Chem. Soc., 97, 591 (1975).

159. G.M. McNamee, B.C. Willett, D.M. LaPerriere, and D.G. Peters, to appear in J. Am. Chem. Soc., June, 1977.

160. K. Alias, W.R. Fawcett, and R. Parsons, J.C.S. Faraday I, 70, 1046 (1974).

161. R.W. Murray and L.K. Hiller, Jr., Anal. Chem., 39, 1221 (1967).

162. W.R. Heineman, J.N. Burnett, and R.W. Murray, Anal. Chem., 40, 1970 (1968).

163. P.R. Singh and R. Sahai, Inorg. Chim. Acta, 2, 102 (1968).

164. A.M.T. Olmedo, R. Pereiro, and D.J. Schiffrin, J. Electroanal. Chem., 74, 19 (1976).

165. J.M. West, "Electrodeposition and Corrosion Processes," 2nd ed., Van Nostrand Reinhold Co., New York, 1970.

166. J.C. Buchholz and G.A. Somorjai, Accts. Chem. Res., 9, 333 (1976).

167. G.A. Somorjai, Accts. Chem. Res., 9, 248 (1976).

168. L.L. Kesmodel and G.A. Somorjai, Accts. Chem. Res., 9, 392 (1976).

169. G.A. Somorjai, J. Colloid. Interface. Sci., 58, 150 (1977).

170. A.J. Bard, Pure Appl. Chem., 25, 379 (1971).

171. P. Zuman, Electrochim. Acta, 21, 687 (1976).

172. J.M. Bobbitt, I. Noguchi, H. Yagi, and K.H. Weisgraber, J. Org. Chem., 41, 845 (1976).

173. D.H. Gerlach, W.G. Peet, and E.L. Muetterties, J. Am. Chem. Soc., 94, 4545 (1972).

174. M. Gargano, P. Ginnoccaro, M. Rossi, G. Vasapollo, and A. Sacco, J.C.S. Dalton Trans., 9 (1975).

175. M. Pankowski, E. Samuel, and M. Bigorgne, J. Organometal. Chem., 97, 105 (1975).

176. G.W. Parshall, Accts. Chem. Res., 3, 139 (1970).

177. J.W. Rathke and E.L. Muetterties, J. Am. Chem. Soc., 97, 3272 (1975).

178. H.P. Waits and G.S. Hammond, J. Am. Chem. Soc., 86, 1911 (1964).

179. "Handbook of Chemistry and Physics," 51st ed., Chemical Rubber Company, Cleveland, Ohio, 1970.

180. "Ryerson Data Book," Joseph T. Ryerson and Son, Inc., 1971, p. 214.

181. "Machinery's Handbook," 18th ed., Industrial Press, N.Y., 1969, p. 2043.

APPENDIX

Uv-visible spectroscopic analysis was performed on a number of electrolysis solutions. Occasionally, these examinations were recorded as a function of time. The general characteristics of a cell and the results of the uv-visible examinations are reported below.

Reaction Number	General Cell Description	Time (hours)	Absorbance [λ(nm) (abs)]
NI106	E_{APP} = 1.5V for 2-electrode cell; Al(unk) electrodes; products present but not quantitatively determined. $Fe(acac)_3$ present at t = 0.	0 20 113 209	353(0.80), 435(0.83) 352(0.76), 433(0.71) 365(0.73) 367(1.32)
NI114	E_{APP} = 1.5V for 2-electrode cell; Al(unk) electrodes; 17.2% RH, 6.2% R(-H), 20.7% R_2; $Fe(acac)_3$ present at t = 0.	0 20 88	353(0.80), 435(0.83 345(0.67), 427(0.50 367(1.34)
NI120	E_{APP} = 1.5V for 2-electrode cell; Al(unk) electrodes; 5.4% RH, 2.6% R(-H), 25.3% R_2; $Fe(acac)_3$ present at t = 0; no Ph_3P used in this cell.	0 21 72	353(0.85), 435(0.86) 350(0.73), 425(0.61) 367(0.97)
NII146	E_{ref} = -0.9V for 3-electrode cell; Stainless steel electrodes; $Fe(acac)_3$ present; no 1-$C_8H_{17}Br$ used in this cell	0 1 3	354(0.74), 437(0.73) 353(0.78), 435(0.71) 344(0.85), 357(0.81, shoulder), 434(0.69)
NII147	E_{ref} = -0.9V for 3-electrode cell; stainless steel working electrode, Pt-counter electrode; $Fe(acac)_3$ present; no 1-$C_8H_{17}Br$ present; TEAP used rather than TEAB.	6 24	354(0.76), 438(0.71) 351(0.70), 444(0.60) Pt counter electrode probably oxidizing Fe(II) to Fe(III).

Appendix A (continued)

Reaction Number	General Cell Description	Time (hours)	Absorbance [λ(nm) (abs)]
NII149	E_{ref} = -0.9V for 3-electrode cell; stainless steel working electrode, Pt counter electrode; $Fe(acac)_3$ present; no $1\text{-}C_8H_{17}Br$ present; TEAB used instead of TEAP.	24 48	354(0.70), 437(0.67) 354(0.63), 437(0.60) Br_2 or Br_3^- probably formed at Pt counter electrode and chemically oxidized Fe(II) to Fe(III).
NII150	E_{ref} = -0.9V for 3-electrode cell; Hg-pool working electrode, Pt counter electrode; same solution conditions as in NII149; little current.	24	354(0.49), 437(0.67)
NII151	E_{ref} = -0.11V for 3-electrode cell; stainless steel working electrode, Pt counter electrode; $Fe(acac)_3$ present, $1\text{-}C_8H_{17}Br$ present; 8.9% RH, trace R(-H), 6.8% R_2, 62.8% rexn.	18 24	354(0.60), 442(0.61) 355(0.59), 447(0.59)
NII153B	E_{ref} = -1.50V for 3-electrode cell; stainless steel working electrode, Pt counter electrode; no $Fe(acac)_3$ present, $1\text{-}C_8H_{17}Br$ present.	20	342(0.63), 400(0.35)
NII155	Solutions of other chromophores were prepared in concentration duplicating the concentrations of $Fe(acac)_3$. These solutions were examined with uv-visible spectroscopy.	Br_2 $FeBr_3$ $Ni(acac)_2$ $Cr(acac)_3$	400(0.15) 390(0.45), 470(0.27) 300(2.00), 315(1.44, shoulder) 339(1.29), 386(0.05)

Appendix A (continued)

Reaction Number	General Cell Description	Time (hours)	Absorbance [λ(nm) (abs)]
NII157	E_{ref} = -0.9V for 3-electrode cell. aluminum 606IT6 electrodes; preelectrolyzed $Fe(acac)_3$ for 24 hours; added $1\text{-}C_8H_{17}Br$ at 24 hours and continued electrolysis for additional 12 hours; 8.3% RH, 2.8% R(-H), 39.0% R_2 66.0% rexn.	24 36	350(0.48), 366(0.43) 357(0.50), 367(0.51)
NII160	E_{ref} = -0.9V for 3-electrode cell; aluminum 606IT6 electrodes; $Fe(acac)_3$ preelectrolyzed for 48 hours, electrodes removed and $1\text{-}C_8H_{17}Br$ added; 0.04 mmol RH, 0.06 mmol R(-H).	24 48 68	350(0.34), 365(0.30) 351(0.37), 367(0.34) 352(0.34), 367(0.34)
NII161	E_{ref} = -0.9V for 3-electrode cell; electrodes from NII160; iron-free solution containing $1\text{-}C_8H_{17}Br$; 9.2% RH, 3.1% R(-H), 62.8% R_2, 66.4% rexn; Electrolyzed for 48 hours.	48	351(0.34, shoulder) 377(0.25, shoulder)
NII16B	E_{ref} = -0.9V for 3-electrode cell; 606IT6 working electrode, stainless steel counter; $Fe(acac)_3$ present no $1\text{-}C_8H_{17}Br$.	0 3 21 43	330(0.54, well) 354(0.74), 380(0.39, well), 437(0.74) 330(0.80, well), 343(0.83), 357(0.77), 380(0.43, well), 435(0.65) 330(1.58), 340(1.50), 357 (0.85, shoulder), 380(0.50, well), 423(0.54) 321(1.96, well), 354(>2), 455(0.29)

Appendix A (continued)

Reaction Number	General Cell Description	Time (hours)	Absorbance [λ(nm) (abs)]
NII169	E_{ref} = -0.9V for 3-electrode cell; 606IT6 working electrode, Pt counter electrode; $Fe(acac)_3$ present, no $1\text{-}C_8H_{17}Br$.	0 17	355(0.71), 437(0.71) 354(0.67), 437(0.59)
NII170	E_{ref} = -0.9V for 3-electrode cell; Pt working electrode, 606IT6 counter electrode; $Fe(acac)_3$ present, no $1\text{-}C_8H_{17}Br$.	12 22	355(0.59, shoulder), 430(0.41) 355(0.54, shoulder), 430(0.35)
NII173	E_{ref} = -0.9V for 3-electrode cell; stainless steel working electrode, 606IT6 counter electrode; $Fe(acac)_3$ present, $1\text{-}C_8H_{17}Br$ present; 30.1% RH, 17.1% R(-H), 19.1% R_2, 100% rexn.	10 22	370(0.60) 372(0.88)
NII174	E_{ref} = -0.9V for 3-electrode cell; 606IT6 electrodes; $Fe(acac)_3$ not present; $1\text{-}C_8H_{17}Br$ not present	120	no chromophores

Hall, Jeffrey Louis, 1947-
Nonaqueous organometallic electrochemistry heterogeneous coupling of alkyl halides with reduced iron.